UNIVERSIDADE FEDERAL DO PARANÁ

WILLIAN CARLOS LESINHOVSKI

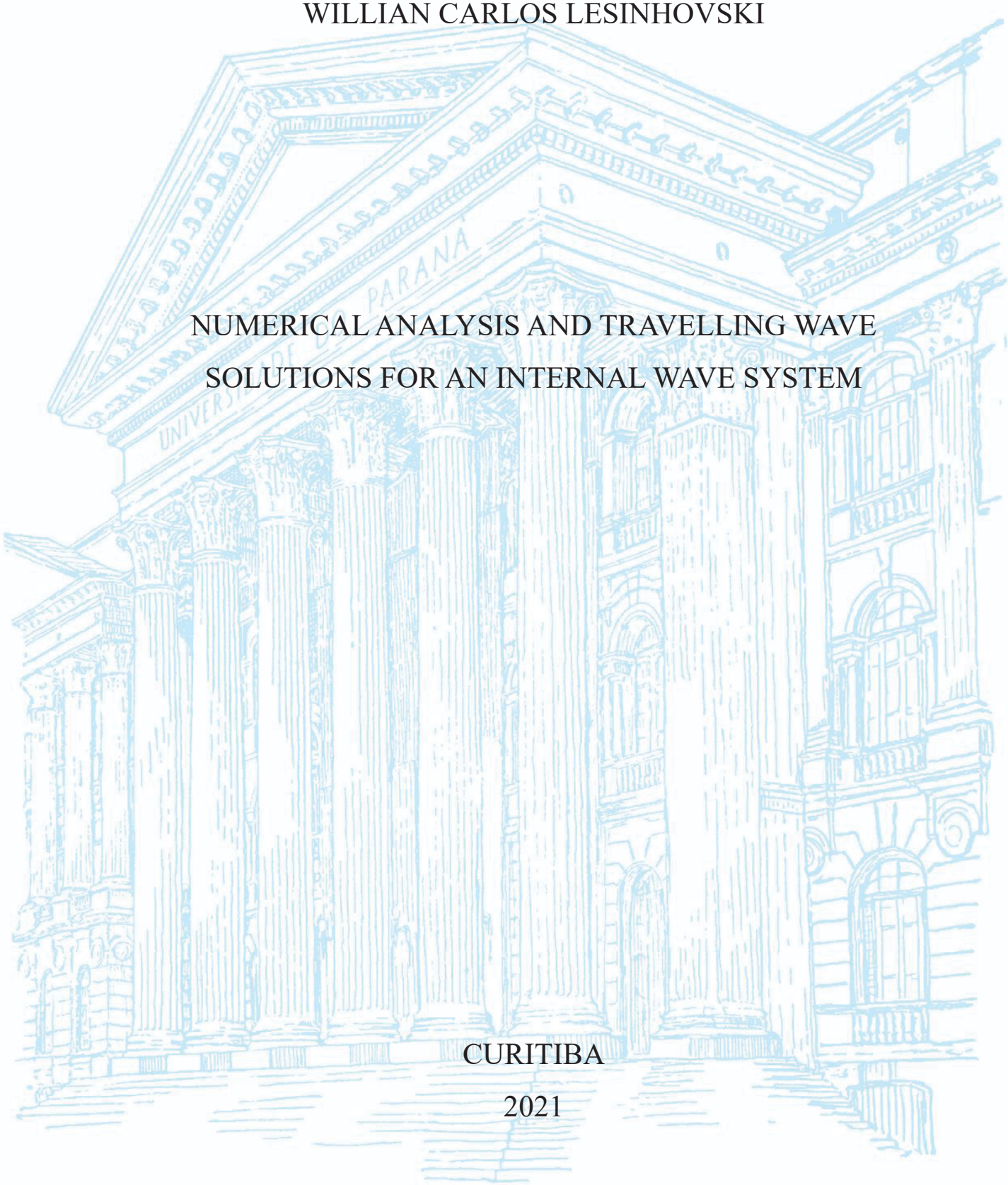

NUMERICAL ANALYSIS AND TRAVELLING WAVE SOLUTIONS FOR AN INTERNAL WAVE SYSTEM

CURITIBA

2021

WILLIAN CARLOS LESINHOVSKI

NUMERICAL ANALYSIS AND TRAVELLING WAVE SOLUTIONS FOR AN INTERNAL WAVE SYSTEM

Tese de Doutorado apresentada ao Programa de Pós-Graduação em Matemática, Setor de Ciências Exatas, Universidade Federal do Paraná, como requisito parcial à obtenção do título de Doutor em Matemática.

Orientadora: Prof.ª Dr.ª Ailin Ruiz de Zarate Fabregas

CURITIBA
2021

DADOS INTERNACIONAIS DE CATALOGAÇÃO NA PUBLICAÇÃO (CIP)
UNIVERSIDADE FEDERAL DO PARANÁ
SISTEMA DE BIBLIOTECAS – BIBLIOTECA CIÊNCIA E TECNOLOGIA

Lesinhovski, Willian Carlos
Numerical analysis and travelling wave solutions for an internal wave system. / Willian Carlos Lesinhovski. – Curitiba, 2021.
1 recurso on-line : PDF.

Tese (Doutorado) – Universidade Federal do Paraná, Setor de Ciências Exatas, Programa de Pós-Graduação em Matemática.
Orientadora: Profa. Dra. Ailin Ruiz de Zarate Fabregas.

1. Matemática. 2. Von Neumann, John, 1903-1957. 3. Métodos matemáticos. 4. Análise numérica. I. Fabregas, Ailin Ruiz de Zarate. II. Universidade Federal do Paraná. Programa de Pós-Graduação em Matemática. III. Título.

Bibliotecário: Nilson Carlos Vieira Junior CRB-9/1797

TERMO DE APROVAÇÃO

Os membros da Banca Examinadora designada pelo Colegiado do Programa de Pós-Graduação em MATEMÁTICA da Universidade Federal do Paraná foram convocados para realizar a arguição da tese de Doutorado de **WILLIAN CARLOS LESINHOVSKI** intitulada: **Numerical analysis and travelling wave solutions for an internal wave system**, sob orientação da Profa. Dra. AILIN RUIZ DE ZARATE FABREGAS, que após terem inquirido o aluno e realizada a avaliação do trabalho, são de parecer pela sua APROVAÇÃO no rito de defesa.

A outorga do título de doutor está sujeita à homologação pelo colegiado, ao atendimento de todas as indicações e correções solicitadas pela banca e ao pleno atendimento das demandas regimentais do Programa de Pós-Graduação.

CURITIBA, 26 de Fevereiro de 2021.

Assinatura Eletrônica
26/02/2021 22:15:21.0
AILIN RUIZ DE ZARATE FABREGAS
Presidente da Banca Examinadora

Assinatura Eletrônica
28/02/2021 19:13:06.0
DANIEL GREGÓRIO ALFARO VIGO
Avaliador Externo (UNIVERSIDADE FEDERAL DO RIO DE JANEIRO)

Assinatura Eletrônica
01/03/2021 15:05:02.0
ANDRE NACHBIN
Avaliador Externo (ASSOCIAÇÃO INSTITUTO NACIONAL DE MATEMÁTICA PURA E APLICADA)

Assinatura Eletrônica
26/02/2021 21:18:37.0
GIOVANI LOPES VASCONCELOS
Avaliador Externo (UNIVERSIDADE FEDERAL DO PARANÁ)

Assinatura Eletrônica
26/02/2021 22:18:20.0
NELSON LUÍS DA COSTA DIAS
Avaliador Externo (UNIVERSIDADE FEDERAL DO PARANÁ)

Assinatura Eletrônica
27/02/2021 10:59:49.0
TOBIAS BERNWARD BLENINGER
Avaliador Externo (UNIVERSIDADE FEDERAL DO PARANÁ)

Agradecimentos

Aos meus pais, Carlos e Eliane, pelo incentivo, apoio e educação que sempre me deram.

A minha orientadora, Ailin Ruiz de Zarate Fabregas, por aceitar o convite para me orientar e por me ajudar no desenvolvimento desse trabalho.

À Capes, pelo auxílio financeiro recebido através da bolsa de estudos.

RESUMO

Neste trabalho nos concentramos em aproximações de soluções de ondas viajantes para um modelo não linear bidirecional reduzido do tipo Boussinesq envolvendo um operador não-local. Três abordagens para calcular ondas viajantes são propostas e comparadas. Para isso, um esquema eficiente e estável para o sistema não linear, baseado em uma análise de estabilidade de von Neumann para o problema linearizado, é utilizado para capturar a evolução de soluções aproximadas de ondas viajantes. Além disso, uma equação unidirecional é deduzida a partir do modelo bidirecional e é provada a existência de ondas viajantes periódicas para esta equação. Por fim, um esquema para a versão de fundo rugoso do sistema não linear é apresentado e validado. Os resultados obtidos por este esquema são comparados com os obtidos para fundo plano.

Palavras-chave: Método espectral. Modelos dispersivos. Análise de estabilidade. Ondas viajantes.

ABSTRACT

In this work we focus on approximations of travelling wave solutions for a reduced bidirectional nonlinear model of Boussinesq type involving a nonlocal operator. Three approaches to calculate travelling waves are proposed and compared. For this an efficient and stable scheme for the nonlinear system, based on a von Neumann stability analysis for the linearized problem, is used to capture the evolution of approximate travelling wave solutions. Also, an unidirectional equation is deduced from the bidirectional model and we proved that this equation admits a periodic travelling wave solution. Lastly, a scheme for the corrugated bottom version of the nonlinear system is proposed and validated. The results obtained by this scheme are compared with the ones from the flat bottom.

Key words: Spectral method. Dispersive models. Stability analysis. Travelling waves

List of Figures

Contents

Chapter 1

Introduction

Internal ocean waves are gravity waves that appear in stratified fluids. Stratification is a consequence of variations in density due mainly to differences in temperature and salinity. Internal ocean waves are relevant for marine and submarine human activity. For example, the dead water phenomenon experienced by vessels when they travel through a relative thin layer of fresh water that does not mix with a denser layer below affects nautical operations, as originally reported by Nansen in [21]. Internal waves are essential in ocean dynamics because of the amount of mass and energy transported by them, ultimately producing wave breaking and mixing and the distribution of nutrients among other kind of matter. Internal waves can also occur in the atmosphere, lakes and reservoirs. For a broad discussion about internal waves, not limited to their presence in oceans, see [28].

Abrupt variations in density justify the use of a layered model, the simplest of which is considered here and consists of a two-layer fluid configuration limited by a rigid lid at the top and a flat bottom. Each layer contains an inviscid, incompressible, irrotational fluid of constant density. The two fluids are immiscible and of different densities, the denser one is located below. An internal wave propagates at the interface between layers and the whole system evolves according to the Euler equations together with appropriate boundary conditions as detailed in [9, 25]. This simplified model retains the main features that enable the study of travelling wave solutions which reproduce the behaviour of well-identified disturbances that move with effectively constant speed for long periods of time as described in [13, 2].

The system considered in the present work was obtained by Ruiz de Zarate in [25] using asymptotic analysis of the Euler equations and it is a generalization of the system presented by Choi and Camassa in [9]. The asymptotic analysis consists of reducing a general model into one that is simpler and easier to deal with, both from a theoretical and computational point of view, but which maintains the behavior and properties of the phenomenon to be studied. We remark that the models obtained by this process are approximations of the original model that can be improved depending on the order of expansion and how it is done.

The model proposed by Choi and Camassa uses an expansion of order 1 with the dispersive parameter β, which is the squared ratio between the fluid layer thickness and the typical wavelength. Ruiz de Zarate considered an expansion of order $3/2$ and obtained a model that reproduces better the dispersive effects of the problem than the previous one. Along with dispersion, another important mechanism present in this system is nonlinearity. Considering the weakly nonlinear regime, the effects of nonlinearity are quantified by the nonlinearity parameter α, which is the ratio between the wave amplitude and the fluid layer thickness and accompanies the nonlinear terms of the system. Let's assume here that α and β are positive, small and have the same order of magnitude.

There are published results about the weakly nonlinear system considered here and its linearized version. The existence of a solution for both systems as a Cauchy problem in Sobolev

spaces has already been proven by Brodzinski in [7]. Considering the characteristics of the linearized system, very efficient numerical methods to calculate approximate solutions of both systems were presented by the author in [16] using as basis the method proposed by Alfaro Vigo and collaborators in [1] for the linearized version of the system of Choi and Camassa. However, there are important topics about the problem to be studied.

The existence of travelling waves is of utmost importance in wave models. In this work three efficient methods to calculate approximate travelling waves for the weakly nonlinear system are proposed, tested and compared. These are improvements of a first attempt at the method presented by the author in [16] but whose results were not satisfactory. Furthermore, the existence of periodic travelling waves is proven for a unidirectional equation that is obtained from the weakly nonlinear system.

The model presented by Ruiz de Zarate in [25] also consider a more general case where there is an irregular topography on the bottom that can be described by an arbitrary curve. The inclusion of the irregular topography bottom in the model makes it considerably more difficult to deal with, both analytically and numerically. Fortunately, it is possible to adapt the numerical method for the flat-bottom systems to the non-flat bottom systems since a single coefficient contains the topography information and the domain is uniform and one-dimensional.

This work is organized as follows. In Chapter 2 a bibliographic review about the models considered in this work and related wave models is presented. In Chapter 3 the main results to be used in this work are presented. In Chapter 4 discretizations for both linear and nonlinear systems are described including three possibilities for spatial derivatives and the von Neumann analysis for each method is performed in Section 4.1. We remark that these results were obtained by the author in [16]. In addition we present here a comparison between stability conditions of different numerical methods for systems (2.6) and (2.7). In Section 4.2 the stability conditions obtained in the previous chapter are exemplified in numerical tests and extended for the nonlinear case. Also, a convergence analysis for both methods is made in Section 4.3. The study and the deduction of the unidirectional equation from the weakly nonlinear system is presented in Chapter 5 where the existence of periodic travelling waves for the model is proven in Section 5.1. In Chapter 6 numerical methods to obtain approximated travelling wave solutions for the weakly nonlinear system are presented and the results are validated. In Chapter 7 the numerical methods for the non-flat models are proposed. Also, the influence of the bottom in the solutions obtained and in the stability conditions are illustrated in experiments.

Chapter 2

State of the art for asymptotic reduced models

Asymptotic analysis of the Euler equations is a successful method for the study of internal ocean waves. Several internal wave models described in the literature are derived by this process, for example, the Intermediate Long Wave (ILW) equation in the intermediate depth regime and the Benjamin-Ono (BO) equation in the deep water regime [15, 4].

For the case of intermediate depth for the lower layer and shallow upper layer, a strongly nonlinear model for internal waves was obtained by Choi and Camassa in [9]. The model describes the evolution of the interface $\eta(x,t)$ between the fluids and the upper layer averaged horizontal velocity $u(x,t)$, where x and t represent the spatial and temporal variables, respectively. The coordinate system is set at the undisturbed interface between layers and subscripts x and t stand for partial derivatives. The thickness $h_1 > 0$ of the upper layer is much smaller than the characteristic wavelength $L > 0$ at the interface. The thickness $h_2 > 0$ of the lower layer is comparable with L. The densities of the upper and lower fluids are denoted by ρ_1 and ρ_2, respectively. For a stable stratification, let $\rho_2 > \rho_1 > 0$. Figure 2.1 illustrates this configuration. Considering g as the gravitational acceleration, the dimensional form of the system proposed in [9], written in the variables and notation adopted here is

$$\begin{cases} \eta_t = \left[(h_1 - \eta)u\right]_x, \\ u_t + uu_x + g\left(1 - \dfrac{\rho_2}{\rho_1}\right)\eta_x = \dfrac{\rho_2}{\rho_1}\mathcal{T}_{h_2}\left[(h_1 - \eta)u\right]_{xt}. \end{cases} \tag{2.1}$$

The nonlocal operator $\mathcal{T}_{h_2}$ is known as Hilbert transform on the strip and acts on boundary data of Neumann problems involving the Laplace equation for the velocity potential of the bottom layer by mapping normal derivatives onto tangential derivatives along the boundary. For numerical purposes we focus on the case where solutions are periodic functions in space with period $2l$. In this case the nonlocal operator $\mathcal{T}_{h_2}$ is defined by the symbol

$$\widehat{\mathcal{T}_{h_2}[f]}(k) = \boldsymbol{i}\coth(h_2\pi k/l)\widehat{f}(k), \quad k \in \mathbb{Z}^*,$$

where $\boldsymbol{i}$ denotes the imaginary unit. For more details about the operator $\mathcal{T}_{h_2}$ see [25] or [1].

In the same configuration, Ruiz de Zarate proposed in [25] a generalization of the model

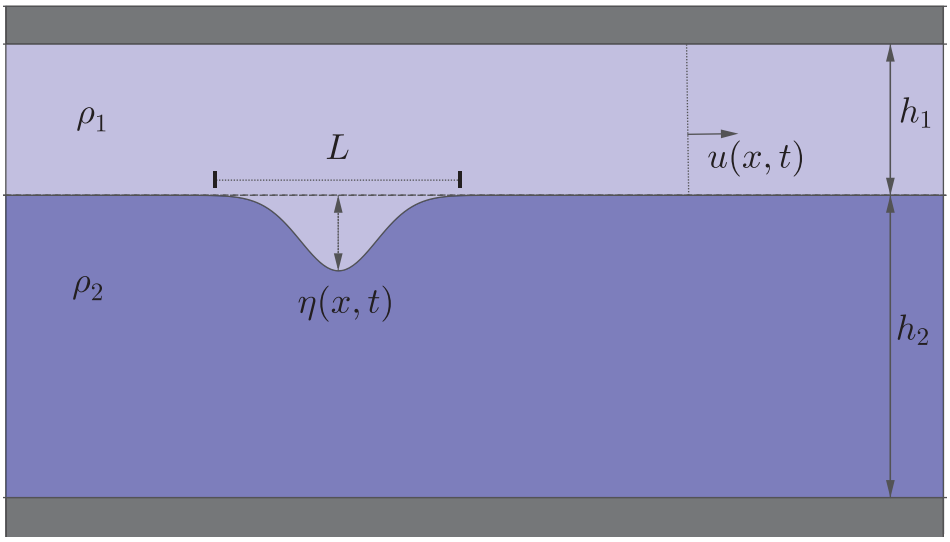

Figure 2.1: Two fluids configuration.

presented by Choi and Camassa. In the dimensional variables this system reads,

$$\begin{cases} \eta_t = \left[(h_1-\eta)u\right]_x, \\ u_t + uu_x + g\left(1-\frac{\rho_2}{\rho_1}\right)\eta_x = \frac{\rho_2}{\rho_1}\mathcal{T}_{h_2}\left[(h_1-\eta)u\right]_{xt} + \\ +\frac{1}{3(h_1-\eta)}\left((h_1-\eta)^3\left(u_{xt}+uu_{xx}-u_xu_x\right)\right)_x + \frac{\rho_2}{\rho_1}\mathcal{T}_{h_2}\left[\eta\mathcal{T}_{h_2}\left[(h_1-\eta)u\right]_x\right]_{xt} + \\ +\frac{\rho_2}{\rho_1}\left(\eta\big((h_1-\eta)u\big)_{xt} + \frac{1}{2L}\big((h_1-\eta)u\big)_x^2\right)_x + \frac{1}{2}\frac{\rho_2}{\rho_1}\left(\mathcal{T}_{h_2}\left[\big((h_1-\eta)u\big)_x\right]^2\right)_x. \end{cases} \tag{2.2}$$

Note that dimensional forms of both systems are consistent in the sense that the common terms agree. This system was derived considering nondimensional variables using a higher order asymptotic expansion with the nondimensional dispersion parameter $\beta = (h_1/L)^2$ which is small. In nondimensional variables system (2.2) reads:

$$\begin{cases} \eta_t = \left[(1-\eta)u\right]_x, \\ u_t + u\,u_x + \left(1-\frac{\rho_2}{\rho_1}\right)\eta_x = \sqrt{\beta}\,\frac{\rho_2}{\rho_1}\mathcal{T}_\delta\left[(1-\eta)u\right]_{xt} + \\ +\frac{\beta}{3(1-\eta)}\left((1-\eta)^3\left(u_{xt}+u\,u_{xx}-u_x\,u_x\right)\right)_x + \beta\,\frac{\rho_2}{\rho_1}\mathcal{T}_\delta\left[\eta\,\mathcal{T}_\delta\left[(1-\eta)u\right]_x\right]_{xt} + \\ +\beta\,\frac{\rho_2}{\rho_1}\left(\eta\big((1-\eta)u\big)_{xt} + \frac{1}{2}\big((1-\eta)u\big)_x^2\right)_x + \frac{\beta}{2}\,\frac{\rho_2}{\rho_1}\left(\mathcal{T}_\delta\left[\big((1-\eta)u\big)_x\right]^2\right)_x, \end{cases} \tag{2.3}$$

where $\delta = h_2/L$.

The second equation in system (2.3) is an approximation of order $\beta^{3/2}$ while the first equation is exact, this means that it is a direct consequence of the Euler equations and no approximation from the asymptotic expansion was made [25, 26]. Thus, system (2.3) is a generalization of the model derived in [9] using a higher order asymptotic expansion that includes terms of order β which are not present in the model considered in [9].

Moreover, we can compare the dispersion relations obtained from the linearized versions of

these models. According to [26], the dispersion relation of system (2.2) is

$$\omega_h^2 = \frac{g(\rho_2-\rho_1)k^2}{\frac{\rho_1}{h_1}+\frac{1}{3}h_1\rho_1k^2+\rho_2k\coth(kh_2)},$$

while the dispersion relation of system (2.1) is given by

$$\omega_l^2 = \frac{g(\rho_2-\rho_1)k^2}{\frac{\rho_1}{h_1}+\rho_2k\coth(kh_2)},$$

also, the full dispersion relation that comes from the linearized Euler equations, in dimensional form, is given by

$$\omega_f^2 = \frac{g(\rho_2-\rho_1)k^2}{\rho_1k\coth(kh_1)+\rho_2k\coth(kh_2)}.$$

Noting that

$$\frac{\rho_1}{h_1}\rho_1k\coth(kh_1) = \frac{\rho_1}{h_1}\left(1+\frac{(h_1\rho_1)^2}{3}+\mathcal{O}\left((h_1\rho_1)^4\right)\right),$$

we can see that ω_h is a better approximation to ω_f than ω_l. That is, system (2.2) approximates better the dispersive effect of the problem than system (2.1).

Considering a weakly nonlinear wave propagation regime, the nonlinearity parameter α, which is the ratio between the typical absolute wave amplitude value and the thickness h_1, is introduced in system (2.3) by scaling $\eta = \alpha\eta^*$, $u = \alpha u^*$ where it is imposed that $\alpha = \mathcal{O}(\beta)$. Thus, omitting the asterisks we obtain the system

$$\begin{cases} \eta_t = \left[(1-\alpha\eta)u\right]_x, \\ u_t + \alpha uu_x + \left(1-\dfrac{\rho_2}{\rho_1}\right)\eta_x = \sqrt{\beta}\,\dfrac{\rho_2}{\rho_1}\mathcal{T}_\delta\left[(1-\alpha\eta)u\right]_{xt} + \\ \quad + \dfrac{\beta}{3(1-\alpha\eta)}\left((1-\alpha\eta)^3\left(u_{xt}+\alpha uu_{xx}-\alpha u_xu_x\right)\right)_x + \\ \quad + \beta\alpha\dfrac{\rho_2}{\rho_1}\left(\eta\big((1-\alpha\eta)u\big)_{xt}+\dfrac{1}{2}\big((1-\alpha\eta)u\big)_x^2\right)_x + \\ \quad + \beta\alpha\dfrac{\rho_2}{\rho_1}\mathcal{T}_\delta\left[\eta\,\mathcal{T}_\delta\big[(1-\alpha\eta)u\big]_x\right]_{xt} + \dfrac{\beta\alpha}{2}\,\dfrac{\rho_2}{\rho_1}\left(\mathcal{T}_\delta\left[\big((1-\alpha\eta)u\big)_x\right]^2\right)_x. \end{cases} \tag{2.4}$$

As a result, gathering the terms with order $\mathcal{O}(\alpha\sqrt{\beta})$, $\mathcal{O}(\alpha\beta)$ and $\mathcal{O}(\beta^{3/2})$ in system (2.4), the following weakly nonlinear system with normalized shallow water velocity is obtained

$$\begin{cases} \eta_t - \big[(1-\alpha\eta)u\big]_x = 0, \\ u_t + \alpha u\,u_x - \eta_x = \sqrt{\beta}\,\dfrac{\rho_2}{\rho_1}\mathcal{T}_\delta\left[u\right]_{xt} + \dfrac{\beta}{3}u_{xxt} + \mathcal{O}\left(\alpha\sqrt{\beta},\alpha\beta,\beta^{3/2}\right). \end{cases} \tag{2.5}$$

Due to the rescaling the amplitude of η and u can be as far as $1/\alpha$. Besides, its linearized version around the zero equilibrium is

$$\begin{cases} \eta_t = u_x, \\ u_t - \dfrac{\rho_2}{\rho_1}\sqrt{\beta}\,\mathcal{T}_\delta[u]_{xt} - \dfrac{\beta}{3}u_{xxt} = \eta_x. \end{cases} \tag{2.6}$$

A study about the existence and uniqueness of solution for both systems in periodic Sobolev

spaces was presented by Brodzinski in [7].

In order to implement the method of lines for the system (2.6), the author considered in [16] a fourth order finite difference scheme for spatial derivatives while a spectral approach for the dispersive terms was considered in the semi-discretization and the classical fourth order Runge-Kutta (RK4) scheme is used for time advancing. This combination proved to be the best since along the imaginary axis (where the eigenvalues of the spatial discretization operators lie) the RK4 method has the largest stability interval if compared with the fifth order, four steps Adams-Moulton scheme and the fourth order, three steps Adams-Moulton scheme; see, for instance, [3].

Also, compared with other schemes for spatial derivatives in semi-discretization, namely spectral differentiation and piecewise B-splines, the fourth order finite difference scheme presents less restrictive stability conditions and a lower computational cost. The stability conditions were validated in numerical tests and extended to the scheme for the nonlinear system (2.5) which includes the discretization of the nonlinear terms $\alpha(\eta u)_x$ and $\alpha u u_x$ as presented in [16].

The numerical method presented above for the linear system (2.6) is based in the one proposed by Alfaro Vigo and collaborators in [1] for the system

$$\begin{cases} \eta_t = u_x, \\ u_t - \dfrac{\rho_2}{\rho_1}\sqrt{\beta}\,\mathcal{T}_\delta[u]_{xt} = \eta_x, \end{cases} \tag{2.7}$$

which is the linearization around the zero equilibrium of the nondimensional form of system (2.1) and differs from system (2.6) in the term involving u_{xxt}. The results of the von Neumann analysis for both systems are analogous; however, the stability conditions obtained in [16] are less restrictive than those presented in [1]. The improvement of the stability conditions is due to the term involving u_{xxt} which is also responsible for the better approximation of the Euler dispersion relation. Thus, the higher order linearized system has better physical and numerical properties.

The model presented by Ruiz de Zarate in [25] also consider a more general case of the intermediate wave system (2.5), where there is an irregular topography on the bottom that can be described by an arbitrary curve. The non-flat version of system (2.5) is given by the system

$$\begin{cases} \eta_t = \dfrac{1}{M(\xi)}\big[(1-\alpha\eta)u\big]_\xi, \\ \\ u_t + \dfrac{\alpha}{M(\xi)}u\,u_\xi - \dfrac{1}{M(\xi)}\eta_\xi = \dfrac{\rho_2}{\rho_1}\dfrac{\sqrt{\beta}}{M(\xi)}\mathcal{T}\big[u\big]_{\xi t} + \dfrac{\beta}{3M(\xi)}\left(\dfrac{u_{\xi t}}{M(\xi)}\right)_\xi, \end{cases} \tag{2.8}$$

where ξ is the horizontal curvilinear coordinate that accompanies the terrain that appears when performing a conformal transformation from the bottom layer to a flat strip $(x,z) \to (\xi,\zeta)$. The variable coefficient $M(\xi)$ contains the irregular topography information and consists of the non-null element of the Jacobian matrix of the conformal mapping evaluated in the interface: $M(\xi) = z_\zeta(\xi,0)$. In the case of a flat bottom $M(\xi) = 1$ and we return to system (2.5). Details can be found in [25].

The inclusion of the irregular topography bottom in the model makes it considerably more difficult to deal with, both analytically and numerically. However, we take advantage that a single coefficient contains the topography information and the domain is uniform and one-dimensional to propose in this work a numerical method for system (2.8) based on the one for the nonlinear system (2.5). The effects of the topography in the solutions and in the stability conditions are illustrated and compared with the solutions for the flat bottom cases.

An important research topic in the study of water waves is the existence of travelling waves.

These solutions do not change their shapes and propagate at constant speed by maintaining a balance between the nonlinear and the dispersive effects of the model. It is also important to know if the travelling wave solutions are stable to small perturbations, otherwise any physical or numerical disturbance will eventually destroy them [11].

Different techniques can be employed to prove the existence of travelling waves depending on the model and if the solution is periodic or non-periodic. For example, the exact expression of non-periodic travelling wave solutions of KdV and ILW equations can be found explicity, see [15] and Appendix A. Also, periodic travelling waves for these models are obtained in [22] by making a periodization of the non-periodic travelling waves. In other cases an exact expression is not available and different approaches can be adopted.

In [24], Pipicano and Grajales proved the existence of periodic travelling solutions for an internal wave model similar to system (2.5) using a fixed point method. The system in [24] consider an infinite depth for the lower fluid and can be written as

$$\begin{cases} \eta_t - \big[(1-\alpha\eta)u\big]_x = \dfrac{\epsilon^2}{6}\eta_{xxt}, \\ u_t + \alpha u\, u_x + \left(1 - \dfrac{\rho_2}{\rho_1}\right)\eta_x = \epsilon\dfrac{\rho_2}{\rho_1}\mathcal{H}\,[u]_{xt} + \dfrac{\epsilon^2}{6}u_{xxt}, \end{cases}$$

where the nonlocal operator $\mathcal{H}$ is the Hilbert transform with symbol $\widehat{\mathcal{H}[f]}(k) = \boldsymbol{i}\,\mathrm{sign}(k)\hat{f}(k)$. The existence of the term with η_{xxt} in the first equation is crucial for the technique employed in [24] to be successful. Therefore, this technique could not be used for system (2.5) and the theoretical proof of the existence of travelling waves for this model is still an open problem. Since we have no theoretical results about existence of these kind of solutions for system (2.5), in the present work we continue to investigate the existence of travelling waves from a numerical point of view.

A first numerical approach to generate approximated travelling waves was proposed by the author in [16]. Although the obtained profiles do not change very much in a given time interval, the results are far from good. Three new methods to obtain travelling waves for the nonlinear system (2.5) are proposed and compared improving the approach presented in [16].

Furthermore, in order to better understand the behaviour of system (2.5), we reduce it to an unidirectional equation for η in an analogous way to what was done to get the KdV equation from the Boussinesq system in [29]. The resulting is a regularized finite depth version of the Benjamin equation which is given by

$$\eta_t + \eta_x - \frac{3\alpha}{2}\eta\eta_x - \frac{\sqrt{\beta}}{2}\frac{\rho_2}{\rho_1}\mathcal{T}_\delta[\eta_{xt}] - \frac{\beta}{6}\eta_{xxt} = 0. \tag{2.9}$$

The Benjamin equation was derived by Benjamin in [5] and has the form

$$\eta_t + \eta_x + 2\eta\eta_x - a\mathcal{H}[\eta_{xx}] - b\eta_{xxx} = 0.$$

Equation (2.9) is the regularized finite depth version of the Benjamin equation in the sense that one of the x-derivatives in the dispersive terms is replaced by a t-derivative and the nonlocal operator $\mathcal{H}$ is the limit of $\mathcal{T}_\delta$ when $\delta \to +\infty$, that is, when the depth grows to infinity. The existence of periodic travelling waves for the Benjamin equation was proven by Benjamin in [6] using a fixed point technique similar to that one used in [24].

Chapter 3

Theoretical Background

In this chapter we will present some definitions and results relevant to the development of the work. The proofs can be found in the cited references.

3.1 Fourier transforms and Sobolev spaces

In the following we will present some definitions and results about Fourier transforms and Sobolev spaces following Iorio in [14] and [1, 27].

Definition 1. *Let $l > 0$ be a constant. A function $f : \mathbb{R} \to \mathbb{C}$ is called l-periodic if $f(x + l) = f(x),\ \forall x \in \mathbb{R}$.*

In many cases it is convenient to write a periodic function as a sum of complex exponentials, that is, to write it as a Fourier series in the form

$$f(x) = \sum_{k=-\infty}^{\infty} c_k \exp(\boldsymbol{i}k\pi x/l), \tag{3.1}$$

where the coefficients c_k are given by

$$c_k = \frac{1}{2l}\int_{-l}^{l} f(x)\exp(-\boldsymbol{i}k\pi x/l)dx. \tag{3.2}$$

It is common to use the notation $c_k = \hat{f}(k)$ for the Fourier Series coefficients. Among the many properties of the Fourier Series, we present here only those that we will use in this work:

$$(\widehat{af})(k) = a\hat{f}(k),\ a \in \mathbb{R},$$

$$(\widehat{f+g})(k) = \hat{f}(k) + \hat{g}(k),$$

$$(\widehat{f'})(k) = (\boldsymbol{i}k\pi/l)\hat{f}(k).$$

Definition 2. *We define $L^2_{per}([-l, l]) = L^2_{per}$ as the space of all $2l$-periodic measurable functions $f : \mathbb{R} \to \mathbb{R}$ such that*

$$\|f\| = \left(\int_{-l}^{l} |f(x)|^2 dx\right)^{1/2} < \infty.$$

Definition 3. *We define $l_2(\mathbb{Z})$ as the space of all complex valued sequences $\upsilon = \{\upsilon_k\}_{k\in\mathbb{Z}}$ which satisfy*

$$\|\upsilon\|_2 = \left(\sum_{k\in\mathbb{Z}} |\upsilon_k|^2\right)^{1/2} < \infty.$$

In view of the linearity properties of the Fourier coefficients, it is possible to define a linear operator between the spaces L^2_{per} and $l_2(\mathbb{Z})$.

Definition 4. *The Periodic Fourier Transform is the linear operator*

$$\begin{array}{rccc} \hat{} : L^2_{per} & \to & l_2(\mathbb{Z}) \\ f & \mapsto & \{\hat{f}(k)\}_{k\in\mathbb{Z}} \end{array}$$

such that

$$\hat{f}(k) = \frac{1}{2l}\int_{-l}^{l} f(x)\exp(-\boldsymbol{i}k\pi x/l)dx.$$

In fact, the Periodic Fourier Transform is a linear bijection between L^2_{per} and $l_2(\mathbb{Z})$, thus we can define its inverse as below

Definition 5. *The Inverse Periodic Fourier Transform is a linear operator*

$$\begin{array}{rcl} \check{} : l_2(\mathbb{Z}) & \to & L^2_{per} \\ \{\alpha_k\}_{k\in\mathbb{Z}} & \mapsto & f \end{array}$$

such that

$$f(x) = \sum_{k=-\infty}^{\infty} \alpha_k \exp(\boldsymbol{i}k\pi x/l).$$

It is not difficult to verify that $(\hat{f})^{\check{}} = f$ and α_k corresponds to $\hat{f}(k)$.
Now we can define the periodic Sobolev spaces.

Definition 6. *The Sobolev space $H^s_{per}([-l,l]) = H^s_{per}$, $s \geqslant 0$ is the space of all $f \in L^2_{per}$ such that*

$$||f||_s = \left(\sum_{k\in\mathbb{Z}} \left(1+|k|^2\right)^s |\widehat{f}(k)|^2\right)^{1/2} < +\infty.$$

Firstly, note that $L^2_{per} = H^0_{per}$. In addition, Sobolev spaces have very useful properties, some of them, which will be used in this work, are listed below.

Theorem 3.1. *Let $s, r \in \mathbb{R}, s \geqslant r$. Then $H^s_{per} \hookrightarrow H^r_{per}$, that is, H^s_{per} is continuously and densely embedded in H^r_{per}, since the following inequality is valid:*

$$||f||_r \leqslant ||f||_s,\ \forall f \in H^s_{per}.$$

Theorem 3.2. *Let $f, g \in H^s_{per}$ be two functions and $s > \frac{1}{2}$. Then, $fg \in H^s_{per}$ and there exists a constant $C > 0$ depending only on s such that*

$$\|fg\|_s \leqslant C\|f\|_s\|g\|_s.$$

Theorem 3.3. *Let $s > 0$. If $f \in H^s_{per}$ then*

$$\|\partial_x f\|_{s-1} \leqslant \|f\|_s.$$

Theorem 3.4. *Let $s \geqslant \frac{1}{2}$. Then H^s_{per} is continuously and densely embedded in the space of continuous functions.*

We reinforce that the proofs of the results presented above can be found in [14].

3.1.1 Discrete Fourier Transform

Let us present the discrete version of the periodic Fourier transform to be used in numerical methods. Basically, it consists in an approximation of the integral involved in the definition of the Fourier coefficients by the repeated trapezoidal rule. Taking into consideration the periodicity, instead of the interval $[-l, l]$, let us consider the interval $[0, 2l]$. Thus, setting a uniform grid on the interval $[0, 2l]$, that is, $x_j = j\Delta x,\ j = 1, \ldots, N$ where $N \in \mathbb{N}$ is even and $\Delta x = 2l/N$, we define the discrete Fourier Transform as bellow:

Definition 7. *Let $f : \mathbb{R} \to \mathbb{C}$, be a $2l$-periodic function and $f_j = f(x_j),\ j = 1, 2, \ldots, N$. The discrete Fourier transform is given by*

$$\hat{f}_k = \hat{f}(k) = \frac{1}{N}\sum_{j=1}^{N} f_j \exp(-\boldsymbol{i}k\pi x_j/l),\ k = -\frac{N}{2} + 1, \ldots, \frac{N}{2}.$$

Also, its inverse transform is given by

$$f_j = \frac{1}{2l}\sum_{k=-N/2+1}^{N/2} \hat{f}_k w_N^{jk},\ j = 1, 2, \ldots, N,$$

where

$$w_N = \exp(\boldsymbol{i}2\pi/N).$$

We can write the discrete Fourier Transform in a matrix version through the Fourier matrix F given by

$$F_{m,j} = \exp(-2\pi\boldsymbol{i}(m - N/2)j/N), 1 < m, j < N.$$

Denoting $\boldsymbol{f} = [f_1, \ldots, f_N]^T$ and $\hat{\boldsymbol{f}} = [\hat{f}_{-N/2+1}, \ldots, \hat{f}_{N/2}]^T$ we have

$$\hat{\boldsymbol{f}} = \Delta x F \boldsymbol{f} \text{ e } \boldsymbol{f} = \frac{1}{2l}\overline{F}^T \hat{\boldsymbol{f}}.$$

We can use the discrete Fourier Transform and its inverse to, for example, compute approximate derivatives. To approximate the first derivative of a periodic function f we define a diagonal matrix $D = \text{diag}(\boldsymbol{i}k\pi/l)$, $k = -N/2 + 1, \ldots, N/2$ and compute $\boldsymbol{g} = \frac{1}{N}\overline{F}^T DF\boldsymbol{f}$. Thus we have that $\boldsymbol{g}$ approximates f' in the uniform grid defined previously.

An interesting property to note is that the Fourier matrix diagonalizes circulating Toeplitz matrices.

Definition 8. *Let $c_1, c_2, \ldots, c_N$, be given real values, a circulating Toeplitz matrix C is defined as*

$$C_{i,j} = \begin{cases} c_{1+j-i}, & i \leqslant j, \\ c_{N+1+j-i}, & i > j. \end{cases} \tag{3.3}$$

If C is a circulating Toeplitz matrix, then there exists a diagonal matrix D such that $C = \frac{1}{N}\overline{F}^T DF$. This fact is proven in [27]. The following theorem gives a simple formula for calculating the eigenvalues of a circulating Toeplitz matrix.

Theorem 3.5. *The eigenvalues of a circulating Toeplitz matrix C defined by values $c_1, c_2, \ldots, c_N$ are given by*

$$\lambda_k(C) = \sum_{m=1}^{N} c_m \exp(\boldsymbol{i}(m-1)\theta_k), \text{ where } \theta_k = \frac{2\pi k}{N}.$$

3.2 Flat bottom models' properties

As mentioned earlier, the existence of solution for the flat bottom models (2.6) and (2.5) in Sobolev spaces is proven by Brodzinski in [7]. The main results are the following:

Theorem 3.6. *Let $\eta^0 \in H^s_{per}$ and $u^0 \in H^{s+1}_{per}$ be real functions and $s > 0$. Then the initial value problem for the flat bottom linear system (2.6) admits a unique global solution $(\eta(t), u(t)) \in H^s_{per} \times H^{s+1}_{per}$ such that $\eta^0 = \eta(0)$ and $u^0 = u(0)$.*

Theorem 3.7. *Let $\eta^0 \in H^{s+1}_{per}$ and $u^0 \in H^{s+1}_{per}$ be real functions and $s > \frac{3}{2}$. Then here exists $T > 0$ such that the initial value problem for the flat bottom nonlinear system (2.5) admits a unique local solution $(\eta(t), u(t)) \in H^s_{per} \times H^{s+1}_{per}$ for $t \in [0, T]$, such that $\eta^0 = \eta(0)$ and $u^0 = u(0)$.*

In addition, we can obtain the conservation of mass law for system (2.5) as follows: integrating the first equation of (2.5) on x we obtain

$$0 = \int_{-l}^{l} \eta_t - \big[(1-\alpha\eta)u\big]_x dx = \frac{d}{dt}\int_{-l}^{l} \eta dx,$$

since u is periodic on the x-variable. Therefore, there exists an arbitrary constant d such that

$$\int_{-l}^{l} \eta(x,t)dx = d, \tag{3.4}$$

which is valid for any value of t in a time interval where the solution is defined. As η comes from a perturbation of the interface at rest and the coordinate system is set at the undisturbed interface we set $d = 0$. Note that the conservation law (3.4) is also valid for system (2.6).

As found in [25, 7] the phase velocity $\omega/k = v(k)$ of system (2.6) is given by

$$v(k) = \left(1 + \frac{\rho_2}{\rho_1}\frac{\sqrt{\beta}}{\delta}\phi(k\delta) + k^2\frac{\beta}{3}\right)^{-1/2},$$

where ϕ is the symbol in the frequency domain for the composition of one spatial derivative with the operator $\mathcal{T}_\delta$, that is

$$\phi(k) = \begin{cases} 1, & k = 0, \\ k\coth k, & k \neq 0. \end{cases} \tag{3.5}$$

Thus, the system in the frequency domain can be written as

$$\begin{bmatrix} \widehat{\eta}_t(k) \\ \widehat{u}_t(k) \end{bmatrix} = A(k) \begin{bmatrix} \widehat{\eta}(k) \\ \widehat{u}(k) \end{bmatrix}, \quad k \in \mathbb{Z},$$

where

$$A(k) = \begin{bmatrix} 0 & \boldsymbol{i}k \\ \boldsymbol{i}kv^2(k) & 0 \end{bmatrix}.$$

The matrix $A(k)$ has pure imaginary eigenvalues $\lambda(k) = \pm\boldsymbol{i}kv(k)$. The numerical method presented by the author in [16] is defined to preserve this property of the spectrum.

3.3 Conformal mapping

Here we will summarize some results about complex functions and conformal mapping following Nachbin and Ruiz de Zarate in [20] and Brown and Churchill [8].

Definition 9. *Let $G \subset \mathbb{C}$ be an open set. Then a complex valued function $f : G \to \mathbb{C}$ is called analytic if it is continuously differentiable in G.*

Definition 10. *A path in a set $G \subset \mathbb{C}$ is a continuous function $\gamma : [a, b] \to G$ for some interval $[a, b] \subset \mathbb{R}$. If $\gamma'(t)$ exists for each $t \in [a, b]$ and $\gamma' : [a, b] \to \mathbb{C}$ is continuous then γ is a differentiable path.*

It is easy to verify that an analytic function preserves differentiable paths. In fact, if γ is a differentiable path in G and $f : G \to \mathbb{C}$ is analytic, then $\sigma = f \circ \gamma$ is also a differentiable path.

If $\gamma : [a, b] \to G$ is a differentiable path and for some $t_0 \in (a, b), \gamma'(t_0) \neq 0$, then γ has a tangent line at the point $z_0 = \gamma(t_0)$. This line goes through the point z_0 in the direction of the vector $\gamma'(t_0)$. Because of that we can define the angle between two differentiable paths.

Definition 11. *If γ_1 and γ_2 are two differentiable paths with $\gamma_1(t_1) = \gamma_2(t_2) = z_0$, $\gamma_1'(t_1) \neq 0$ and $\gamma_2'(t_2) \neq 0$ then define the angle between the paths* $\arg \gamma_2'(t_2) - \arg \gamma_1'(t_1)$.

Theorem 3.8. *If $f : G \to \mathbb{C}$ is analytic then f preserves angles at each point $z \in G$ where $f'(z) \neq 0$.*

Definition 12. *A conformal map is a function $f : G \to \mathbb{C}$ which has the angle preserving property and also exists the limit*

$$\lim_{z \to a} \frac{|f(z) - f(a)|}{|z - a|}.$$

If f is analytic and $f'(z) \neq 0$ for any z then f is a conformal mapping. The converse of this statement is also true as presented in [20]. In fact, some authors define a conformal mapping as an analytic function whose derivative never equals zero.

A classical example of conformal map is the Möbius transformation.

Example 1. *A mapping of the form*

$$S(z) = \frac{az + b}{cz + d},$$

is called a linear fractional transformation. If $ad - bc \neq 0$ then $S(z)$ is called a Möbius transformation.

Another important property of the conformal mapping is that it transforms the Laplacian of a certain function into another multiplied by a factor, that is, considering a conformal mapping f as a change of variables $f(z) = f(x, y) = (\xi, \zeta)$ a Laplacian in (x, y) becomes a Laplacian in (ξ, ζ) as follows:

$$\frac{\partial^2 \phi}{\partial x^2} + \frac{\partial^2 \phi}{\partial x^2} = |f'(z)|^2 \left(\frac{\partial^2 \psi}{\partial \xi^2} + \frac{\partial^2 \psi}{\partial \zeta^2} \right).$$

Therefore, the conformal mapping between the regular strip and the irregular strip of the lower layer of our configuration preserves the Laplace equation for the velocity potential in the new variables.

To ensure the existence of a conformal mapping between the regular and the irregular strips we use the Riemann mapping theorem and the Schwarz-Christoffel transformation.

Theorem 3.9 (Riemann mapping theorem)**.** *Let G be a non-empty simply connected open subset of $\mathbb{C}$, $G \neq \mathbb{C}$, then there exists a holomorphic bijective mapping f from G onto the open unit disk whose inverse is also analytic.*

Applying de Chain rule in the relation $f^{-1}(f(z)) = z$ we can see that $f'(z) \neq 0 \; \forall z \in G$, thus f is a conformal mapping.

Theorem 3.10 (Schwarz-Christoffel transformation)**.** *Let P be the interior of a polygon Γ having vertices $w_1, \ldots, w_n$ and interior angles $\alpha_1\pi, \ldots, \alpha_n\pi$ in counterclockwise order. Let f be any conformal mapping from the upper half-plane of $\mathbb{C}$ to P with $f(\infty) = w_n$. Then*

$$f(z) = A + C \int^z \prod_{k=1}^{n-1} (\zeta - z_k)^{\alpha_k - 1} \, d\zeta,$$

for some complex constants A and C, where $w_k = f(z_k)$ for $k = 1, \ldots, n-1$.

Therefore, using the results described here and mapping compositions, we can guarantee the existence of a conformal mapping that transforms an irregular strip into a flat one, as required.

Chapter 4

Numerical methods for flat bottom models

For the discretization of the linearized system (2.6), in order to find numerical approximate solutions, we proceed in a similar way as in [1]. Let us define the auxiliary function

$$\psi = u - \frac{\rho_2}{\rho_1}\sqrt{\beta}\,\mathcal{T}_\delta[u]_x - \frac{\beta}{3}u_{xx}, \tag{4.1}$$

and rewrite system (2.6) as

$$\begin{cases} \eta_t = u_x, \\ \psi_t = \eta_x. \end{cases}$$

Since u and η are $2l$-periodic with respect to the variable x, we define a uniform grid on the interval $[0, 2l]$, that is, $x_j = j\Delta x,\ j = 1, \ldots, N$ where $N \in \mathbb{N}$ is even and $\Delta x = 2l/N$, the last element x_N is also identified with $x = 0$. Define $\boldsymbol{u}(t) = [u_1, \ldots, u_N]^T$ and $\boldsymbol{\eta}(t) = [\eta_1, \ldots, \eta_N]^T$ where $u_j \approx u(x_j, t)$ and $\eta_j \approx \eta(x_j, t)$, $j = 1, \ldots, N$. The spatial discretization results in a system of Ordinary Differential Equations in the matrix form below

$$\begin{cases} \boldsymbol{\eta}_t = C\boldsymbol{u}, \\ P\boldsymbol{u}_t = C\boldsymbol{\eta}. \end{cases} \tag{4.2}$$

Matrix C comes from the discretization of the first order x-derivative and matrix P is obtained using the Discrete Fourier Transform (DFT) in order to get $\boldsymbol{\psi} = P\boldsymbol{u}$ with $\boldsymbol{\psi}(t) = [\psi_1, \ldots, \psi_N]^T$, where ψ_j approximates the expression (4.1) evaluated at (x_j, t).

The DFT of a vector $\boldsymbol{w} = [w_1, \cdots, w_N]^T \in \mathbb{R}^N$ is denoted by the vector $\widehat{\boldsymbol{w}} = [\widehat{w}_{-N/2+1}, \ldots, \widehat{w}_{N/2}]^T \in \mathbb{C}^N$, which is defined by the relation

$$\widehat{w}_k = \frac{1}{N}\sum_{j=1}^{N} w_j \exp(-\boldsymbol{i}k\pi x_j/l),\ k = -\frac{N}{2} + 1, \ldots, \frac{N}{2}. \tag{4.3}$$

Its inverse is given by

$$w_j = \frac{1}{2l}\sum_{k=-N/2+1}^{N/2} \widehat{w}_k \exp(\boldsymbol{i}2\pi/N)^{jk},\ j = 1, 2, \ldots, N. \tag{4.4}$$

Defining the Fourier matrix F componentwise by $F_{m,j} = \exp(-2\pi\boldsymbol{i}(m - N/2)j/N)$, $1 <$

$m, j < N$, the relations (4.3) and (4.4) can be written in the vector form

$$\begin{cases} \widehat{\boldsymbol{w}} = \Delta x F \boldsymbol{w}, \\ \boldsymbol{w} = \dfrac{1}{2l}\overline{F}^T \widehat{\boldsymbol{w}}. \end{cases}$$

Now, using that the composition of one spatial derivative with the operator $\mathcal{T}_\delta$ has the symbol defined by equation (3.5) and some properties of the Fourier series, we can calculate $\widehat{\psi}(k)$ as

$$\begin{aligned} \widehat{\psi}(k) &= \widehat{u}(k) - \frac{\rho_2}{\rho_1}\sqrt{\beta}\,(\widehat{\mathcal{T}_\delta[u]_x})(k) - \frac{\beta}{3}\widehat{u}_{xx}(k) \\ &= \widehat{u}(k) + \frac{\rho_2}{\rho_1}\frac{\sqrt{\beta}}{\delta}\phi(k\pi\delta/l)\widehat{u}(k) + (k\pi/l)^2\,\frac{\beta}{3}\widehat{u}(k) \\ &= v(k\pi/l)^{-2}\widehat{u}(k). \end{aligned}$$

Defining $\widehat{P} = \operatorname{diag}\left(\lambda_{-N/2+1}(\widehat{P}), \ldots, \lambda_{N/2}(\widehat{P})\right)$ as the diagonal matrix whose entries are given by

$$\lambda_k(\widehat{P}) = v(k\pi/l)^{-2},\ k = -N/2+1, \ldots, N/2,$$

and considering the approximation $\widehat{\psi}(k) = v(k\pi/l)^{-2}\widehat{u}(k)$, we get $\widehat{\boldsymbol{\psi}} = \widehat{P}\widehat{\boldsymbol{u}}$, thus

$$\boldsymbol{\psi} = \frac{1}{2l}\overline{F}^T\widehat{\boldsymbol{\psi}} = \frac{1}{2l}\overline{F}^T\widehat{P}\widehat{\boldsymbol{u}} = \frac{1}{2l}\overline{F}^T\widehat{P}\Delta x F\boldsymbol{u} = \frac{1}{N}\overline{F}^T\widehat{P}F\boldsymbol{u} = P\boldsymbol{u}. \tag{4.5}$$

We remark that the matrix $(1/\sqrt{N})F$ is orthogonal and diagonalizes the matrix P, that is

$$P = \frac{1}{\sqrt{N}}\overline{F}^T\widehat{P}\frac{1}{\sqrt{N}}F.$$

For the first order x-derivative, as in [1], we choose numerical schemes such that $u_x(x_j) \approx (Cu)_j$ where C is a real, skew-symmetric and Toeplitz circulant matrix. These assumptions are made in order to preserve the property of the spectrum described earlier and the periodicity of the spatial domain. Also, we can obtain a fair comparison between the methods for the linearized systems (2.6) and (2.7).

A Toeplitz circulant matrix C is defined by the elements $c_1, \ldots, c_N$ of its first row by

$$C_{i,j} = \begin{cases} c_{1+j-i}, & i \leqslant j, \\ c_{N+1+j-i}, & i > j. \end{cases}$$

It is shown in [1] that the skew-symmetric Toeplitz circulant matrix C is diagonalized by the matrix $(1/\sqrt{N})F$ and its eigenvalues are given by

$$\lambda_k(C) = \frac{\boldsymbol{i}}{\Delta x}\gamma(\theta_k),$$

where,

$$\gamma(\theta) = 2\Delta x \sum_{m=1}^{N/2-1} c_{1+m}\sin(m\theta) \text{ and } \theta_k = \frac{2\pi k}{N}.$$

Therefore, from the diagonal matrix $\widehat{C} = \operatorname{diag}\left(\lambda_{-N/2+1}(C), \ldots, \lambda_{N/2}(C)\right)$ we recover

$$C = \frac{1}{\sqrt{N}}\overline{F}^T\widehat{C}\frac{1}{\sqrt{N}}F.$$

Three possibilities for the matrix C are studied that correspond to each of the following discretizations for the first order spatial derivative: five-point fourth order finite difference, piecewise linear B-splines and the spectral scheme. As shown in [1], their respective functions γ are given by

$$\gamma^{FD}(\theta) = \frac{4}{3}\sin\theta - \frac{1}{6}\sin 2\theta,$$

$$\gamma^{BS}(\theta) = \frac{3}{2}\left(\frac{\sin(\theta)}{1+\cos(\theta)/2}\right),$$

$$\gamma^{SP}(\theta) = \begin{cases} \theta, & \theta \in (-\pi, \pi) \\ 0, & \theta = \pm\pi. \end{cases}$$

For the time integration let us rewrite system (4.2) as

$$\begin{bmatrix} \boldsymbol{\eta}_t \\ \boldsymbol{u}_t \end{bmatrix} = D \begin{bmatrix} \boldsymbol{\eta} \\ \boldsymbol{u} \end{bmatrix}, \qquad D = \begin{bmatrix} \mathbf{0} & C \\ P^{-1}C & \mathbf{0} \end{bmatrix}. \tag{4.6}$$

Denoting the eigenvalues of P and D by $\lambda_k(P)$ and $\lambda_k(D)$, respectively, it is not difficult to prove that $\lambda_k(D) = \pm\lambda_k(C)/\sqrt{\lambda_k(P)}$ since matrices C and P are diagonalized by the same matrix. Note the similarity between the eigenvalues of the matrices $A(k)$ and D in the sense that $1/\sqrt{\lambda_k(P)} = v(k\pi/l)$ and $\lambda_k(C)$ approximates $\boldsymbol{i}k\pi/l$. In fact, for the spectral scheme we have $\lambda_k^{SP}(C) = \boldsymbol{i}k\pi/l$ and for finite difference and B-splines figure 4.1 illustrates that γ^{FD} and γ^{BS} approximate well γ^{FD} around zero, thus, $\lambda_k^{FD}(C)$ and $\lambda_k^{BS}(C)$ are good approximations of $\boldsymbol{i}k\pi/l$ for small values of wavenumber k.

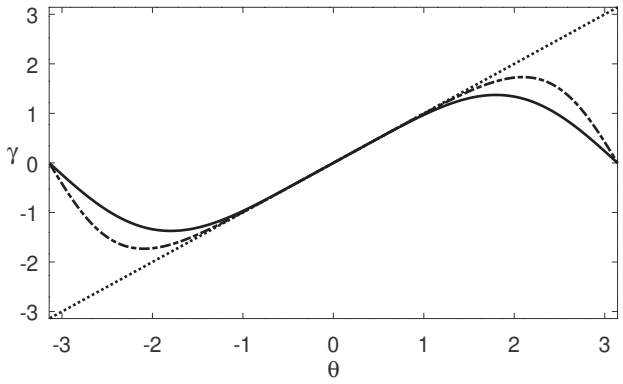

Figure 4.1: Graphics of γ^{SP} $(\cdots)$, γ^{BS} $(-\cdot-)$ and γ^{FD} (—).

Since $\lambda_k(D)$ is purely imaginary, the classic fourth order Runge-Kutta method is appropriate for this problem. Applying the RK4 method in system (4.6) we get

$$\begin{bmatrix} \boldsymbol{\eta}^{n+1} \\ \boldsymbol{u}^{n+1} \end{bmatrix} = \left(I + \Delta t D + \frac{\Delta t^2}{2}D^2 + \frac{\Delta t^3}{3!}D^3 + \frac{\Delta t^4}{4!}D^4\right) \begin{bmatrix} \boldsymbol{\eta}^{n} \\ \boldsymbol{u}^{n} \end{bmatrix}, \tag{4.7}$$

where $\boldsymbol{\eta}^n$ and $\boldsymbol{u}^n$ are the approximations for $\boldsymbol{\eta}(t_n)$ and $\boldsymbol{u}(t_n)$, respectively.

Once the discretization of the linear system is complete, let us obtain the discretization of the nonlinear system. For that, let us rewrite system (2.5) as

$$\begin{cases} \eta_t &= E_1(\eta, u), \\ \psi_t &= E_2(\eta, u), \end{cases}$$

where $E_1(\eta, u) = u_x - \alpha\eta u_x - \alpha u\eta_x$ and $E_2(\eta, u) = \eta_x - \alpha u u_x$.

Considering the spatial mesh defined before, the x-derivatives in E_1 and E_2 are approximated using one of the numerical schemes described previously, that is, five-point finite difference, piecewise linear B-splines and the spectral scheme. The variable $\boldsymbol{\psi}$ is calculated by equation (4.5) as in the linear case. The time integration is done with the fourth-order Runge-Kutta method. Note that in the problem that motivated this study α is of the same order of β, but setting $\alpha = 0$ we obtain scheme (4.7).

4.1 Von Neumann analysis

In order to prove that the numerical scheme (4.7) is stable, let us define the following norm

$$||\boldsymbol{w}||_{N,s}^2 = 2\pi \sum_{k=-N/2+1}^{N/2} \left(1 + (k\pi/l)^2\right)^s |\widehat{w}_k|^2,\ s \geqslant 0,$$

where $\boldsymbol{w} \in \mathbb{R}^N$ and $\widehat{\boldsymbol{w}}$ is its DFT. Our aim is to prove that there exists a positive constant C_s which does not depend on n and Δt such that

$$\left\|[\boldsymbol{\eta}^n, \boldsymbol{u}^n]^T\right\|_{N,s,s+1} \leqslant C_s \left\|[\boldsymbol{\eta}^0, \boldsymbol{u}^0]^T\right\|_{N,s,s+1},\ \forall\, n\Delta t \leqslant T, \tag{4.8}$$

where

$$\left\|[\boldsymbol{w_1}, \boldsymbol{w_2}]^T\right\|_{N,s,s+1}^2 = ||\boldsymbol{w_1}||_{N,s}^2 + ||\boldsymbol{w_2}||_{N,s+1}^2,$$

and both vectors $\boldsymbol{w_1}$ and $\boldsymbol{w_2}$ belong to $\mathbb{R}^N$.

Substituting matrix D in scheme (4.7) by its blocks described in (4.6) and using that $(1/\sqrt{N})F$ diagonalizes matrices C, P and P^{-1}, we proceed as in [1] to transform scheme (4.7) to the Fourier space obtaining

$$\begin{cases} \widehat{\boldsymbol{\eta}}^{n+1} = \left[I + \dfrac{\Delta t^2}{2}\widehat{P}^{-1}\widehat{C}^2 + \dfrac{\Delta t^4}{4!}\widehat{P}^{-2}\widehat{C}^4\right]\widehat{\boldsymbol{\eta}}^n + \left[\Delta t\widehat{C} + \dfrac{\Delta t^3}{3!}\widehat{P}^{-1}\widehat{C}^3\right]\widehat{\boldsymbol{u}}^n, \\ \widehat{\boldsymbol{u}}^{n+1} = \left[\Delta t\widehat{P}^{-1}\widehat{C} + \dfrac{\Delta t^3}{3!}\widehat{P}^{-2}\widehat{C}^3\right]\widehat{\boldsymbol{\eta}}^n + \left[I + \dfrac{\Delta t^2}{2}\widehat{P}^{-1}\widehat{C}^2 + \dfrac{\Delta t^4}{4!}\widehat{P}^{-2}\widehat{C}^4\right]\widehat{\boldsymbol{u}}^n, \end{cases}$$

that can be written for each wavenumber k in the form

$$\begin{bmatrix} \widehat{\eta}_k^{n+1} \\ \widehat{u}_k^{n+1} \end{bmatrix} = \begin{bmatrix} \mathrm{c}(\theta_k, \sigma, \Delta x) & \boldsymbol{i}v^{-1}\left(\frac{\theta_k}{\Delta x}\right)\mathrm{s}(\theta_k, \sigma, \Delta x) \\ \boldsymbol{i}v\left(\frac{\theta_k}{\Delta x}\right)\mathrm{s}(\theta_k, \sigma, \Delta x) & \mathrm{c}(\theta_k, \sigma, \Delta x) \end{bmatrix} \begin{bmatrix} \widehat{\eta}_k^n \\ \widehat{u}_k^n \end{bmatrix} = G_k \begin{bmatrix} \widehat{\eta}_k^n \\ \widehat{u}_k^n \end{bmatrix}, \tag{4.9}$$

for $-N/2 + 1 \leqslant k \leqslant N/2$, where $\sigma = \Delta t/\Delta x$ is the Courant number and

$$\begin{aligned} \mathrm{c}(\theta, \sigma, \Delta x) &= 1 - \frac{1}{2}\sigma^2 v^2\left(\tfrac{\theta}{\Delta x}\right)\gamma^2(\theta) + \frac{1}{4!}\sigma^4 v^4\left(\tfrac{\theta}{\Delta x}\right)\gamma^4(\theta), \\ \mathrm{s}(\theta, \sigma, \Delta x) &= \sigma v\left(\tfrac{\theta}{\Delta x}\right)\gamma(\theta) - \frac{1}{3!}\sigma^3 v^3\left(\tfrac{\theta}{\Delta x}\right)\gamma^3(\theta). \end{aligned}$$

It is easy to verify that we can write $G_k = V(k\pi/l)\,\tilde{G}_k\,V(k\pi/l)^{-1}$, where

$$V(\kappa) = \begin{bmatrix} 1 & 0 \\ 0 & v(\kappa) \end{bmatrix}, \qquad \tilde{G}_k = \begin{bmatrix} \mathrm{c}(\theta_k, \sigma, \Delta x) & \boldsymbol{i}\mathrm{s}(\theta_k, \sigma, \Delta x) \\ \boldsymbol{i}\mathrm{s}(\theta_k, \sigma, \Delta x) & \mathrm{c}(\theta_k, \sigma, \Delta x) \end{bmatrix},$$

and that the eigenvalues of G_k and $\tilde{G}_k$ are given by $g_k^{\pm} = g^{\pm}(\theta_k, \sigma, \Delta x)$, where

$$g^{\pm}(\theta, \sigma, \Delta x) = \mathrm{c}(\theta, \sigma, \Delta x) \mp \boldsymbol{i}\,\mathrm{s}(\theta, \sigma, \Delta x).$$

Before enunciating the proposition which gives a sufficient condition for stability we need the following lemma which is proven in [7].

Lemma 4.1. *There exist positive constants c_1 and c_2 such that $\forall\, y \in \mathbb{R}$*

$$c_1 \leqslant \frac{1}{v(y)^2(1+y^2)} \leqslant c_2. \tag{4.10}$$

Proposition 4.2. *Let $\beta > 0$ and $s \geqslant 0$. The numerical scheme (4.7) is stable, that is, inequality (4.8) holds, if $g^{\pm}(\theta, \sigma, \Delta x)$ satisfy*

$$|g^{\pm}(\theta, \sigma, \Delta x)| \leqslant 1, \ \forall\, \theta \in (-\pi, \pi]. \tag{4.11}$$

Proof:

Let $[\boldsymbol{\eta}^n, \boldsymbol{u}^n]^T$ be the solution given by the method (4.7). For $s \geqslant 0$ we have

$$\begin{aligned}
\|[\boldsymbol{\eta}^n, \boldsymbol{u}^n]^T\|^2_{N,s,s+1} &= \|\boldsymbol{\eta}^n\|^2_{N,s} + \|\boldsymbol{u}^n\|^2_{N,s+1} \\
&= \frac{1}{2l} \sum_{k=-N/2+1}^{N/2} \left[1 + (k\pi/l)^2\right]^s \left(|\widehat{\eta}_k^n|^2 + \left[1 + (k\pi/l)^2\right] |\widehat{u}_k^n|^2\right) \\
&= \frac{1}{2l} \sum_{k=-N/2+1}^{N/2} \left[1 + (k\pi/l)^2\right]^s \left\|B(k\pi/l)[\widehat{\eta}_k^n, \widehat{u}_k^n]^T\right\|_2^2,
\end{aligned}$$

where $\|\cdot\|_2$ denotes the usual Euclidean norm and

$$B(\kappa) = \begin{bmatrix} 1 & 0 \\ 0 & \sqrt{1+\kappa^2} \end{bmatrix}.$$

Thus, it is enough to prove that there exists a positive constant C_s such that

$$\left\|B(k\pi/l)[\widehat{\eta}_k^n, \widehat{u}_k^n]^T\right\|_2^2 \leqslant C_s^2 \left\|B(k\pi/l)[\widehat{\eta}_k^0, \widehat{u}_k^0]^T\right\|_2^2.$$

Using equality (4.9) recursively we get $[\widehat{\eta}_k^n, \widehat{u}_k^n]^T = G_k^n [\widehat{\eta}_k^0, \widehat{u}_k^0]^T$, then

$$\begin{aligned}
\left\|B(k\pi/l)[\widehat{\eta}_k^n, \widehat{u}_k^n]^T\right\|_2^2 &= \left\|B(k\pi/l)(G_k)^n B^{-1}(k\pi/l) B(k\pi/l)[\widehat{\eta}_k^0, \widehat{u}_k^0]^T\right\|_2^2 \\
&\leqslant \left\|B(k\pi/l)(G_k)^n B^{-1}(k\pi/l)\right\|_2^2 \left\|B(k\pi/l)[\widehat{\eta}_k^0, \widehat{u}_k^0]^T\right\|_2^2.
\end{aligned}$$

Thereby, using that $G_k = V(k\pi/l)\, \tilde{G}_k\, V(k\pi/l)^{-1}$ we get

$$\begin{aligned}
\left\|B(k\pi/l)(G_k)^n B^{-1}(k\pi/l)\right\|_2^2 &= \left\|B(k\pi/l)V(k\pi/l)\tilde{G}_k^n \left(B(k\pi/l)V(k\pi/l)\right)^{-1}\right\|_2^2 \\
&\leqslant \|B(k\pi/l)V(k\pi/l)\|_2^2 \, \|\tilde{G}_k\|_2^{2n} \left\|\left(B(k\pi/l)V(k\pi/l)\right)^{-1}\right\|_2^2.
\end{aligned}$$

Since matrix $\tilde{G}_k$ has eigenvalues $g^{\pm}(\theta_k, \sigma, \Delta x)$, by the hypothesis (4.11) we obtain

$$\|\tilde{G}_k\|_2^{2n} \leqslant \sup_{|\theta| \leqslant \pi} \left\{ |g^{\pm}(\theta, \sigma, \Delta x)|^{2n} \right\} \leqslant 1.$$

On the other hand,

$$\|B(k\pi/l)V(k\pi/l)\|_2^2\| \left(B(k\pi/l)V(k\pi/l)\right)^{-1} \|_2^2 = \max\left\{v(k\pi/l)^2(1+(k\pi/l)^2), \frac{1}{v(k\pi/l)^2(1+(k\pi/l)^2)}\right\}.$$

By inequality (4.10) we get

$$\frac{1}{v(k\pi/l)^2(1+(k\pi/l)^2)} \leqslant c_2, \quad \text{and} \quad v(k\pi/l)^2(1+(k\pi/l)^2) \leqslant 1/c_1.$$

Then,

$$\|B(k\pi/l)V(k\pi/l)\|_2^2 \left\|\left(B(k\pi/l)V(k\pi/l)\right)^{-1}\right\|_2^2 \leqslant \max\{1/c_1, c_2\} = C_s^2.$$

Therefore,

$$\left\|B\left(k\pi/l\right)\left[\widehat{\eta}_k^n, \widehat{u}_k^n\right]^T\right\|_2^2 \leqslant C_s^2 \left\|B\left(k\pi/l\right)\left[\widehat{\eta}_k^0, \widehat{u}_k^0\right]^T\right\|_2^2,$$

which leads us to conclude that

$$\left\|[\boldsymbol{\eta}^n, \boldsymbol{u}^n]^T\right\|_{N,s,s+1} \leqslant C_s \left\|[\boldsymbol{\eta}^0, \boldsymbol{u}^0]^T\right\|_{N,s,s+1}.$$

■

Condition (4.11) guarantees stability but it is not practical for numerical implementations. As shown in [1], we can write the squared amplification factor as

$$|g_k^{\pm}|^2 = 1 + p\left(\sigma v\left(\tfrac{\theta_k}{\Delta x}\right)\gamma(\theta_k)\right),$$

where $p(y) = y^6(y^2-8)/576$. Note that $p(y) \leqslant 0$ if $|y| \leqslant 2\sqrt{2}$, then the scheme is stable if

$$\max_{|\theta|<\pi} \sigma \left|v\left(\tfrac{\theta}{\Delta x}\right)\gamma(\theta)\right| \leqslant 2\sqrt{2}. \tag{4.12}$$

In view of the previous computations, theorem 4.3 provides three practical conditions to guarantee stability.

Theorem 4.3. *The numerical scheme (4.7) is stable if at least one of the following inequalities holds:*

$$\sigma = \frac{\Delta t}{\Delta x} \leqslant \gamma_1 \sqrt{1 + \frac{\rho_2}{\rho_1}\frac{\sqrt{\beta}}{\delta}}, \quad \gamma_1 = 2\sqrt{2}\left(\sup_{|\theta|\leqslant\pi}|\gamma(\theta)|\right)^{-1}, \tag{4.13}$$

$$\mu = \frac{\Delta t}{\sqrt{\Delta x}} \leqslant \gamma_2 \sqrt{\sqrt{\beta}\left(1+\frac{\rho_2}{\rho_1}\right)}, \quad \gamma_2 = 2\sqrt{2}\left(\sup_{|\theta|\leqslant\pi}\left\{\frac{|\gamma(\theta)|}{\sqrt{|\theta|}}\right\}\right)^{-1}, \tag{4.14}$$

$$\Delta t \leqslant \gamma_3 \sqrt{\frac{\beta}{3}}, \quad \gamma_3 = 2\sqrt{2}\left(\sup_{|\theta|\leqslant\pi}\left\{\frac{|\gamma(\theta)|}{|\theta|}\right\}\right)^{-1}. \tag{4.15}$$

Proof:
As previously stated, we just need to prove that each condition leads to inequality (4.12). For this we will use the following inequalities

$$\phi(y) \geqslant 1, \forall y \in \mathbb{R}, \tag{4.16}$$

$$\phi(y) \geqslant |y|, \forall y \in \mathbb{R}, \tag{4.17}$$

proven in [7] and also

$$1 + \frac{\beta}{3}y^2 > \sqrt{\beta}|y|, \forall y \in \mathbb{R}, \text{ for } \beta > 0, \tag{4.18}$$

which is proven in [16]. The first condition is established using inequality (4.16) to obtain

$$v(\kappa) = \frac{1}{\sqrt{1 + \frac{\rho_2}{\rho_1}\frac{\sqrt{\beta}}{\delta}\phi(\kappa\delta) + \kappa^2\frac{\beta}{3}}} \leqslant \frac{1}{\sqrt{1 + \frac{\rho_2}{\rho_1}\frac{\sqrt{\beta}}{\delta}}}.$$

Therefore,

$$\left|v\left(\tfrac{\theta}{\Delta x}\right)\gamma(\theta)\right| \leqslant \sup_{|\theta|\leqslant\pi} v\left(\tfrac{\theta}{\Delta x}\right) \sup_{|\theta|\leqslant\pi} |\gamma(\theta)| \leqslant \left[1 + \frac{\rho_2}{\rho_1}\frac{\sqrt{\beta}}{\delta}\right]^{-1/2} \sup_{|\theta|\leqslant\pi} |\gamma(\theta)|. \tag{4.19}$$

Multiplying inequality (4.19) by σ, applying condition (4.13) and making some simplifications we guarantee inequality (4.12).

For the second condition we use inequalities (4.17) and (4.18) to get

$$v(\kappa) = \frac{1}{\sqrt{1 + \frac{\rho_2}{\rho_1}\frac{\sqrt{\beta}}{\delta}\phi(\kappa\delta) + \kappa^2\frac{\beta}{3}}} \leqslant \frac{1}{\sqrt{\frac{\rho_2}{\rho_1}\frac{\sqrt{\beta}}{\delta}|\kappa\delta| + \sqrt{\beta}|\kappa|}},$$

thus

$$\begin{aligned}\left|v\left(\tfrac{\theta}{\Delta x}\right)\gamma(\theta)\right| &\leqslant \sup_{|\theta|\leqslant\pi}\left\{\frac{|\gamma(\theta)|}{\sqrt{\frac{\rho_2}{\rho_1}\frac{\sqrt{\beta}}{\delta}|\theta\delta/\Delta x| + \sqrt{\beta}|\theta/\Delta x|}}\right\} \\ &= \left(\sqrt{\frac{\Delta x}{\sqrt{\beta}\left(1 + \frac{\rho_2}{\rho_1}\right)}}\right) \sup_{|\theta|\leqslant\pi}\left\{\frac{|\gamma(\theta)|}{\sqrt{|\theta|}}\right\}.\end{aligned}$$

Multiplying inequality (4.14) by $\left|v\left(\frac{\theta}{\Delta x}\right)\gamma(\theta)\right|/\sqrt{\Delta x}$ and applying the inequality above we obtain condition (4.12).

For the last condition we use that $\phi(y) > 0, \forall y \in \mathbb{R}$, then

$$\left|v\left(\tfrac{\theta}{\Delta x}\right)\gamma(\theta)\right| \leqslant \sup_{|\theta|\leqslant\pi}\left\{\frac{|\gamma(\theta)|}{\sqrt{\frac{\beta}{3}(\theta/\Delta x)^2}}\right\} = \left(\frac{\Delta x}{\sqrt{\frac{\beta}{3}}}\right) \sup_{|\theta|\leqslant\pi}\left\{\frac{|\gamma(\theta)|}{|\theta|}\right\}.$$

Using this inequality and condition (4.15) similarly to what was done previously we obtain inequality (4.12).

Therefore, if one of the conditions (4.13), (4.14) or (4.15) holds, the method is stable.

■

The values of γ_1, γ_2 and γ_3 depend on the spatial discretization used to obtain matrix C. Table 4.1 shows approximations for these values for each of the discretizations presented earlier in this chapter. The finite difference scheme provides larger values of γ_1, γ_2 and γ_3 when compared to piecewise linear B-splines and the spectral scheme, thus its stability conditions are less restrictive than those provided by the other schemes.

	Finite Difference	B-Splines	Spectral Differentiation
γ_1	2.061	1.633	0.900
γ_2	2.651	2.300	1.595
γ_3	2.828	2.828	2.828

Table 4.1: Values of γ_i for each method.

In general, we want the largest possible value of Δt in order to reduce the computational cost while maintaining stability and a good approximation. Denoting by Δt_σ, Δt_μ and Δt_c the largest values of Δt for a given Δx obtained respectively by conditions (4.13), (4.14) and (4.15), figure 4.2 illustrates the criteria for choosing the most appropriate stability condition for the finite difference spatial discretization. Defining

$$\chi_1 = \left(\frac{\gamma_3}{\gamma_2}\right)^2 \frac{\rho_1\beta/3}{\sqrt{\beta}(\rho_1+\rho_2)} \text{ and } \chi_2 = \left(\frac{\gamma_2}{\gamma_1}\right)^2 \frac{\sqrt{\beta}(\rho_1+\rho_2)}{\rho_1+\sqrt{\beta}\rho_2/\delta},$$

and considering $\sqrt{\beta}/\delta = h_1/h_2 < 1$ and $\gamma_2^2/\gamma_1 \geqslant \gamma_3/\sqrt{3}$, it is proven in [16] that $\chi_1 < \chi_2$. Therefore, if $\Delta x < \chi_1$ condition (4.15) provides the largest values of Δt, if $\Delta x \in (\chi_1, \chi_2)$ condition (4.14) is the most appropriate and if $\Delta x > \chi_2$ we use condition (4.13). Since we aim at good precision at a reasonable computational cost, in most of the cases condition (4.14) is used.

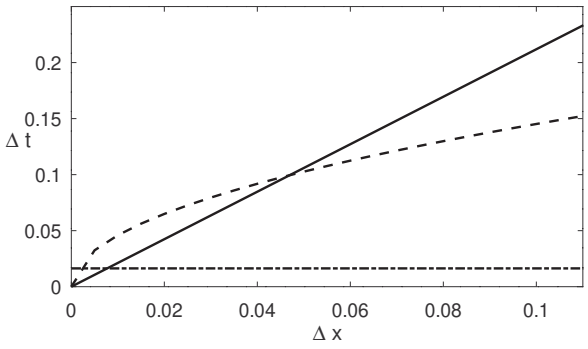

Figure 4.2: Δt_σ (—), Δt_μ $(--)$ and Δt_c $(- \cdot -)$ as functions of Δx for $\beta = 0.0001$, $h_2/h_1 = 35.05$ and $\rho_1/\rho_2 = 0.5$.

Now we can compare the method (4.7) for our dispersive system and the scheme presented in [1] for system (2.7), which has the following stability conditions:

$$\sigma = \frac{\Delta t}{\Delta x} \leqslant \gamma_1\sqrt{1+\frac{\rho_2}{\rho_1}\frac{\sqrt{\beta}}{\delta}}, \quad \gamma_1 = 2\sqrt{2}\left(\sup_{|\theta|\leqslant\pi}|\gamma(\theta)|\right)^{-1},$$
$$\mu = \frac{\Delta t}{\sqrt{\Delta x}} \leqslant \gamma_2\sqrt{\sqrt{\beta}\left(\frac{\rho_2}{\rho_1}\right)}, \quad \gamma_2 = 2\sqrt{2}\left(\sup_{|\theta|\leqslant\pi}\left\{\frac{|\gamma(\theta)|}{\sqrt{|\theta|}}\right\}\right)^{-1}.$$

Due to the term $(\beta/3)u_{xxt}$ that leads to the term $(\beta/3)k^2$ in $v(k)$, the condition for $\Delta t/\sqrt{\Delta x}$ is less restrictive for system (2.6) than for system (2.7). Moreover, we can obtain a stability condition independent of Δx for the scheme (4.7) which is not possible for the case of system (2.7) where there is no quadratic term like $(\beta/3)k^2$ in $v(k)$ and any inequality must rely on the linear growth of ϕ. The condition for the Courant number $\Delta t/\Delta x$ is the same in both cases.

4.2 Numerical stability tests

In this section we will perform a sequence of numerical experiments in order to validate the methods and the stability conditions. The implementations were done in Octave. For the spatial derivative we choose the finite difference approximation because it has a low computational cost compared to the other schemes (piecewise linear B-splines and spectral scheme) and provides the largest values of γ_1, γ_2 and γ_3, as shown in table 4.1.

The conservation law (3.4), which is valid for all systems considered here, is approximated by the trapezoidal rule defining the function

$$I(t_i) = \Delta x \sum_{j=1}^{N} \eta_j^i,$$

in order to verify how well the numerical solutions satisfy it. Since $d = 0$ in relation (3.4), the initial condition must satisfy $I(0) = 0$, so we choose as initial configuration the profile

$$\eta_0(x) = \overline{\eta}(x) - a,$$

where $\overline{\eta}(x) = 0.1\exp(-2(x-l)^2)$ and a is calculated by the trapezoidal rule

$$a = \frac{1}{N}\sum_{j=1}^{N} \overline{\eta}_j, \tag{4.20}$$

as an approximation of the value of

$$\frac{1}{2l}\int_{-l}^{l} \overline{\eta} dx.$$

We set u_0 so that η only propagates to the right in the linear system, that is, $\widehat{u}_0(k) = v(k\pi/l)\widehat{\eta}_0(k)$. For the nonlinear system u_0 is set in the same way. For the numerical experiments we set $\rho_1 = 1$, $\rho_2 = 2$, $h_1 = 0.1$ and $h_2 = 3.505$ as in [9]. The values of β, α, l, N and Δt are defined in each test. The other values are calculated by the relations $L = h_1/\sqrt{\beta}$ and $\delta = h_2/L$.

Figure 4.3 presents the graphics of the numerical solution of system (2.6) at different instants for $\beta = 0.0001$ and $l = 10\pi$ with $\Delta x = 0.03068$ and $\Delta t = 0.08043$ which satisfy the stability condition (4.14). We can see the dispersion acting on η and u because of the wave trains that form as time advances. In fact, as the phase velocity $v(k)$ decreases to zero when $|k| \to +\infty$ the high wavenumber components of the solution propagate more slowly and form the aforementioned wave trains.

Figure 4.4 shows how the amplification factor $|g_k^{\pm}|$ grows as Δt increases while Δx is kept constant. If $\Delta x = 0.03068$ and $\Delta t = 0.08043$, conditions (4.14) and (4.11) are satisfied. If $\Delta t = 0.08847$, none of the conditions required for stability in theorem 4.3 is satisfied, but condition (4.11) still holds as the dashed line in figure 4.4 shows. For $\Delta t = 0.09460$, condition (4.11) is not satisfied because $|g^{\pm}(\pi/2, \sigma, \Delta x)| = 1.0029$. In the last case, since no stability condition holds, high wavenumber components permeate the numerical solution as shown in figure 4.5 for $t = 1800\Delta t$. Note that this phenomenon is different from dispersion in which the components propagate with different speeds. In this case, besides the dispersion effect of the system (2.6), the amplitude of high wavenumber components increases anomalously and the numerical solution is compromised. This example illustrates the relevance of a proper stability

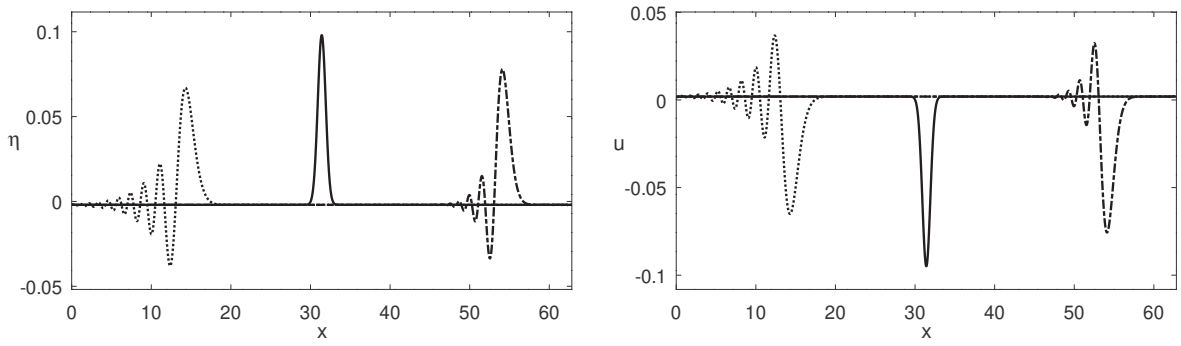

(a) η (b) u

Figure 4.3: Approximate solutions for the linear system (2.6) at times $t = 0$ (—), $t = 1100\Delta t$ $(- \cdot -)$ and $t = 2200\Delta t$ $(\cdots)$ with $l = 10\pi$, $\beta = 0.0001$, $N = 2^{11}$, $\Delta x = 0.03068$, $\Delta t = 0.08043$.

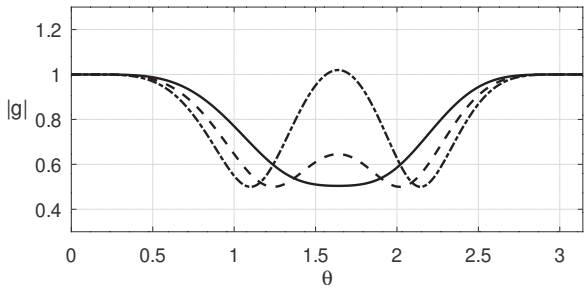

Figure 4.4: $|g^{\pm}(\theta, \sigma, \Delta x)|$ for $\Delta x = 0.03068$, $\Delta t = 0.08043$ (—), $\Delta t = 0.08847$ $(--)$ and $\Delta t = 0.09460$ $(- \cdot -)$ with $\beta = 0.0001$.

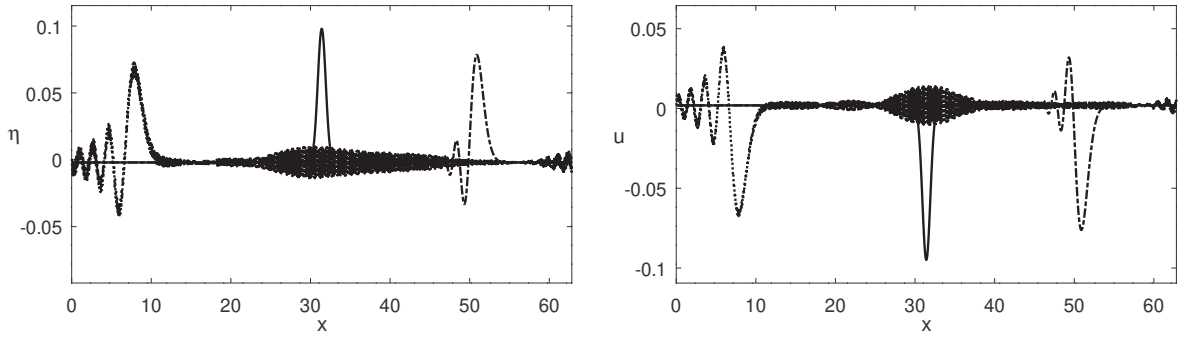

(a) η (b) u

Figure 4.5: Approximate solutions for the linear system (2.6) at times $t = 0$ (—), $t = 900\Delta t$ $(- \cdot -)$ and $t = 1800\Delta t$ $(\cdots)$ with $l = 10\pi$, $\beta = 0.0001$, $N = 2^{11}$, $\Delta x = 0.03068$, $\Delta t = 0.09460$.

analysis even when the stability conditions are less restrictive.

Figure 4.6 presents the graphics of the numerical solution of system (2.6) for $l = 10\pi$, $\beta = 0.001$ using $\Delta x = 0.00383$ and $\Delta t = 0.05163$ which satisfy the stability condition (4.15). We see that increasing the parameter β the phase velocity $v(k)$ decreases to zero faster, thus a wider wave train is formed.

Figure 4.7 shows how the amplification factor grows as Δt increases while Δx is kept constant. If $\Delta x = 0.00383$ and $\Delta t = 0.05163$ we have a stable solution as shown in figure 4.6.

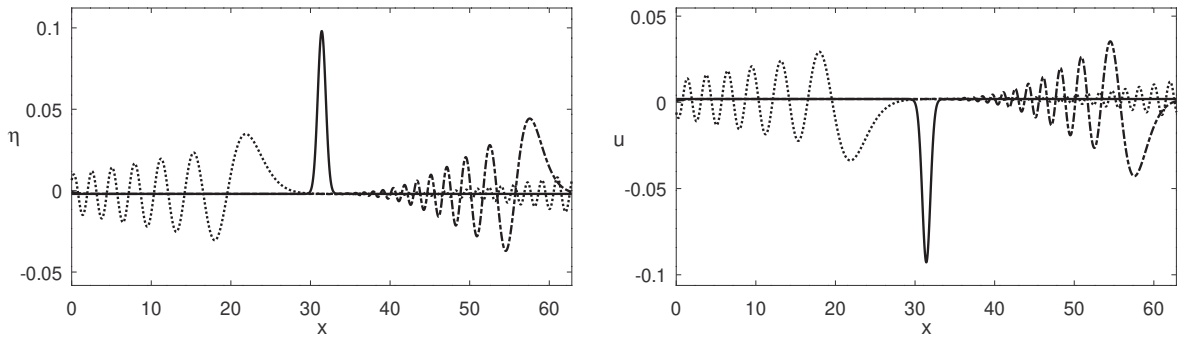

(a) η (b) u

Figure 4.6: Approximate solutions for the linear system (2.6) at times $t = 0$ (—), $t = 1800\Delta t$ $(- \cdot -)$ and $t = 3600\Delta t$ $(\cdots)$ with $l = 10\pi$, $\beta = 0.001$, $N = 2^{14}$, $\Delta x = 0.00383$, $\Delta t = 0.05163$.

If $\Delta t = 0.06196$, none of the stability conditions in theorem 4.3 is satisfied, but condition (4.11) still holds as the dashed line in figure 4.7 illustrates. For $\Delta t = 0.07026$, condition (4.11) is not satisfied since we have $|g^{\pm}(1.12, \sigma, \Delta x)| = 1.0062$ and the solution obtained is unstable as shown in figure 4.8.

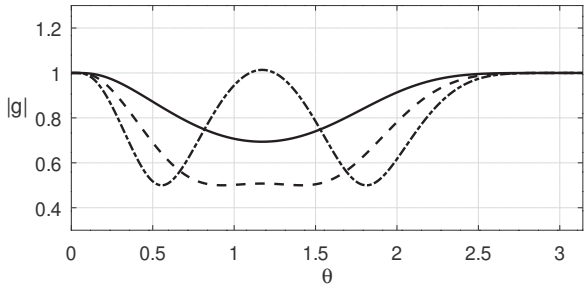

Figure 4.7: $|g^{\pm}(\theta, \sigma, \Delta x)|$ for $\Delta t = 0.05163$ (—), $\Delta t = 0.06196$ $(--)$ and $\Delta t = 0.07027$ $(- \cdot -)$ with $\Delta x = 0.00383$ and $\beta = 0.001$.

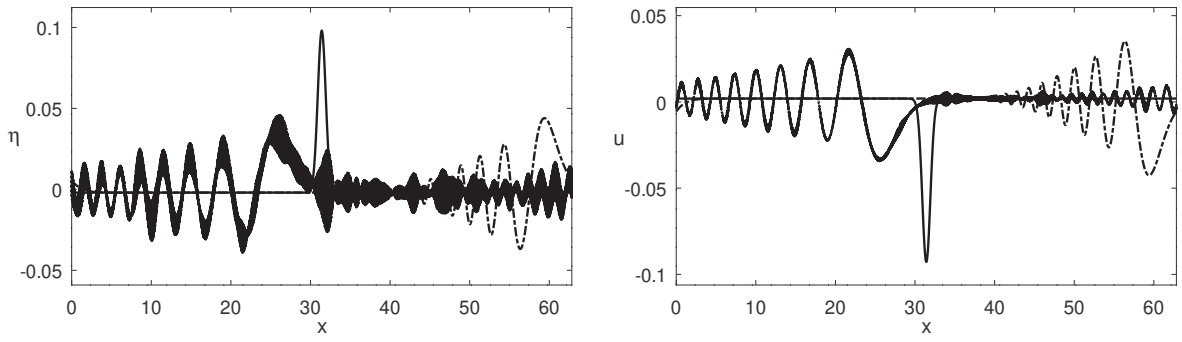

(a) η (b) u

Figure 4.8: Approximate solutions for the linear system (2.6) at times $t = 0$ (—), $t = 1350\Delta t$ $(- \cdot -)$ and $t = 2700\Delta t$ $(\cdots)$ with $l = 10\pi$, $\beta = 0.001$, $N = 2^{14}$, $\Delta x = 0.00383$, $\Delta t = 0.07026$.

The stability performance exhibited illustrates the fact that theorem 4.3 provides sufficient,

not necessary restrictions for stability. Rather than the best possible condition, theorem 4.3 provides sufficient stability conditions which are useful for implementation codes.

Figure 4.9 shows the graphic of the mean I for the computed solutions presented in figures 4.3 and 4.6, respectively. We can see that the numerical solutions of the linear system preserve very well the conservation law (3.4) since the absolute value of I is bounded by 10^{-14} in both cases.

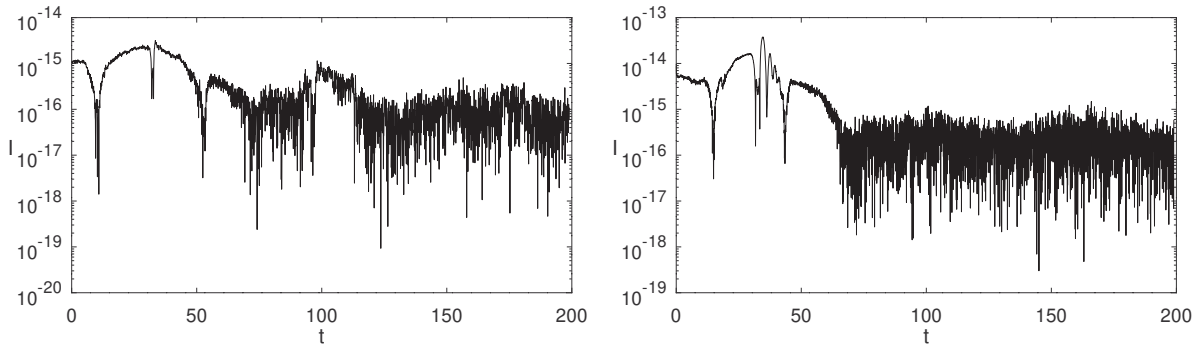

(a) $\Delta x = 0.03068$, $\Delta t = 0.08043$ (b) $\Delta x = 0.00383$, $\Delta t = 0.05163$

Figure 4.9: Mean I for the results presented in figures 4.3 and 4.6.

Now let us show that the stability conditions in theorem 4.3 are valid to the scheme for the nonlinear system (2.5). Note that condition (4.11) only makes sense in the linear case where there exists an amplification factor. Figure 4.10 shows the graphics of the numerical solutions for system (2.5) for $l = 10\pi$, $\beta = \alpha = 0.0001$ where $\Delta x = 0.03068$ and $\Delta t = 0.08043$ satisfy condition (4.14), also figure 4.11 presents the graphics of the numerical solutions for $l = 10\pi$, $\beta = \alpha = 0.001$ with $\Delta x = 0.00383$ and $\Delta t = 0.05163$ satisfying the stability condition (4.15). We see that the conditions in theorem 4.3 still hold for these nonlinear cases. Figures 4.12 and 4.13 show that if Δt is increased so that no stability condition in theorem 4.3 is satisfied the numerical solution is unstable as in the linear case. Also, we can see that the numerical solutions of the nonlinear system preserve very well the conservation law (3.4) as shown in figure 4.14 for the computed solutions presented in figures 4.10 and 4.11, respectively.

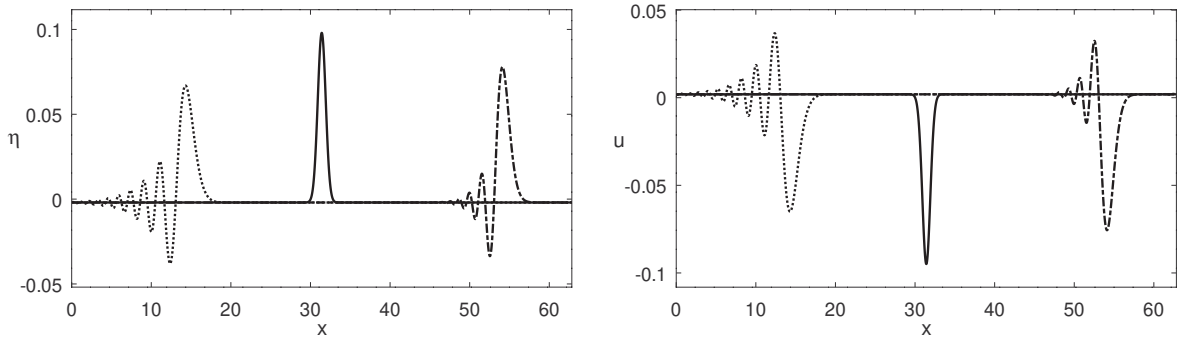

(a) η (b) u

Figure 4.10: Approximate solutions for the nonlinear system (2.5) at times $t = 0$ (—), $t = 1100\Delta t$ $(-\cdot-)$ and $t = 2200\Delta t$ $(\cdots)$ with $l = 10\pi$, $\beta = \alpha = 0.0001$, $N = 2^{11}$, $\Delta x = 0.03068$, $\Delta t = 0.08043$.

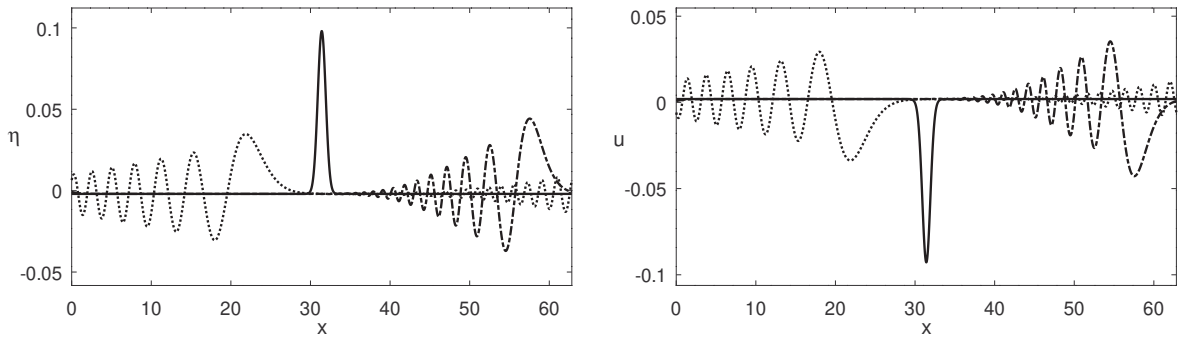

(a) η (b) u

Figure 4.11: Approximate solutions for the nonlinear system (2.5) at times $t = 0$ (—), $t = 1800\Delta t$ $(- \cdot -)$ and $t = 3600\Delta t$ $(\cdots)$ with $l = 10\pi$, $\beta = \alpha = 0.001$, $N = 2^{14}$, $\Delta x = 0.00383$, $\Delta t = 0.05163$.

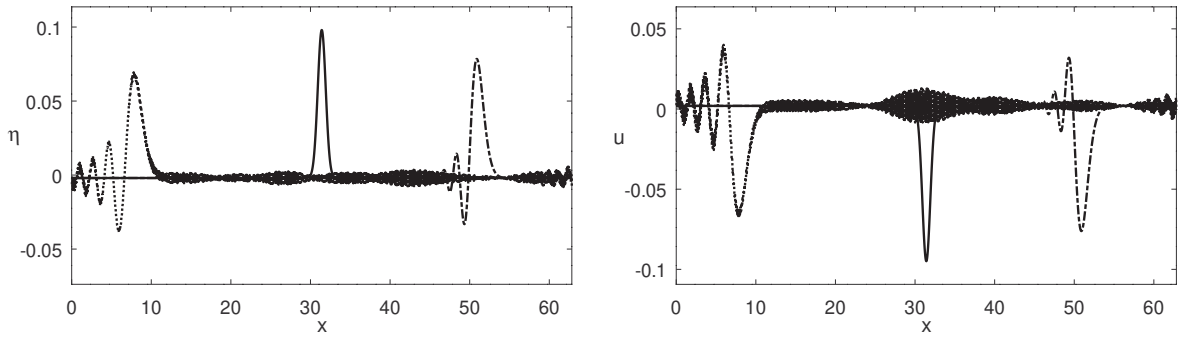

(a) η (b) u

Figure 4.12: Approximate solutions for the nonlinear system (2.5) at times $t = 0$ (—), $t = 900\Delta t$ $(- \cdot -)$ and $t = 1800\Delta t$ $(\cdots)$ with $l = 10\pi$, $\beta = \alpha = 0.0001$, $N = 2^{11}$, $\Delta x = 0.03068$, $\Delta t = 0.09460$.

Solutions for the nonlinear system (2.5) have a similar appearance to solutions for the linear system (2.6) with the same set of common parameters and starting from the same initial conditions. In order to compare them we compute the Euclidean norm of the vector that results from their difference at several instants. Table 4.2 shows that the Euclidean norm of the difference grows as time advances and it is larger for the larger value of the nonlinear parameter. In particular, the values at the intersection of the rows identified by $\beta = 0.0001$ and the columns identified by $\overline{\eta}(x) = \exp(-2x^2)$ correspond to the two experiments that generate figures 4.3 and 4.10. Analogously, the values at the intersection of the rows identified by $\beta = 0.001$ and the columns identified by $\overline{\eta}(x) = \exp(-2x^2)$ correspond to the two experiments that generate figures 4.6 and 4.11. Besides, table 4.2 shows that if $\overline{\eta}(x)$ changes from $0.1\exp(-2x^2)$ to $\exp(-2x^2)$ and therefore the initial values for η and u change by the same factor (keeping all the parameters equal), the Euclidean norm of the corresponding difference is multiplied approximately by one hundred, confirming that the nonlinear effects are present and are more noticeable for higher amplitude profiles.

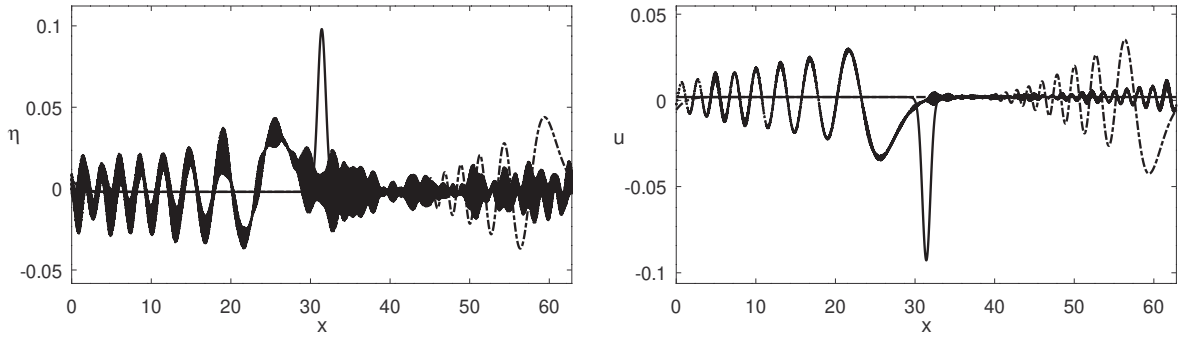

(a) η (b) u

Figure 4.13: Approximate solutions for the nonlinear system (2.5) at times $t = 0$ (—), $t = 1350\Delta t$ $(- \cdot -)$ and $t = 2700\Delta t$ $(\cdots)$ with $l = 10\pi$, $\beta = \alpha = 0.001$, $N = 2^{14}$, $\Delta x = 0.00383$, $\Delta t = 0.07026$.

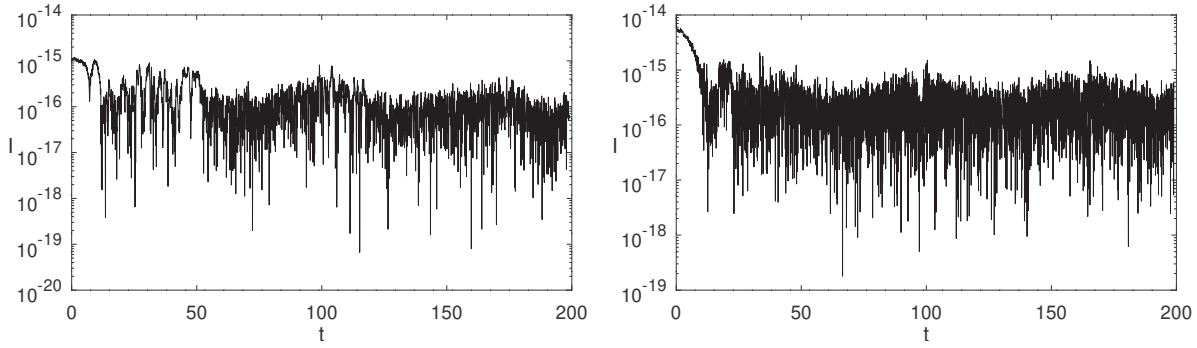

(a) $\Delta x = 0.03068$, $\Delta t = 0.08043$ (b) $\Delta x = 0.00383$, $\Delta t = 0.05163$

Figure 4.14: Mean I for the results presented in figures 4.10 and 4.11.

		$\overline{\eta}(x) = 0.1\exp(-2x^2)$		$\overline{\eta}(x) = \exp(-2x^2)$	
β	time	norm (η)	norm (u)	norm (η)	norm (u)
0.0001	$100\Delta t = 8.043$	0.0000495	0.0000475	0.0049454	0.0047532
	$500\Delta t = 40.213$	0.0002119	0.0002041	0.0211847	0.0204099
	$1100\Delta t = 88.468$	0.0003597	0.0003474	0.0359573	0.0347279
	$2200\Delta t = 176.937$	0.0005106	0.0004941	0.0510226	0.0493752
0.001	$150\Delta t = 7.745$	0.0011563	0.0010590	0.1156249	0.1059029
	$700\Delta t = 36.142$	0.0025461	0.0023993	0.2542572	0.2395679
	$1800\Delta t = 92.938$	0.0031029	0.0029502	0.3092888	0.2940249
	$3600\Delta t = 185.875$	0.0033832	0.0032392	0.3365037	0.3221350

Table 4.2: Euclidean norm of the difference between the solutions of the linear system (2.6) and the nonlinear system (2.5).

4.3 Numerical convergence study

Now let us study the convergence of the method on the temporal and spatial variables. Since the exact solution is not available for the nonlinear system, in order to compare with the numerical approximations, we substitute it by an accurate numerical solution $(\overline{\boldsymbol{\eta}}, \overline{\boldsymbol{u}})$ that is calculated with small values of $\Delta x = \Delta x^*$ and $\Delta t = \Delta t^*$. For a given time $T > 0$ we define

the time error by

$$E_t(\eta, \Delta t, \Delta t^*, \Delta x^*, T) = \|\boldsymbol{\eta}^n - \overline{\boldsymbol{\eta}}^m\|_2,\ n\Delta t = m\Delta t^* = T.$$

We can estimate the temporal convergence rate p making successive refinements dividing Δt by 2 while keeping $\Delta x = \Delta x^*$ and computing

$$p \approx \frac{\log(E_t(\eta, \Delta t/2, \Delta t^*, \Delta x^*, T)/E_t(\eta, \Delta t, \Delta t^*, \Delta x^*, T))}{\log(1/2)}.$$

The error and rate for u are defined analogously.

Since the classical Runge-Kutta method has fourth order of convergence, it is expected for the rate p to be close to 4. This is confirmed for the linear and nonlinear cases for different values of β and α as shown in tables 4.3-4.6.

	η		u	
Δt	error	rate	error	rate
0.286039	0.054823619180		0.049861071184	
0.143020	0.007747620293	2.82297	0.006884781170	2.85643
0.071510	0.000527767899	3.87578	0.000467186526	3.88134
0.035755	0.000033095045	3.99522	0.000029291581	3.99544
0.017877	0.000002061352	4.00495	0.000001824437	4.00496
0.008939	0.000000121261	4.08740	0.000000107324	4.08740

Table 4.3: Convergence study on the temporal variable t for the linear system (2.6) with $\beta = 0.001$, $l = 10\pi$, $\Delta x = 0.122718$, $\Delta t^* = 0.004469$ and $T = 99.827624$.

	η		u	
Δt	error	rate	error	rate
0.160852	0.015553630790		0.014882034096	
0.080426	0.001239195834	3.64978	0.001182218375	3.65400
0.040213	0.000078402189	3.98237	0.000074783623	3.98263
0.020106	0.000004901891	3.99948	0.000004675617	3.99949
0.010053	0.000000305267	4.00519	0.000000291176	4.00520
0.005027	0.000000017957	4.08744	0.000000017128	4.08744

Table 4.4: Convergence study on the temporal variable t for the linear system (2.6) with $\beta = 0.0001$, $l = 10\pi$, $\Delta x = 0.122718$, $\Delta t^* = 0.002513$ and $T = 99.888826$.

For spatial convergence we define the error $E_x(\eta, \Delta x, \Delta x^*, \Delta t^*, T)$ analogously to E_t, but we consider only the points where all numerical solutions are calculated and the same value of $\Delta t = \Delta t^*$ in each solution. We perform successive refinements of the spatial mesh dividing Δx by 2 and estimating the spatial convergence rate by

$$p \approx \frac{\log(E_x(\eta, \Delta x/2, \Delta x^*, \Delta t^*, T)/E_x(\eta, \Delta x, \Delta x^*, \Delta t^*, T))}{\log(1/2)}.$$

As in the temporal convergence study, a fourth order convergence rate is expected in the spatial variable since the finite difference formula has order 4 and the Fourier approximation has

	η		u	
Δt	error	rate	error	rate
0.286039	0.054926091446		0.049952905618	
0.143020	0.007771557556	2.82122	0.006905599111	2.85473
0.071510	0.000529584107	3.87527	0.000468751769	3.88087
0.035755	0.000033209536	3.99519	0.000029390166	3.99542
0.017877	0.000002068486	4.00495	0.000001830579	4.00496
0.008939	0.000000121681	4.08740	0.000000107686	4.08740

Table 4.5: Convergence study on the temporal variable t for the nonlinear system (2.5) with $\beta = \alpha = 0.001$, $l = 10\pi$, $\Delta x = 0.122718$, $\Delta t^* = 0.004469$ and $T = 99.827624$.

	η		u	
Δt	error	rate	error	rate
0.160852	0.015568274218		0.014895959522	
0.080426	0.001240645307	3.64945	0.001183590855	3.65368
0.040213	0.000078495424	3.98234	0.000074871868	3.98260
0.020106	0.000004907726	3.99948	0.000004681140	3.99949
0.010053	0.000000305630	4.00519	0.000000291520	4.00520
0.005027	0.000000017979	4.08744	0.000000017148	4.08744

Table 4.6: Convergence study on the temporal variable t for the nonlinear system (2.5) with $\beta = \alpha = 0.0001$, $l = 10\pi$, $\Delta x = 0.122718$, $\Delta t^* = 0.002513$ and $T = 99.888826$.

spectral convergence. Again, the estimated convergence rate is confirmed in the experiments for the linear and nonlinear cases considering different values of β and α as shown in tables 4.7-4.10.

	η		u	
Δx	error	rate	error	rate
0.122718	0.026010268439		0.023104571640	
0.061359	0.001918149846	3.76129	0.001688775393	3.77413
0.030680	0.000120901867	3.98781	0.000106417207	3.98817
0.015340	0.000007568352	3.99771	0.000006661369	3.99777
0.007670	0.000000471502	4.00464	0.000000414994	4.00466
0.003835	0.000000027739	4.08730	0.000000024414	4.08730

Table 4.7: Convergence study on spatial variable x for the linear system (2.6) with $\beta = 0.001$, $l = 10\pi$, $\Delta x^* = 0.001917$, $\Delta t = 0.035755$ and $T = 99.970644$.

	η		u	
Δx	error	rate	error	rate
0.122718	0.027538640823		0.026333212505	
0.061359	0.002079925294	3.72685	0.001982864179	3.73123
0.030680	0.000131165768	3.98707	0.000125033612	3.98720
0.015340	0.000008211104	3.99767	0.000007827135	3.99769
0.007670	0.000000511549	4.00463	0.000000487626	4.00464
0.003835	0.000000030095	4.08730	0.000000028687	4.08730

Table 4.8: Convergence study on spatial variable x for the linear system (2.6) with $\beta = 0.0001$, $\Delta x^* = 0.001917$, $\Delta t = 0.020106$ and $T = 99.989358$.

	η		u	
Δx	error	rate	error	rate
0.122718	0.026091160182		0.023175239719	
0.061359	0.001926156970	3.75976	0.001695616565	3.77270
0.030680	0.000121412422	3.98774	0.000106852992	3.98811
0.015340	0.000007600350	3.99771	0.000006688679	3.99776
0.007670	0.000000473496	4.00464	0.000000416696	4.00465
0.003835	0.000000027856	4.08730	0.000000024514	4.08730

Table 4.9: Convergence study on spatial variable x for the nonlinear system (2.5) with $\beta = \alpha = 0.001$, $l = 10\pi$, $\Delta x^* = 0.001917$, $\Delta t = 0.035755$ and $T = 99.970644$.

	η		u	
Δx	error	rate	error	rate
0.122718	0.027568752268		0.026361860047	
0.061359	0.002083124595	3.72621	0.001985887091	3.73060
0.030680	0.000131371169	3.98703	0.000125227617	3.98716
0.015340	0.000008223982	3.99767	0.000007839299	3.99768
0.007670	0.000000512351	4.00463	0.000000488384	4.00464
0.003835	0.000000030142	4.08730	0.000000028732	4.08730

Table 4.10: Convergence study on spatial variable x for the nonlinear system (2.5) with $\alpha = \beta = 0.0001$, $l = 10\pi$, $\Delta x^* = 0.001917$, $\Delta t = 0.020106$ and $T = 99.989358$.

Chapter 5

Unidirectional equation

In this chapter we will prove the existence of travelling wave solution for the unidirectional equation (2.9) using a fixed point method. Firstly, let us present the derivation of the regularized equation from system (2.5) using asymptotic expansion.

Considering $\alpha = \beta = 0$ in system (2.5) we get

$$\begin{cases} \eta_t - u_x = 0, \\ u_t - \eta_x = 0. \end{cases} \tag{5.1}$$

Note that from system (5.1) we can obtain the wave equation for η and u with speed $c^2 = 1$, that is,

$$\begin{cases} \eta_{tt} - \eta_{xx} = 0, \\ u_{tt} - u_{xx} = 0. \end{cases} \tag{5.2}$$

Looking for travelling solutions for system (5.1) of the form $\eta(x,t) = f(x - ct)$, $u(x,t) = g(x - ct)$ we get, after substitution of these expressions, the following system:

$$\begin{cases} -cf' - g' = 0, \\ -cg' - f' = 0. \end{cases} \tag{5.3}$$

From (5.3) we can conclude that $c = \pm 1$ which is consistent with the wave equations in system (5.2). Since we want a wave propagating to the right we choose $c = 1$. So, returning to system (5.3), we obtain that $g' = -f'$ and consequently $u = -\eta + a$, where a is constant. Then $\eta_t = u_x = -\eta_x$ and $u_t = \eta_x = -u_x$, that is,

$$\begin{cases} \eta_t + \eta_x = 0, \\ u_t + u_x = 0. \end{cases} \tag{5.4}$$

Thus, in view of $u = -\eta + a$, let us consider

$$u = -\eta + \alpha P + \beta Q + \sqrt{\beta} R + \mathcal{O}(\alpha\sqrt{\beta}, \beta^{3/2}), \tag{5.5}$$

where P, Q and R are functions to be determined. Differentiating (5.5) with respect to t and x we have

$$u_t = -\eta_t + \alpha P_t + \beta Q_t + \sqrt{\beta} R_t + \mathcal{O}(\alpha\sqrt{\beta}, \beta^{3/2}), \tag{5.6}$$

$$u_x = -\eta_x + \alpha P_x + \beta Q_x + \sqrt{\beta} R_x + \mathcal{O}(\alpha\sqrt{\beta}, \beta^{3/2}). \tag{5.7}$$

The equations in (5.4) suggest to replace the t derivatives of η and u in (5.6) by minus the x

derivative, which results in

$$-u_x = \eta_x + \alpha P_t + \beta Q_t + \sqrt{\beta} R_t + \mathcal{O}(\alpha\sqrt{\beta}, \beta^{3/2}). \tag{5.8}$$

Adding expressions (5.7) and (5.8) we have

$$0 = \alpha(P_t + P_x) + \beta(Q_t + Q_x) + \sqrt{\beta}(R_t + R_x) + \mathcal{O}(\alpha\sqrt{\beta}, \beta^{3/2}). \tag{5.9}$$

In order to satisfy equation (5.9) we obtain the following equations

$$\begin{cases} P_t + P_x = 0, \\ Q_t + Q_x = 0, \\ R_t + R_x = 0. \end{cases} \tag{5.10}$$

Substituting expression (5.5) in the first equation of system (2.5) and making some simplifications we obtain

$$\eta_t + \eta_x - \alpha(P_x + (\eta^2)_x) - \beta Q_x - \sqrt{\beta} R_x + \mathcal{O}(\alpha\sqrt{\beta}, \beta^{3/2}) = 0. \tag{5.11}$$

Analogously, substituting expression (5.5) in the second equation of system (2.5) we get

$$-\eta_t - \eta_x + \alpha(P_t + \eta\eta_x) + \beta\left(Q_t + \frac{1}{3}\eta_{xxt}\right) + \sqrt{\beta}\left(R_t + \frac{\rho_2}{\rho_1}\mathcal{T}_\delta[\eta_{xt}]\right) = \mathcal{O}(\alpha\sqrt{\beta}, \beta^{3/2}). \tag{5.12}$$

Now, equating terms with α, β and $\sqrt{\beta}$ in equations (5.11) and (5.12) we have

$$\begin{cases} P_x + (\eta^2)_x = P_t + \eta\eta_x, \\ Q_x = Q_t + \dfrac{1}{3}\eta_{xxt}, \\ R_x = R_t + \dfrac{\rho_2}{\rho_1}\mathcal{T}_\delta[\eta_{xt}]. \end{cases}$$

From the equations in (5.10) we obtain

$$\begin{cases} P_x = -\dfrac{(\eta^2)_x}{4}, \\ Q_x = \dfrac{1}{6}\eta_{xxt}, \\ R_x = \dfrac{\rho_2}{2\rho_1}\mathcal{T}_\delta[\eta_{xt}]. \end{cases} \tag{5.13}$$

Substituting the equations in (5.13) in equation (5.11) we have

$$\eta_t + \eta_x - \alpha\left(-\frac{1}{2}\eta\eta_x + (\eta^2)_x\right) - \beta\frac{1}{6}\eta_{xxt} - \sqrt{\beta}\frac{\rho_2}{2\rho_1}\mathcal{T}_\delta[\eta_{xt}] + \mathcal{O}(\alpha\sqrt{\beta}, \beta^{3/2}) = 0,$$

which leads us to the regularized finite depth Benjamin equation

$$\eta_t + \eta_x - \frac{3\alpha}{2}\eta\eta_x - \frac{\sqrt{\beta}}{2}\frac{\rho_2}{\rho_1}\mathcal{T}_\delta[\eta_{xt}] - \frac{\beta}{6}\eta_{xxt} = 0.$$

Rewriting equation (2.9) in the general form

$$\eta_t + \eta_x - c_1\eta\eta_x - c_2\mathcal{T}_\delta[\eta_{xt}] - c_3\eta_{xxt} = 0, \tag{5.14}$$

we can calculate the phase velocity of its linear version

$$\eta_t + \eta_x - c_2\mathcal{T}_\delta[\eta_{xt}] - c_3\eta_{xxt} = 0. \tag{5.15}$$

Substituting $\eta(x,t) = \exp(\boldsymbol{i}(kx - \omega t))$ in equation (5.15) we obtain

$$\left(-\boldsymbol{i}\omega + \boldsymbol{i}k - \boldsymbol{i}\omega\frac{c_2}{\delta}\phi(\delta k) - \boldsymbol{i}\omega c_3 k^2\right)\exp(\boldsymbol{i}(kx - \omega t)) = 0,$$

thus the phase velocity is given by

$$\frac{\omega(k)}{k} = \frac{1}{1 + \frac{c_2}{\delta}\phi(\delta k) + c_3 k^2}.$$

Figure 5.1 shows the graphics of the phase velocities of system (2.5) and equation (2.9). The phase velocity of both models are very similar for small values of k, but the difference increases for larger values of k. In addition, the equation has a slower phase velocity than the system, which tends to generate a larger wave train.

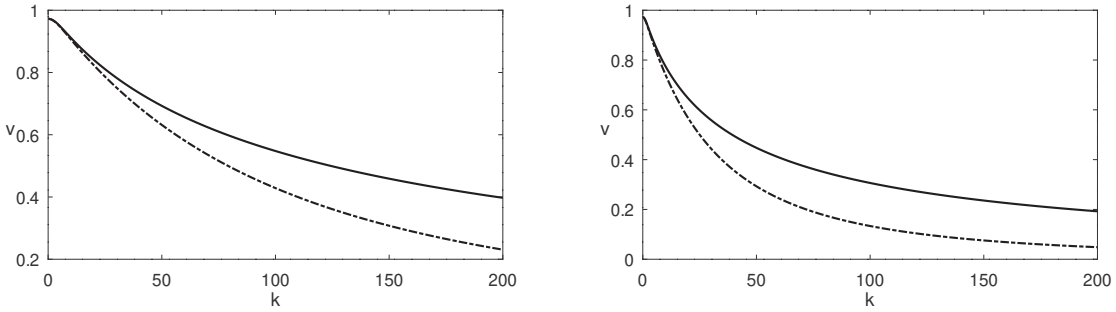

(a) $\beta = 0.0001$ (b) $\beta = 0.001$

Figure 5.1: Graphics of the phase velocity of system (2.5) (—) and equation (2.9) $(- \cdot -)$.

5.1 Travelling waves of the regularized equation

In this section we will study the existence of periodic travelling wave solutions for equation (5.14). We will use the fixed point method used to prove the existence of travelling wave solutions for the Benjamin equation in [6] adapting some results and notations from [24].

A classical solution for the equation must be at least three times differentiable, but initially we will consider weak solutions. In this case we will change the problem to another formulation where the solution can be a function in the L^2_{per} space. At the end we will prove that the obtained solution has enough regularity to be a classical solution of the equation.

Making the change of variables $\eta^* = -\frac{c_1}{2}\eta$ in equation (5.14) and dropping the asterisks we obtain

$$\eta_t + \eta_x + 2\eta\eta_x - c_2\mathcal{T}_\delta[\eta_{xt}] - c_3\eta_{xxt} = 0.$$

Supposing that this equation admits a travelling wave solution $\eta(x,t) = \varphi(x - ct)$ let us substitute this expression in it. Integrating the resulting equation once and considering the integration constant to be equal to zero we have

$$-c\varphi + \varphi + \varphi^2 + c_2 c\mathcal{T}_\delta[\varphi'] + c_3 c\varphi'' = 0.$$

Making another change of variables $\varphi = c\varphi^*$ and dropping the asterisks we get

$$B\varphi - c_2\mathcal{T}_\delta[\varphi'] - c_3\varphi'' = \varphi^2, \tag{5.16}$$

where $B = \frac{c-1}{c}$. In the following computations it will be necessary that $B > 0$, thus we suppose that $c > 1$. Note that equation (5.16) has two trivial solutions $\varphi \equiv 0$ and $\varphi \equiv B$ although we want to prove that it admits a non-trivial solution.

Let us suppose that the travelling wave φ is $2l$-periodic and even, so its Fourier series can be written as

$$\varphi(x) = \sum_{k\in\mathbb{Z}} a_k \cos(k\pi x/l), \tag{5.17}$$

where

$$a_k = \frac{1}{l}\int_0^l \varphi(x)\cos(k\pi x/l)dx = a_{-k}.$$

Since the Fourier coefficients of φ^2 are given by the convolution $(a * a)_k = \sum_{m\in\mathbb{Z}} a_{k+m}a_m$ see, for example, [6], substituting expression (5.17) in equation (5.16) we can see that coefficients a_k satisfy

$$a_k = \frac{1}{w_k}(a * a)_k,\ k \in \mathbb{Z}, \tag{5.18}$$

where $w_k = B + \frac{c_2}{\delta}\phi(\delta k\pi/l) + c_3(k\pi/l)^2$. Note that the sequences corresponding to $\varphi \equiv 0$ and $\varphi \equiv B$ are solutions of equation (5.18). However, we want a solution that is a non-trivial sequence which will correspond to a non-trivial solution of equation (5.16).

We can write (5.18) in an operator form $a = \mathcal{A}a$ where $(\mathcal{A}a)_k = w_k^{-1}(a * a)_k$. The operator $\mathcal{A} : l_2(\mathbb{Z}) \to l_2(\mathbb{Z})$ is well defined because by Holder's inequality, $|(a * a)_k| \leqslant \|a\|_2^2$ for all $k \in \mathbb{Z}$ and $w^{-1} = \{w_k^{-1}\}_{k\in\mathbb{Z}} \in l_2(\mathbb{Z})$. Thus, if we find a real sequence a which is a non-trivial fixed point of $\mathcal{A}$ we will obtain a weak solution $\varphi \in L^2_{\text{per}}$ of equation (5.16).

Now let us state the main results of the fixed point index method to be used.

Definition 13. *A subset K in a Banach space is a cone if the following three statements are valid:*

- $0 \in K$.
- *if $x \in K$ then $\lambda x \in K$ for all $\lambda \geqslant 0$.*
- *if $-x$ and x belongs to K then $x = 0$.*

Let K be a closed convex cone in a Banach space and $A\colon K \to K$ a continuous and compact operator. If $\Omega \subset K$ is open in the relative topology of K and there are no fixed points of A on $\partial\Omega$ then we denote by $i(A, K, \Omega)$ the fixed point index of A in Ω. The definition of the integer number $i(A, K, \Omega)$ is quite technical but can be found in detail in [23]. For our purposes, it is enough to sumarize here that the index i has the following properties:

- Let $\Omega \subset K$ be an open subset in the relative topology of K. If $Ax = x_0$, $\forall x \in \Omega \subset K$ for some $x_0 \in \Omega$ then $i(A, K, \Omega) = 1$;
- Let $\Omega_1, \Omega_2 \subset K$ be two open and disjoint subsets in the relative topology of K. If $\overline{\Omega}_1 \cap \overline{\Omega}_2$ is an empty set then

$$i(A, K, \Omega_1 \cup \Omega_2) = i(A, K, \Omega_1) + i(A, K, \Omega_2);$$

- Let $\Omega \subset K$ be an open subset in the relative topology of K. If $i(A, K, \Omega) \neq 0$ then A has a fixed point in Ω.

For $0 < r < R$ let us define $K_r = \{x \in K; \|x\| < r\}$, $\partial K_r = \{x \in K; \|x\| = r\}$ and $K_r^R = \{x \in K; r < \|x\| < R\}$. The following lemma is adapted from [24].

Lemma 5.1. *Let K be a convex cone in a Banach space and $A : K \to K$ a continuous and compact operator. Then the three following statements are valid:*

1. *Let $r > 0$ be a constant. If $x - tAx \neq 0$, $\forall x \in \partial K_r$ and $t \in [0, 1]$ then $i(A, K, K_r) = 1$;*
2. *Let $r > 0$ be a constant. If there exists $\zeta \in K$ with $\zeta \neq 0$ such that $x - Ax \neq s\zeta$, $\forall x \in \partial K_r$ and $s \geqslant 0$ then $i(A, K, K_r) = 0$;*
3. *Let $\Omega \subset K$ be an open subset in the relative topology of K such that A has no fixed points in $\partial\Omega$. If there exists $\zeta \in K$ with $\zeta \neq 0$ such that $x - Ax \neq s\zeta$, $\forall x \in \partial\Omega$ and $s \geqslant 0$ then $i(A, K, \Omega) = 0$.*

Let us define an appropriate cone for the domain of $\mathcal{A}$ in order to ensure that the operator satisfies the hypothesis of lemma 5.1. Denoting $\lambda = \|w^{-1}\|_2$ we define the cone $\mathcal{K}$ as

$$\mathcal{K} = \{a \in l_2(\mathbb{Z}); \|a\|_2 \leqslant \lambda w_0 a_0 \text{ and } a_k = a_{-k} \geqslant 0 \; \forall k \in \mathbb{Z}\}.$$

Note that $\mathcal{K}$ admits non-trivial sequences since $\lambda w_0 > 1$ and it is a convex subset by the triangular inequality. For $a \in \mathcal{K}$ we have that $b = \mathcal{A}a \in l_2(\mathbb{Z})$ moreover, $b_k = b_{-k} \geqslant 0$ since $w_k = w_{-k} \geqslant 0$. On the other hand, we obtain that $b_k \leqslant \frac{1}{w_k}\|a\|_2^2$ and in particular $b_0 = \frac{1}{w_0}\|a\|_2^2$, therefore we have $\|b\|_2 \leqslant \lambda\|a\|_2^2 = \lambda w_0 b_0$, that is $b \in \mathcal{K}$ and $\mathcal{A}$ maps $\mathcal{K}$ into itself.

Lemma 5.2. *The operator $\mathcal{A} : \mathcal{K} \to \mathcal{K}$ is continuous and compact.*

Proof. To prove the continuity of $\mathcal{A}$ let $a, b \in \mathcal{K}$. Thus we obtain

$$\begin{aligned}
|(a * a)_k - (b * b)_k| &= |\sum_{m\in\mathbb{Z}} a_{k+m}a_k - b_{k+m}b_k| \\
&= |\sum_{m\in\mathbb{Z}} a_{k+m}(a_k - b_k) + b_k(b_{k+m} - a_{m+k})| \\
&\leqslant |\sum_{m\in\mathbb{Z}} a_{k+m}(a_k - b_k)| + |\sum_{m\in\mathbb{Z}} b_k(b_{k+m} - a_{m+k})|.
\end{aligned}$$

By Holder's inequality we have

$$|\sum_{m\in\mathbb{Z}} a_{k+m}(a_k - b_k)| \leqslant \|a\|_2\|a - b\|_2 \text{ and } |\sum_{m\in\mathbb{Z}} b_k(b_{k+m} - a_{m+k})| \leqslant \|b\|_2\|a - b\|_2.$$

Therefore, $|(a * a)_k - (b * b)_k| \leqslant (\|a\|_2 + \|b\|_2)\|a - b\|_2$. Thus we get

$$\|\mathcal{A}a - \mathcal{A}b\|_2 \leqslant \sqrt{\sum_{k\in\mathbb{Z}} w_k^{-2}|(a * a)_k - (b * b)_k|^2} \leqslant \lambda(\|a\|_2 + \|b\|_2)\|a - b\|_2.$$

Therefore, $\mathcal{A}$ is continuous.

For the compactness let us consider the family of operators $\mathcal{A}_N$ which are defined by

$$(\mathcal{A}_N a)_k = \begin{cases} (\mathcal{A}a)_k & \text{for } |k| \leqslant N, \\ 0 & \text{for } |k| > N. \end{cases}$$

Observe that $\|\mathcal{A}_N a - \mathcal{A}a\|_2^2 \leqslant \sum_{|k|>N} w_k^{-2}\|a\|_2^2$. In bounded sets, since $\sum_{|k|>N} w_k^{-2} \to 0$ as $N \to \infty$, $\mathcal{A}$ is the uniform limit of finite rank operators and therefore is compact.

□

Lemma 5.3. *let r be a positive constant. If $r < 1/\lambda$, then $i(\mathcal{A}, \mathcal{K}, \mathcal{K}_r) = 1$.*

Proof. Consider $a \in \partial\mathcal{K}_r$ and take the component $k = 0$ of $a - t\mathcal{A}a$. Using that $a_0 = \|a\|_2/(\lambda w_0)$ we get

$$a_0 - \frac{t}{w_0}\|a\|_2^2 = \frac{1}{w_0}\left(\frac{1}{\lambda} - t\|a\|_2\right)\|a\|_2,$$

since $\|a\|_2 < \frac{1}{\lambda}$ and $t \in [0,1]$ we obtain $(a - t\mathcal{A}a)_0 > 0$. Therefore $a - t\mathcal{A}a \neq 0\ \forall a \in \partial\mathcal{K}_r$ and $t \in [0,1]$. By item 1 of lemma 5.1 $i(\mathcal{A}, \mathcal{K}, \mathcal{K}_r) = 1$.

□

Lemma 5.4. *Let R be a positive constant. If $R > w_0$ then $i(\mathcal{A}, \mathcal{K}, \mathcal{K}_R) = 0$.*

Proof. Let $\zeta \in \mathcal{K}$ such that $\zeta_0 > 0$. Consider $a \in \partial\mathcal{K}_R$ and take the component $k = 0$ of $a - \mathcal{A}a$, since $\|a\|_2 > w_0$,

$$a_0 - \frac{1}{w_0}\|a\|_2^2 < \|a\|_2 - \frac{1}{w_0}\|a\|_2^2 < 0,$$

then $(a - \mathcal{A}a)_0 \neq s\zeta_0\ \forall s \geqslant 0$ and by item 2 of lemma 5.1 we conclude that $i(\mathcal{A}, \mathcal{K}, \mathcal{K}_R) = 0$.

□

With the last lemmas we can conclude that $i(\mathcal{A}, \mathcal{K}, \mathcal{K}_r^R) = -1$. Unfortunately, since $r < w_0 < R$ the sequence corresponding to $\varphi \equiv B$ belongs to $\mathcal{K}_r^R$ and we have no guarantee that there is a non-trivial fixed point of $\mathcal{A}$ in $\mathcal{K}_r^R$. Thus, we must isolate this sequence in a small neighborhood and use item 3 of lemma 5.1 to guarantee that there exists a non-trivial fixed point of $\mathcal{A}$ in $\mathcal{K}_r^R$. Defining the sequence d as $d_0 = w_0$ and $d_k = 0$ for $k \neq 0$ we denote the neighborhood of d by $V_\epsilon(d) = \{a \in \mathcal{K}; \|d - a\|_2 < \epsilon\}$.

Lemma 5.5. *If $2w_0 > w_1$ and $\epsilon > 0$ is chosen sufficiently small then $i(\mathcal{A}, \mathcal{K}, V_\epsilon(d)) = 0$.*

Proof. Note that $b \in \partial V_\epsilon(d)$ is of the form $b = d + h$ where $\|h\|_2 = \epsilon > 0$, thus

$$(b * b)_k = 2w_0 h_k + (h * h)_k,$$

then

$$(b - \mathcal{A}b)_k = d_k + \left(1 - \frac{2w_0}{w_k}\right)h_k - \frac{1}{w_k}(h * h)_k.$$

By the definition of b we have that $h_k \geqslant 0$ for $k \neq 0$, thus

$$-(h * h)_1 < 2|h_0|h_1 < 2\epsilon h_1.$$

Therefore,

$$(b - \mathcal{A}b)_1 = \left(1 - \frac{2w_0}{w_1}\right)h_1 - \frac{1}{w_1}(h * h)_1 < \left(1 - \frac{2w_0}{w_1} + \frac{2\epsilon}{w_1}\right)h_1.$$

Note that if l is chosen large enough then $2w_0 > w_1$ is valid. So, if $\epsilon > 0$ is sufficiently small then $(b - \mathcal{A}b)_1 < 0$. Thus, choosing $\zeta \in K$ so that $\zeta_1 > 0$ we have $b - \mathcal{A}b \neq s\zeta$, $\forall b \in \partial V_\epsilon(d)$ and $s \geqslant 0$. Therefore $i(\mathcal{A}, \mathcal{K}, V_\epsilon(d)) = 0$.

□

Theorem 5.6. *If $2w_0 > w_1$, then operator $\mathcal{A}$ has a non-trivial fixed point in $\mathcal{K}_r^R$ for $0 < r < w_0 < R$.*

Proof. From lemmas 5.3 and 5.4 we have that $i(\mathcal{A}, \mathcal{K}, \mathcal{K}_r^R) = -1$. If $2w_0 > w_1$ and $\epsilon > 0$ is chosen small enough we obtain $i(\mathcal{A}, \mathcal{K}, V_\epsilon(d)) = 0$ by lemma 5.5. Moreover, if ϵ is so that $V_\epsilon(d) \subset \mathcal{K}_r^R$ then we have that $i(\mathcal{A}, \mathcal{K}, \mathcal{K}_r^R \backslash V_\epsilon(d)) = -1$. Therefore, operator $\mathcal{A}$ has a non-trivial fixed point in $\mathcal{K}_r^R \backslash V_\epsilon(d)$.

□

The non-trivial fixed point a of operator $\mathcal{A}$ corresponds to a function $\varphi \in L^2_{\text{per}}$, however we want φ to be a smooth function. So let us enunciate the theorem which will guarantee the existence of a C^∞ travelling solution.

Theorem 5.7. *If the half period l is chosen large enough then there exists a non-trivial $2l$-periodic C^∞ function φ which is a solution of equation (5.16).*

Proof. Due to the considerations made previously, we just need to prove that the function φ corresponding to the non-trivial fixed point a of $\mathcal{A}$ belongs to $H^s_{\text{per}}([-l, l])$ for all $s \geqslant 0$. Since a is a fixed point of $\mathcal{A}$ it satisfies $w_k a_k \leqslant \|a\|_2^2$, then

$$\sum_{k\in\mathbb{Z}} |a_k| \leqslant \sum_{k\in\mathbb{Z}} \frac{\|a\|_2^2}{w_k} = \|a\|_2^2 \sum_{k\in\mathbb{Z}} \frac{1}{w_k} < \infty.$$

So we have

$$\sum_{k\in\mathbb{Z}} w_k |a_k|^2 \leqslant \sum_{k\in\mathbb{Z}} |a_k| \|a\|_2^2 \leqslant \|a\|_2^2 \sum_{k\in\mathbb{Z}} |a_k| < \infty.$$

Observe that w_k grows like $1 + |k|^2$, thus $\sum_{k\in\mathbb{Z}} (1 + |k|^2)|a_k|^2 < \infty$, that is, $\varphi \in H^1_{\text{per}}([-l, l])$. Thus, by Theorem 3.2 we conclude that $\varphi^2 \in H^1_{\text{per}}([-l, l])$ and

$$\sum_{k\in\mathbb{Z}} (1 + |k|^2)|(a * a)_k|^2 = \sum_{k\in\mathbb{Z}} (1 + |k|^2) w_k^2 |a_k|^2 < \infty.$$

Therefore, $\sum_{k\in\mathbb{Z}} (1+|k|^2)^3 |a_k|^2 < \infty$, that is $\varphi \in H^3_{\text{per}}([-l, l])$. Repeating this process we obtain that $\varphi \in H^s_{\text{per}}([-l, l])$ for all $s \geqslant 0$ so φ is a C^∞ function and a solution of equation (5.16).

□

Therefore, returning to the original variables we have that equation (5.14) admits a periodic and C^∞ travelling wave solution. We remark that, with some adaptions, these computations can be applied to prove the existence of travelling waves for the regularized Benjamin equation using the operator $\mathcal{H}$ instead of $\mathcal{T}_\delta$.

Chapter 6

Travelling waves for the flat bottom nonlinear system

In this chapter we will study the existence of travelling wave solutions for the nonlinear system (2.5). In the last chapter we proved the existence of travelling waves for the unidirectional equation (5.14), unfortunately it was not yet possible to show the existence of this type of solution for the nonlinear system. The technique employed by Pipicano and Grajales in [24] could not be used because the system considered by them has dispersive terms in both equations, unlike the system considered here. This dispersive term absent in the first equation proved to be crucial to employ the aforementioned technique in our system.

Since, from a theoretical point of view, we do not have results about travelling waves for the nonlinear system (2.5), we are going to adopt a numerical approach to this problem. We will present three methods to compute travelling waves for this nonlinear system and compare the results obtained by these methods.

A first numerical approach to generate approximated travelling waves was proposed by the author in [16] and was based on the one presented by Santos in [10] for the system

$$\begin{cases} \eta_t - \left[(1-\alpha\eta)u\right]_x = 0, \\ u_t + \alpha u\, u_x - \eta_x = \sqrt{\beta}\,\dfrac{\rho_2}{\rho_1}\mathcal{T}_\delta\left[u\right]_{xt}, \end{cases} \tag{6.1}$$

which was based on the strategy implemented in [25].

The approach proposed in [16] is the following: supposing that system (2.5) admits a travelling wave solution, we define the variable $y = x - ct$ and the functions $\tilde{\eta}(y) = \eta(x-ct,0) = \eta(x,t)$ and $\tilde{u}(y) = u(x-ct,0) = u(x,t)$. Using the chain rule we obtain the system

$$\begin{cases} -c\tilde{\eta}_y - \tilde{u}_y + \alpha(\tilde{\eta}\tilde{u})_y = 0, \\ -c\tilde{u}_y + \alpha\tilde{u}\tilde{u}_y - \tilde{\eta}_y + c\sqrt{\beta}\dfrac{\rho_2}{\rho_1}\mathcal{T}_\delta\big[\tilde{u}_{yy}\big] + c\dfrac{\beta}{3}\tilde{u}_{yyy} = 0. \end{cases}$$

Integrating both equations on y and considering the integration constant to be equal to zero we have

$$\begin{cases} -c\tilde{\eta} - (1-\alpha\tilde{\eta})\tilde{u} = 0, \\ -c\tilde{u} + \dfrac{\alpha}{2}\tilde{u}^2 - \tilde{\eta} + c\sqrt{\beta}\dfrac{\rho_2}{\rho_1}\mathcal{T}_\delta\big[\tilde{u}_y\big] + c\dfrac{\beta}{3}\tilde{u}_{yy} = 0. \end{cases} \tag{6.2}$$

Now we isolate $\tilde{u}$ in the first equation of system (6.2) and use a second order approximation to get

$$\tilde{u} = -\frac{c\tilde{\eta}}{1-\alpha\tilde{\eta}} = -c\tilde{\eta} - c\alpha\tilde{\eta}^2 + \mathcal{O}(\alpha^2). \tag{6.3}$$

Substituting this expression in the second equation of system (6.2) and discarding the terms of order $\mathcal{O}(\alpha\sqrt{\beta}, \alpha\beta, \alpha^2)$ we have,

$$\alpha\frac{3}{2}\tilde{\eta}^2 + \left[1 - \frac{1}{c^2}\right]\tilde{\eta} - \sqrt{\beta}\frac{\rho_2}{\rho_1}\mathcal{T}_\delta\big[\tilde{\eta}_y\big] - \frac{\beta}{3}\tilde{\eta}_{yy} = 0. \tag{6.4}$$

Considering a discretization analogous to the one made in Chapter 4 the following system of equations is obtained

$$\alpha\frac{3}{2}\begin{bmatrix}\tilde{\eta}_1^2\\ \vdots \\ \tilde{\eta}_N^2\end{bmatrix} + \left(\left(1 - \frac{1}{c^2}\right)I - \sqrt{\beta}\frac{\rho_2}{\rho_1}T - \frac{\beta}{3}S\right)\begin{bmatrix}\tilde{\eta}_1\\ \vdots \\ \tilde{\eta}_N\end{bmatrix} = 0, \tag{6.5}$$

where

$$T = \frac{1}{N}\overline{F}^T\hat{T}F, \quad \hat{T} = \operatorname{diag}\left(-\frac{1}{\delta}\phi(k\pi\delta/l)\right)$$

and

$$S = \frac{1}{N}\overline{F}^T\hat{S}F, \quad \hat{S} = \operatorname{diag}\left(-(k\pi/l)^2\right).$$

This system is solved numerically by Newton's method. The resulting profiles have very small amplitude and changes in a given time interval. In fact the method seems to converge to the null vector which is a trivial solution of system (6.5), also the initial conditions were not adequately adjusted for the method.

One of the problems with the method used in [16] is that velocity c is a fixed parameter and we do not know what its value should be. For example, for the unidirectional equation and the system considered in [24], the speed of the travelling waves must be greater than 1, which may indicate that the same must be true for system (2.5), but the numerical results of this chapter indicates the opposite.

As an enhancement to this approach, let us consider c as an unknown variable and complete the system (6.5) with the conservation law (3.4) approximated by the trapezoidal rule (4.20). That is,

$$\frac{1}{N}\sum_{j=1}^{N}\tilde{\eta}_j = d. \tag{6.6}$$

To maintain consistency with the physical settings of the problem, the constant d must be equal to zero, however in this case the null vector is again a solution of the problem. Thus, setting nonzero values of d we avoid the possibility of a null solution and can generate different solutions depending on this parameter. In the numerical tests of this chapter we will consider two options for the constant d. In the first option we set $d = 0$ and make the adjustment in the initial guess for the Newton's method as in Section 4.2. In the other option we do not make the adjustment in the initial guess, set d as the mean of the profile computed by the trapezoidal rule.

Therefore, the first method to generate travelling waves for the nonlinear system (2.5) consists in solve the system of equations composed of (6.5) and (6.6) by Newton's method. With the resulting $\tilde{\eta}$ and c we obtain $\tilde{u}$ using the approximation given by expression (6.3).

Another problem in the original approach is the large number of approximations made, since $\tilde{u}$ appears many times in the second equation of system (6.2), that may compromise the results.

This fact motivates us to propose a new method where no approximations are made. In this case we will obtain an equation on $\tilde{u}$ isolating $\tilde{\eta}$ on the first equation of (6.2) to obtain

$$\tilde{\eta} = \frac{\tilde{u}}{\alpha\tilde{u} - c}, \tag{6.7}$$

and substituting this expression on the second equation of (6.2) to obtain

$$-c\tilde{u} + \frac{\alpha}{2}\tilde{u}^2 - \frac{\tilde{u}}{\alpha\tilde{u} - c} + c\sqrt{\beta}\frac{\rho_2}{\rho_1}\mathcal{T}_\delta\big[\tilde{u}_y\big] + c\frac{\beta}{3}\tilde{u}_{yy} = 0. \tag{6.8}$$

Using the same discretization as before we get the following system

$$\frac{\alpha}{2}\begin{bmatrix} \tilde{u}_1^2 \\ \vdots \\ \tilde{u}_N^2 \end{bmatrix} - \begin{bmatrix} \tilde{u}_1/(\alpha\tilde{u}_1 - c) \\ \vdots \\ \tilde{u}_N/(\alpha\tilde{u}_N - c) \end{bmatrix} + c\left(-I + \sqrt{\beta}\frac{\rho_2}{\rho_1}T + \frac{\beta}{3}S\right)\begin{bmatrix} \tilde{u}_1 \\ \vdots \\ \tilde{u}_N \end{bmatrix} = 0. \tag{6.9}$$

Again c is considered as an unknown and the system is completed with the numerical version of the conservation law (3.4), that due to equality (6.7) becomes

$$\frac{1}{N}\sum_{j=1}^{N}\frac{\tilde{u}_j}{\alpha\tilde{u}_j - c} = d. \tag{6.10}$$

As in the previous case, the system is solved by Newton's method and $\tilde{\eta}$ is calculated by expression (6.7).

Although the second method has no approximations, it is necessary to calculate $\tilde{\eta}$ separately after applying Newton's method. In view of this, in the third method option we consider $\tilde{\eta}$ and $\tilde{u}$ together to discretize the complete system (6.2) which becomes

$$\begin{cases} c\begin{bmatrix} \tilde{\eta}_1 \\ \vdots \\ \tilde{\eta}_N \end{bmatrix} + \begin{bmatrix} (1-\alpha\tilde{\eta}_1)\tilde{u}_1 \\ \vdots \\ (1-\alpha\tilde{\eta}_N)\tilde{u}_N \end{bmatrix} = 0, \\ \dfrac{\alpha}{2}\begin{bmatrix} \tilde{u}_1^2 \\ \vdots \\ \tilde{u}_N^2 \end{bmatrix} - \begin{bmatrix} \tilde{\eta}_1 \\ \vdots \\ \tilde{\eta}_N \end{bmatrix} + c\left(-I + \sqrt{\beta}\dfrac{\rho_2}{\rho_1}T + \dfrac{\beta}{3}S\right)\begin{bmatrix} \tilde{u}_1 \\ \vdots \\ \tilde{u}_N \end{bmatrix} = 0. \end{cases} \tag{6.11}$$

As in the previous cases we will consider c as an unknown variable and complete the system with the conservation law (3.4) approximated by the trapezoidal rule (6.6).

In summary, the three approaches presented in this section are the following: the first approach was given by system (6.5) and equation (6.6), for the second approach we considered system (6.9) and equation (6.10). The third approach was defined by system (6.11) and equation (6.6).

In order to have a quantitative comparison of the methods, we defined the following procedure to compare the results obtained by them. The wave velocity obtained from Newton's method in each test is denoted by c_{met} and the numerical wave speed c_n is computed as follows. For each time $t_j = j\Delta t$, $j = 1, 2, \ldots, J$, J big enough, we find the grid point x_{l_j} that minimizes η_l^j and make a linear regression on the points $\{(t_j, x_{l_j})\}$ to estimate c_n. Using Fourier properties and the DFT, we define $\boldsymbol{\eta}^*$ as the approximation of $\eta(x - c_n t, 0)$ by $\widehat{\eta}_k^* = \exp(-\boldsymbol{i}k\pi c_n t/l)\widehat{\eta}_k^0$. We define the absolute error e_{abs} and the relative error e_{rel} at a chosen $t_n = n\Delta t$, respectively,

by

$$e_{\text{abs}} = \|\boldsymbol{\eta}^* - \boldsymbol{\eta}^n\|_2, \text{ and } e_{\text{rel}} = \frac{\|\boldsymbol{\eta}^* - \boldsymbol{\eta}^n\|_2}{\|\boldsymbol{\eta}^*\|_2}.$$

We will set the parameters as in Section 4.2, $\rho_1 = 1$, $\rho_2 = 2$, $h_1 = 0.1$, $h_2 = 3.505$ and $\Delta x = 0.03068$. The values of β, α, l and Δt are specified in each test. The other values are calculated by the relations $L = h_1/\sqrt{\beta}$ and $\delta = h_2/L$.

6.1 Initial guesses for the methods

Since Newton's method has local convergence we must choose good initial guesses. For that we will consider the BBM and rILW equations, that can be obtained from the unidirectional equation (5.14), whose travelling waves have known expressions. So, discarding the term with η_{xxt} in equation (5.14), we obtain the regularized Intermediate Long Wave (rILW) equation

$$\eta_t + \eta_x - c_1\eta\eta_x - c_2\mathcal{T}_\delta[\eta_{xt}] = 0,$$

and discarding the term with the operator $\mathcal{T}_\delta$ we get the Benjamin-Bona-Mahony (BBM) equation

$$\eta_t + \eta_x - c_1\eta\eta_x - c_3\eta_{xxt} = 0. \tag{6.12}$$

We can see in [25] that a travelling wave solution family for the rILW equation is

$$\eta(y) = \frac{a\cos^2(\theta)}{\cos^2(\theta) + \sinh^2(y/\lambda)},\ y = x - ct, \tag{6.13}$$

with

$$a = \frac{4cc_2\theta\tan\theta}{\delta c_1},\ c = \frac{1}{1 + \frac{2c_2}{\delta}\theta\cot(2\theta)},\ \lambda = \frac{\delta}{\theta},\ 0 < \theta < \pi/2.$$

Also, it is proven in Appendix A that for $c > 1$ the travelling wave solution of the BBM equation (6.12) is

$$\eta(y) = -\frac{3(c-1)}{c_1}\operatorname{sech}^2\left(\frac{\sqrt{c-1}y}{2\sqrt{cc_2}}\right). \tag{6.14}$$

Since we are considering solutions which are periodic on the x variable, periodic travelling wave solutions of the BBM and the rILW equations should be more appropriate as initial guesses. Natali proved in [22] that a periodic travelling wave solution for the KdV equation can be obtained by a periodization of the solitary travelling wave solution, for a period $L > 0$. This fact motivates us to consider as initial guesses periodizations of the waves (6.14) and (6.13) by

$$\eta_p(x) = \sum_{j=-10}^{10} \eta(x + j2l).$$

Before using the BBM and rILW wave profiles as initial guesses for the methods for obtaining travelling waves, let's test them as initial conditions in the numerical method for the nonlinear system and see how they advance in time. Figures 6.1–6.4 present the graphics of the evolution $\boldsymbol{\eta}^n$ for the travelling wave initial condition $\boldsymbol{\eta}^0$ of each equation and the corresponding approximate translation $\boldsymbol{\eta}^*$. For BBM profiles the dispersion appears with loss of amplitude which is more pronounced as β and c increases, however, the wave train is much smaller compared to the results obtained for the Gaussian profile in the Section 4.2. On the other hand, the

rILW profiles preserve well their shapes and the graphics of $\boldsymbol{\eta}^n$ and $\boldsymbol{\eta}^*$ coincide. This fact is confirmed by the small errors presented in tables 6.1–6.4, that is, the rILW profile works fine as travelling wave for the nonlinear system (2.5). In view of that, for the next experiments we will use only the rILW profiles as initial condition. Also, note that the numerical wave velocity c_n is smaller than 1 in all cases, contrary to the theoretical estimate based on similar models presented at the beginning of the chapter.

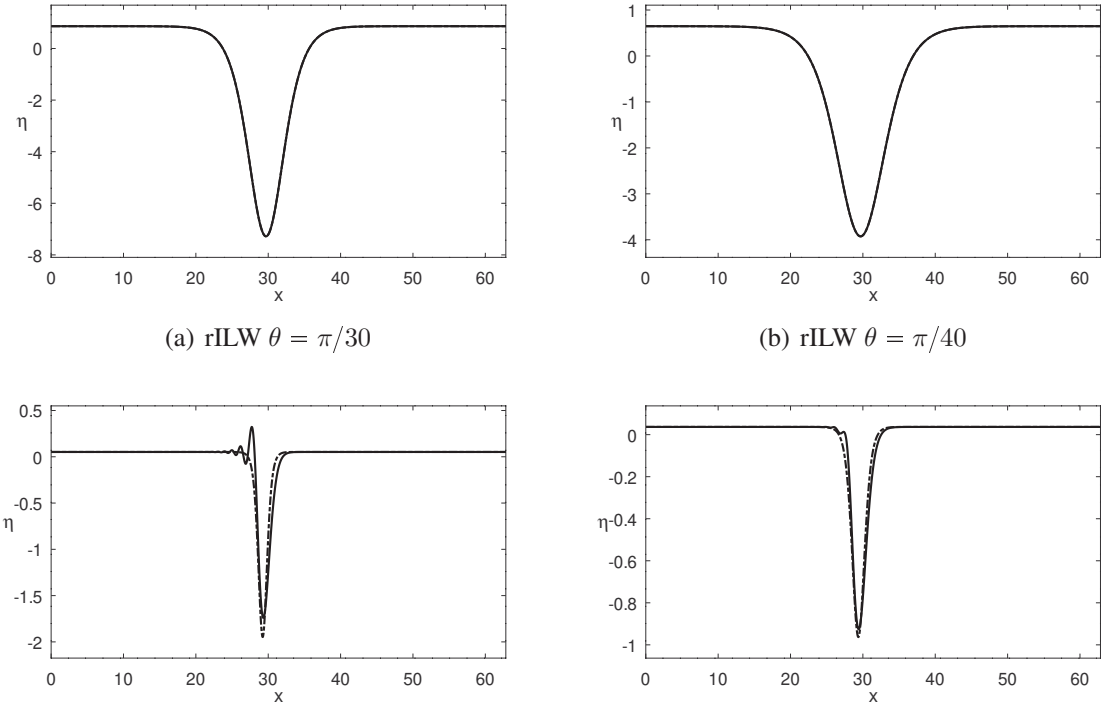

(a) rILW $\theta = \pi/30$

(b) rILW $\theta = \pi/40$

(c) BBM $c = 1 + \alpha$

(d) BBM $c = 1 + \alpha/2$

Figure 6.1: Graphics of $\boldsymbol{\eta}^*$ $(- \cdot -)$ and $\boldsymbol{\eta}^n$ $(—)$ for each initial guess with $l = 10\pi$, $\alpha = \beta = 0.0001$, $\Delta x = 0.03068$, $\Delta t = 0.08043$ at time $t = 62.81254 = 781\Delta t$.

Profiles	e_{abs}	e_{rel}	c_n	c
rILW $\theta = \pi/30$	0.0116351	0.0001295	0.97289	0.97266
rILW $\theta = \pi/40$	0.0221550	0.0003925	0.97273	0.97248
BBM $c = 1 + \alpha$	3.6931012	0.3162016	0.96554	1.00010
BBM $c = 1 + \alpha/2$	1.1554772	0.1677999	0.96778	1.00005

Table 6.1: Errors at time $t = 62.81254 = 781\Delta t$ and wave velocities of η for each initial guess with $l = 10\pi$, $\alpha = \beta = 0.0001$, $\Delta x = 0.03068$, $\Delta t = 0.08043$.

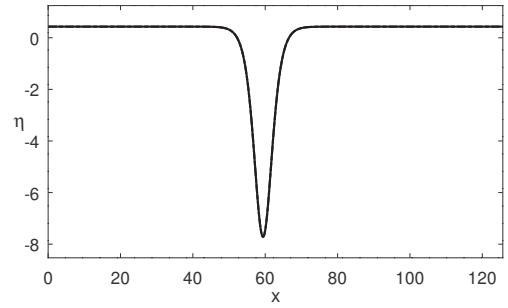

(a) rILW $\theta = \pi/30$

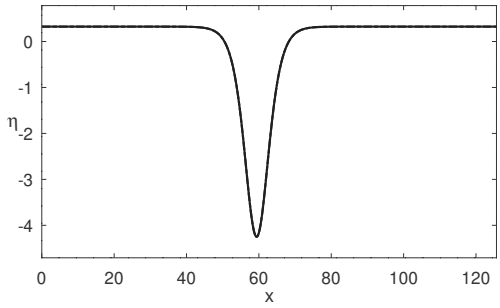

(b) rILW $\theta = \pi/40$

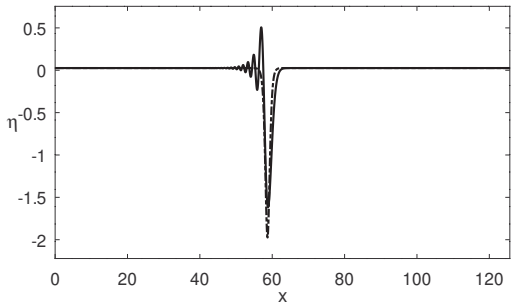

(c) BBM $c = 1 + \alpha$

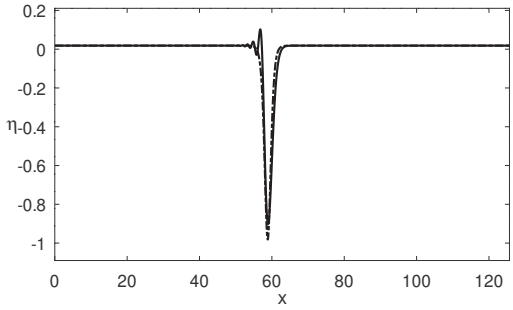

(d) BBM $c = 1 + \alpha/2$

Figure 6.2: Graphics of $\boldsymbol{\eta}^*$ $(- \cdot -)$ and $\boldsymbol{\eta}^n$ $(—)$ for each initial guess with $l = 20\pi$, $\alpha = \beta = 0.0001$, $\Delta x = 0.03068$, $\Delta t = 0.08043$ at time $t = 125.62508 = 1562\Delta t$.

Profiles	e_{abs}	e_{rel}	c_n	c
rILW $\theta = \pi/30$	0.0224622	0.0002389	0.97295	0.97266
rILW $\theta = \pi/40$	0.0171695	0.0002855	0.97279	0.97248
BBM $c = 1 + \alpha$	5.0787804	0.4304986	0.96738	1.00010
BBM $c = 1 + \alpha/2$	1.8279094	0.2616618	0.96861	1.00005

Table 6.2: Errors at time $t = 125.62508 = 1562\Delta t$ and wave velocities of η for each initial guess with $l = 20\pi$, $\alpha = \beta = 0.0001$, $\Delta x = 0.03068$, $\Delta t = 0.08043$.

Profiles	e_{abs}	e_{rel}	c_n	c
rILW $\theta = \pi/30$	0.0037089	0.0003018	0.97259	0.97266
rILW $\theta = \pi/40$	0.0016790	0.0002551	0.97252	0.97248
BBM $c = 1 + \alpha$	8.3822192	0.7175269	0.94978	1.00100
BBM $c = 1 + \alpha/2$	3.6962996	0.5367247	0.95249	1.00050

Table 6.3: Errors at time $t = 62.78557 = 439\Delta t$ and wave velocities of η for each initial guess with $l = 10\pi$, $\alpha = \beta = 0.001$, $\Delta x = 0.03068$, $\Delta t = 0.14302$.

Profiles	e_{abs}	e_{rel}	c_n	c
rILW $\theta = \pi/30$	0.0020079	0.0001332	0.97281	0.97266
rILW $\theta = \pi/40$	0.0008429	0.0000915	0.97269	0.97248
BBM $c = 1 + \alpha$	9.6674115	0.8192695	0.95829	1.00100
BBM $c = 1 + \alpha/2$	4.5562339	0.6521451	0.95902	1.00050

Table 6.4: Errors at time $t = 125.57114 = 878\Delta t$ and wave velocities of η for each initial guess with $l = 20\pi$, $\alpha = \beta = 0.001$, $\Delta x = 0.03068$, $\Delta t = 0.14302$.

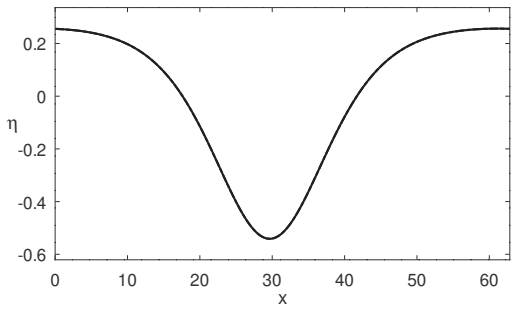

(a) rILW $\theta = \pi/30$

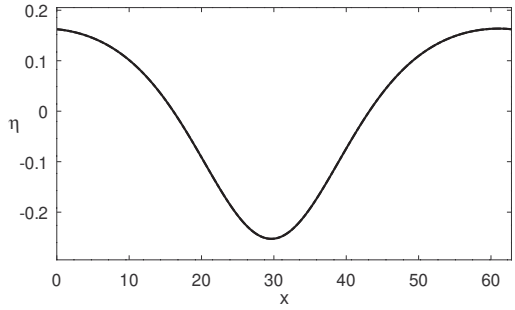

(b) rILW $\theta = \pi/40$

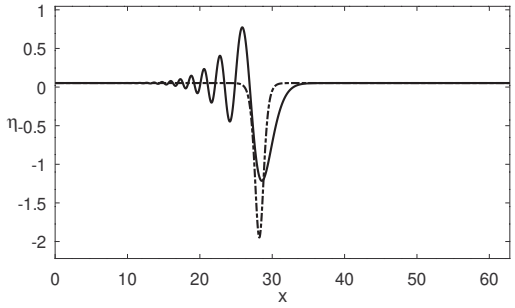

(c) BBM $c = 1 + \alpha$

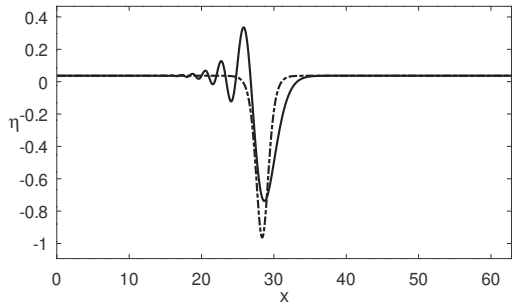

(d) BBM $c = 1 + \alpha/2$

Figure 6.3: Graphics of $\boldsymbol{\eta}^*$ $(- \cdot -)$ and $\boldsymbol{\eta}^n$ $(—)$ for each initial guess with $l = 10\pi$, $\alpha = \beta = 0.001$, $\Delta x = 0.03068$, $\Delta t = 0.14302$ at time $t = 62.78557 = 439\Delta t$.

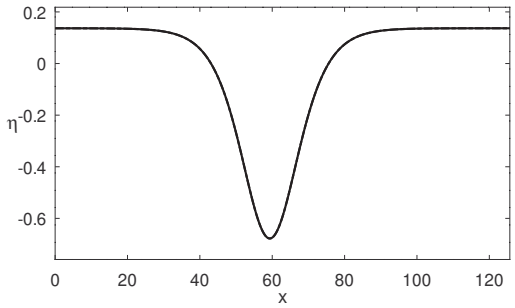

(a) rILW $\theta = \pi/30$

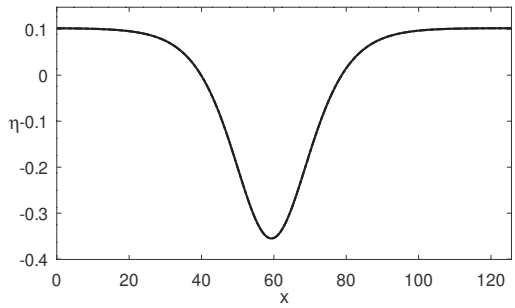

(b) rILW $\theta = \pi/40$

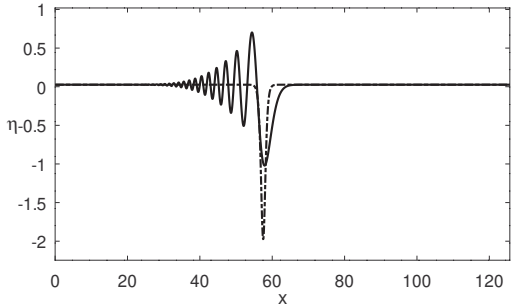

(c) BBM $c = 1 + \alpha$

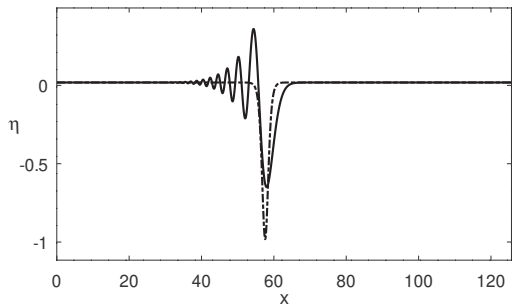

(d) BBM $c = 1 + \alpha/2$

Figure 6.4: Graphics of $\boldsymbol{\eta}^*$ $(- \cdot -)$ and $\boldsymbol{\eta}^n$ $(—)$ for each initial guess with $l = 20\pi$, $\alpha = \beta = 0.001$, $\Delta x = 0.03068$, $\Delta t = 0.14302$ at time $t = 125.57114 = 878\Delta t$.

From the results obtained in these experiments, the question that arises is: why did the rILW profile work so well as a travelling wave for the nonlinear system and the BBM profile did not?

This question can be answered by the phase velocity of these models. Figure 6.5 shows the phase velocities of the rILW and the BBM equations and the nonlinear system (2.5), we can see that the phase velocity of the rILW equation is much closer to the phase velocity of system (2.5) than that from the BBM equation.

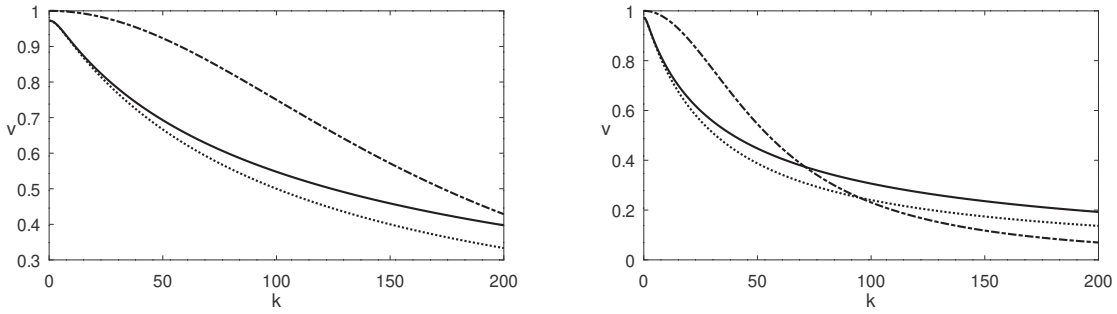

(a) $\beta = 0.0001$ (b) $\beta = 0.001$

Figure 6.5: Graphics of the dispersion relations of system (2.5) (—), rILW equation $(\cdots)$ and BBM equation $(- \cdot -)$.

6.2 Numerical tests for travelling waves

Based on the results obtained by the first method, illustrated in Figures 6.6–6.9, we can see that choosing the constant d has great influence on results. With $d \neq 0$ the initial guesses remain practically unchanged and the errors continue in the same order as in the corresponding tests of the previous section. Therefore, we did not have significant gains in this case.

For $d = 0$ we have very different and interesting results. Wave profiles change considerably in shape and amplitude. For example, in the case $\alpha = 0.0001$ and $l = 10\pi$, the number of oscillations in the period $2l$ increases as shown in Figure 6.6. We also highlight the case $\alpha = 0.0001$, $l = 20\pi$ and $\theta = \pi/40$ where Newton's method did not converge. Despite being quite different from the initial guesses, the wave profiles obtained with $d = 0$ have similar performance to those with $d \neq 0$, with the exception of the case in which Newton's method did not converge. In other words, we got new travelling wave profiles with good performance.

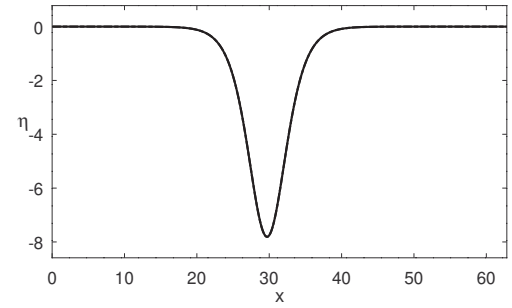

(a) $\theta = \pi/30$, $d \neq 0$

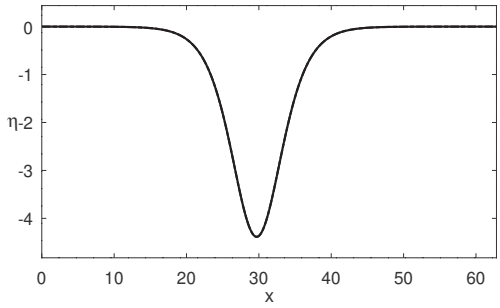

(b) $\theta = \pi/40$, $d \neq 0$

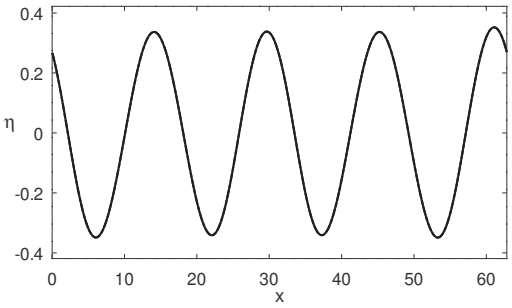

(c) $\theta = \pi/30$, $d = 0$

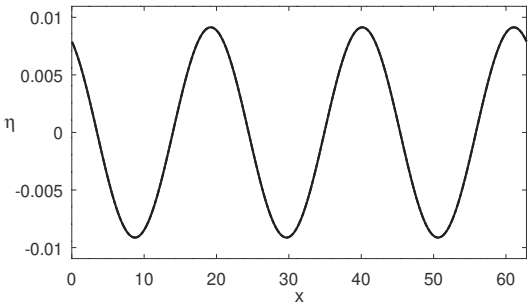

(d) rILW $\theta = \pi/40$, $d = 0$

Figure 6.6: Graphics of $\boldsymbol{\eta}^*$ $(- \cdot -)$ and $\boldsymbol{\eta}^n$ $(—)$ for the first method and each initial guess with $l = 10\pi$, $\alpha = \beta = 0.0001$, $\Delta x = 0.03068$, $\Delta t = 0.08043$ at time $t = 62.81254 = 781\Delta t$.

Profiles	e_{abs}	e_{rel}	c_n	c
$\theta = \pi/30$, $d \neq 0$	0.0260958	0.0002719	0.97303	0.97299
$\theta = \pi/40$, $d \neq 0$	0.0044712	0.0000718	0.97285	0.97284
$\theta = \pi/30$, $d = 0$	0.0089071	0.0008124	0.97248	0.97246
$\theta = \pi/40$, $d = 0$	0.0000311	0.0001065	0.97254	0.97254

Table 6.5: Errors at time $t = 62.81254 = 781\Delta t$ and wave velocities of η for the first method and each initial guess with $l = 10\pi$, $\alpha = \beta = 0.0001$, $\Delta x = 0.03068$, $\Delta t = 0.08043$.

Profiles	e_{abs}	e_{rel}	c_n	c
$\theta = \pi/30$, $d \neq 0$	0.0569211	0.0005931	0.97303	0.97299
$\theta = \pi/40$, $d \neq 0$	0.0142263	0.0002284	0.97286	0.97284
$\theta = \pi/30$, $d = 0$	0.0082445	0.0011949	0.97270	0.97263
$\theta = \pi/40$, $d = 0$	2080.5004823	1.1509963	0.98937	0.97241

Table 6.6: Errors at time $t = 125.62508 = 1562\Delta t$ and wave velocities of η for the first method and each initial guess with $l = 20\pi$, $\alpha = \beta = 0.0001$, $\Delta x = 0.03068$, $\Delta t = 0.08043$.

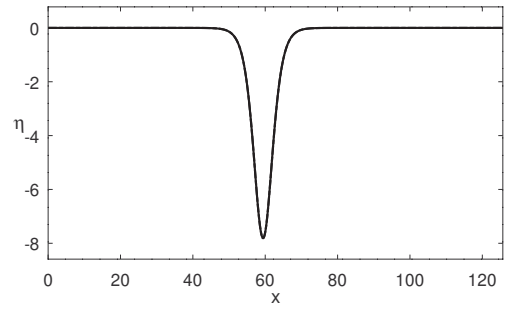

(a) $\theta = \pi/30$, $d \neq 0$

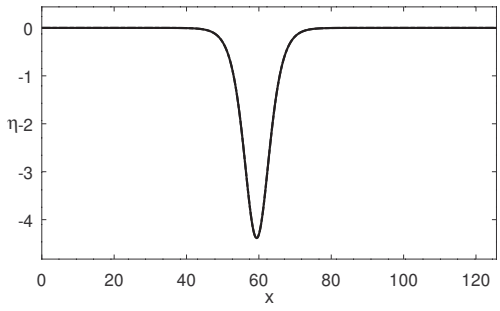

(b) $\theta = \pi/40$, $d \neq 0$

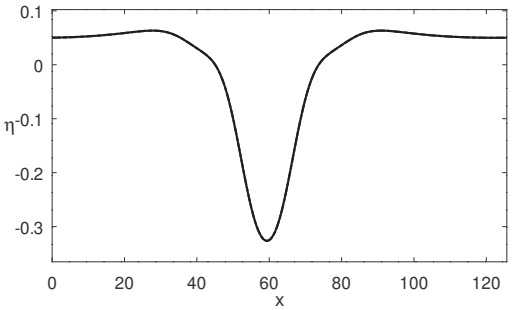

(c) $\theta = \pi/30$, $d = 0$

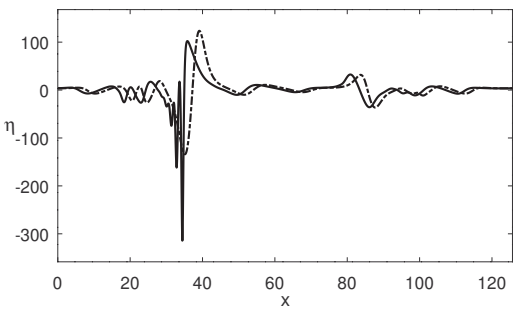

(d) $\theta = \pi/40$, $d = 0$

Figure 6.7: Graphics of $\boldsymbol{\eta}^*$ $(- \cdot -)$ and $\boldsymbol{\eta}^n$ $(—)$ for the first method and each initial guess with $l = 20\pi$, $\alpha = \beta = 0.0001$, $\Delta x = 0.03068$, $\Delta t = 0.08043$ at time $t = 125.62508 = 1562\Delta t$.

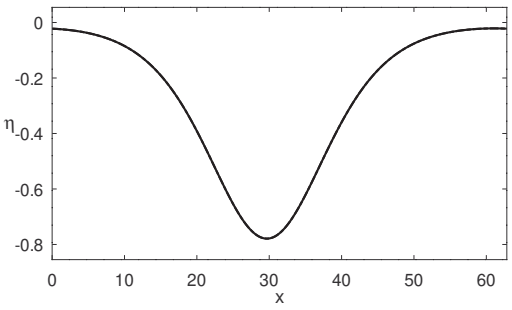

(a) $\theta = \pi/30$, $d \neq 0$

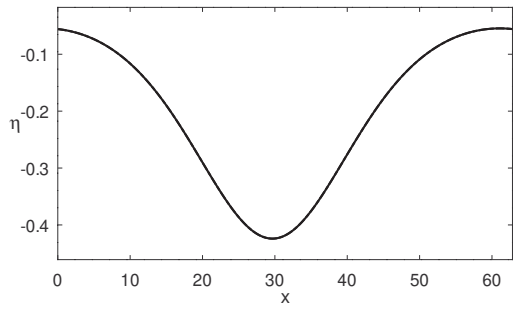

(b) $\theta = \pi/40$, $d \neq 0$

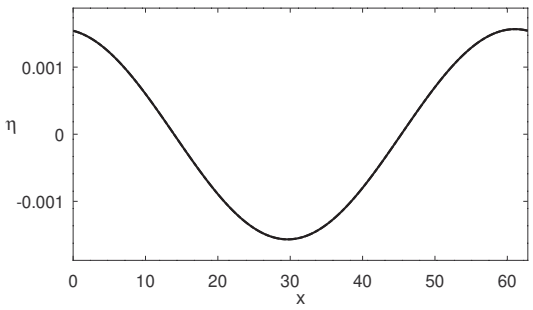

(c) $\theta = \pi/30$, $d = 0$

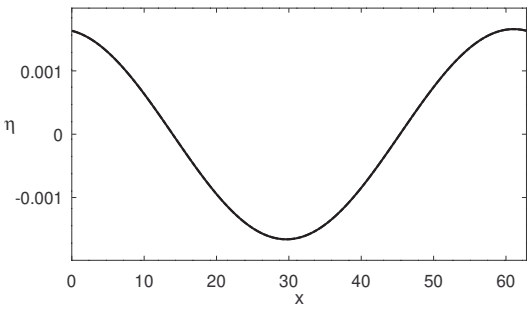

(d) $\theta = \pi/40$, $d = 0$

Figure 6.8: Graphics of $\boldsymbol{\eta}^*$ $(- \cdot -)$ and $\boldsymbol{\eta}^n$ $(—)$ for the first method and each initial guess with $l = 10\pi$, $\alpha = \beta = 0.001$, $\Delta x = 0.03068$, $\Delta t = 0.14302$ at time $t = 62.78557 = 439\Delta t$.

Profiles	e_{abs}	e_{rel}	c_n	c
$\theta = \pi/30,\ d \neq 0$	0.0009426	0.0000553	0.97302	0.97299
$\theta = \pi/40,\ d \neq 0$	0.0001909	0.0000174	0.97285	0.97283
$\theta = \pi/30,\ d = 0$	0.0000006	0.0000124	0.97252	0.97253
$\theta = \pi/40,\ d = 0$	0.0000004	0.0000077	0.97253	0.97253

Table 6.7: Errors at time $t = 62.78557 = 439\Delta t$ and wave velocities of η for the first method and each initial guess with $l = 10\pi$, $\alpha = \beta = 0.001$, $\Delta x = 0.03068$, $\Delta t = 0.14302$.

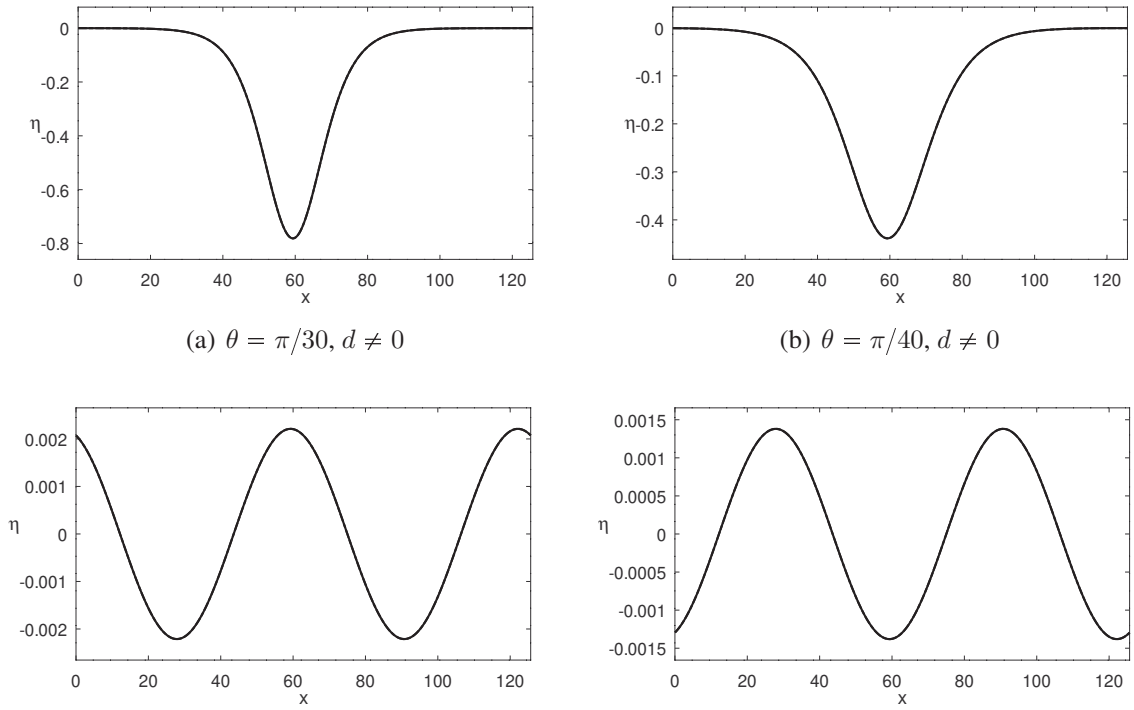

(a) $\theta = \pi/30,\ d \neq 0$

(b) $\theta = \pi/40,\ d \neq 0$

(c) $\theta = \pi/30,\ d = 0$

(d) $\theta = \pi/40,\ d = 0$

Figure 6.9: Graphics of $\boldsymbol{\eta}^*$ $(- \cdot -)$ and $\boldsymbol{\eta}^n$ $(—)$ for the first method and each initial guess with $l = 20\pi$, $\alpha = \beta = 0.001$, $\Delta x = 0.03068$, $\Delta t = 0.14302$ at time $t = 125.57114 = 878\Delta t$.

Profiles	e_{abs}	e_{rel}	c_n	c
$\theta = \pi/30,\ d \neq 0$	0.0026962	0.0001580	0.97303	0.97299
$\theta = \pi/40,\ d \neq 0$	0.0009046	0.0000817	0.97286	0.97284
$\theta = \pi/30,\ d = 0$	0.0000030	0.0000300	0.97253	0.97253
$\theta = \pi/40,\ d = 0$	0.0000081	0.0001299	0.97252	0.97253

Table 6.8: Errors at time $t = 125.57114 = 878\Delta t$ and wave velocities of η for the first method and each initial guess with $l = 20\pi$, $\alpha = \beta = 0.001$, $\Delta x = 0.03068$, $\Delta t = 0.14302$.

Let us now present the results for the second method. In the case $d \neq 0$ the graphs do not show changes as in the first method, however, when we analyze the errors in tables 6.9–6.12 we see that these are greater than the previous ones. When $d = 0$ the profiles obtained are quite different from the initial guesses and those found by the first method, but in this case the amplitude increases and the errors are also greater.

The fact that the errors were larger for the second method was unexpected since we do not use any approximation for the deduction of equation (6.8), unlike the first method. Despite providing new wave profiles, the second method was not useful to generate travelling waves for the nonlinear system since the performance of the initial guesses is already better.

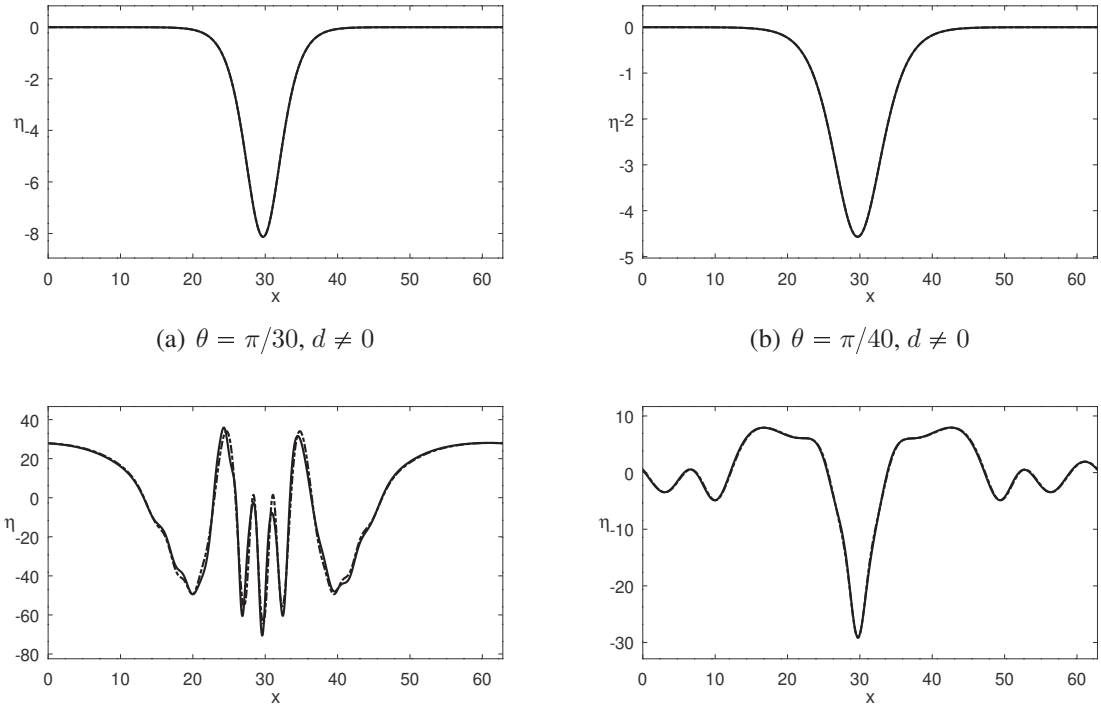

(a) $\theta = \pi/30$, $d \neq 0$ (b) $\theta = \pi/40$, $d \neq 0$

(c) $\theta = \pi/30$, $d = 0$ (d) $\theta = \pi/40$, $d = 0$

Figure 6.10: Graphics of $\boldsymbol{\eta}^*$ $(- \cdot -)$ and $\boldsymbol{\eta}^n$ $(—)$ for the second method and each initial guess with $l = 10\pi$, $\alpha = \beta = 0.0001$, $\Delta x = 0.03068$, $\Delta t = 0.08043$ at time $t = 62.81254 = 781\Delta t$.

Profiles	e_{abs}	e_{rel}	c_n	c
$\theta = \pi/30$, $d \neq 0$	0.1032543	0.0010547	0.97298	0.97632
$\theta = \pi/40$, $d \neq 0$	0.0462858	0.0007281	0.97276	0.97618
$\theta = \pi/30$, $d = 0$	146.5366087	0.1161537	0.97327	0.97135
$\theta = \pi/40$, $d = 0$	9.3485096	0.0280177	0.97360	0.97214

Table 6.9: Errors at time $t = 62.81254 = 781\Delta t$ and wave velocities of η for the second method and each initial guess with $l = 10\pi$, $\alpha = \beta = 0.0001$, $\Delta x = 0.03068$, $\Delta t = 0.08043$.

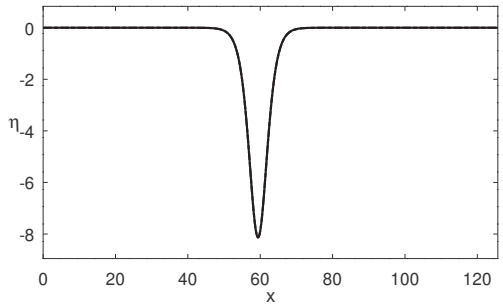

(a) $\theta = \pi/30$, $d \neq 0$

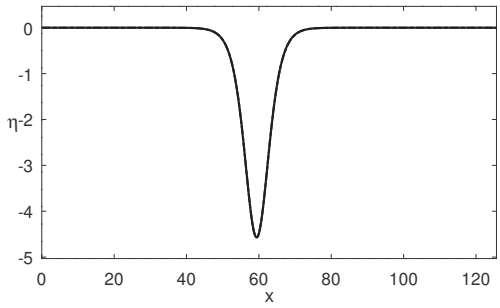

(b) $\theta = \pi/40$, $d \neq 0$

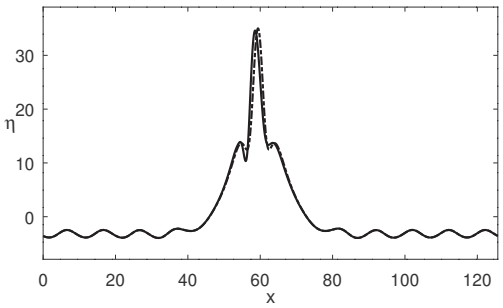

(c) $\theta = \pi/30$, $d = 0$

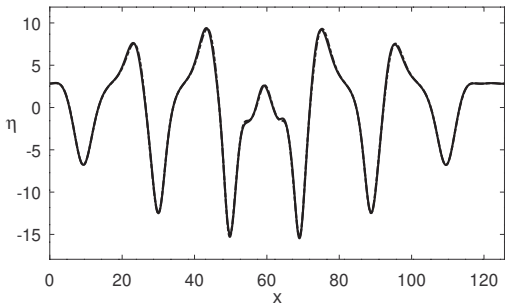

(d) $\theta = \pi/40$, $d = 0$

Figure 6.11: Graphics of $\boldsymbol{\eta}^*$ $(- \cdot -)$ and $\boldsymbol{\eta}^n$ $(—)$ for the second method and each initial guess with $l = 20\pi$, $\alpha = \beta = 0.0001$, $\Delta x = 0.03068$, $\Delta t = 0.08043$ at time $t = 125.62508 = 1562\Delta t$.

Profiles	e_{abs}	e_{rel}	c_n	c
$\theta = \pi/30$, $d \neq 0$	0.2003666	0.0020467	0.97301	0.97632
$\theta = \pi/40$, $d \neq 0$	0.1080727	0.0017001	0.97283	0.97618
$\theta = \pi/30$, $d = 0$	74.6840505	0.1672032	0.97287	0.97267
$\theta = \pi/40$, $d = 0$	10.6721663	0.0294054	0.97290	0.97268

Table 6.10: Errors at time $t = 125.62508 = 1562\Delta t$ and wave velocities of η for the second method and each initial guess with $l = 20\pi$, $\alpha = \beta = 0.0001$, $\Delta x = 0.03068$, $\Delta t = 0.08043$.

Profiles	e_{abs}	e_{rel}	c_n	c
$\theta = \pi/30$, $d \neq 0$	0.0267387	0.0015362	0.97264	0.97632
$\theta = \pi/40$, $d \neq 0$	0.0209795	0.0018516	0.97228	0.97620
$\theta = \pi/30$, $d = 0$	2.3019028	0.0346729	0.97432	0.97429
$\theta = \pi/40$, $d = 0$	0.0851274	0.0046011	0.97278	0.97278

Table 6.11: Errors at time $t = 62.78557 = 439\Delta t$ and wave velocities of η for the second method and each initial guess with $l = 10\pi$, $\alpha = \beta = 0.001$, $\Delta x = 0.03068$, $\Delta t = 0.14302$.

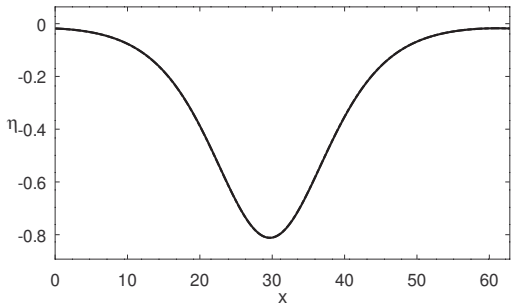

(a) $\theta = \pi/30$, $d \neq 0$

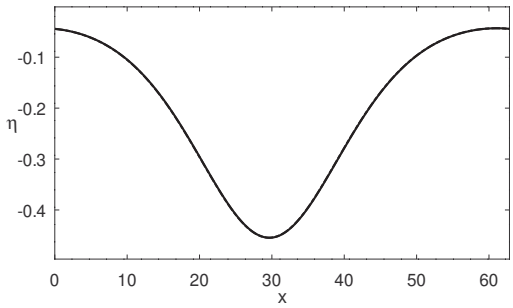

(b) $\theta = \pi/40$, $d \neq 0$

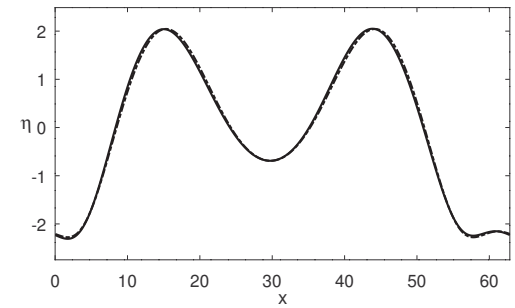

(c) $\theta = \pi/30$, $d = 0$

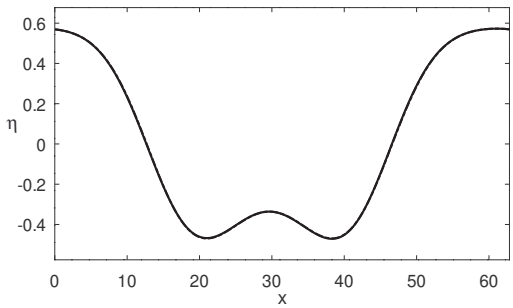

(d) $\theta = \pi/40$, $d = 0$

Figure 6.12: Graphics of $\boldsymbol{\eta}^*$ $(- \cdot -)$ and $\boldsymbol{\eta}^n$ $(—)$ for the second method and each initial guess with $l = 10\pi$, $\alpha = \beta = 0.001$, $\Delta x = 0.03068$, $\Delta t = 0.14302$ at time $t = 62.78557 = 439\Delta t$.

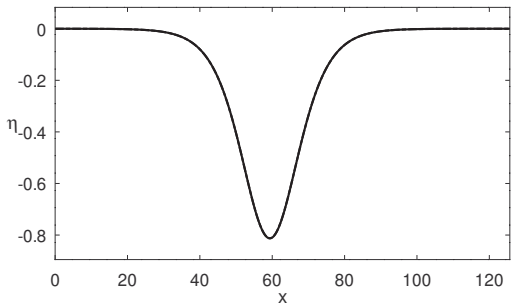

(a) $\theta = \pi/30$, $d \neq 0$

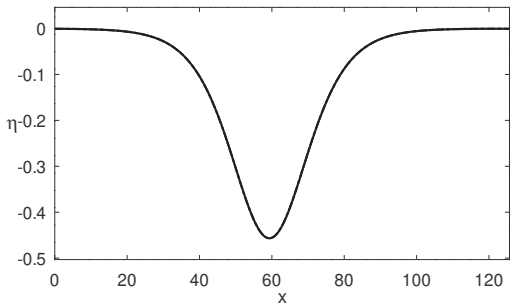

(b) $\theta = \pi/40$, $d \neq 0$

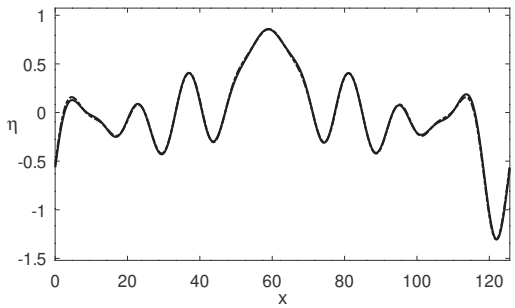

(c) $\theta = \pi/30$, $d = 0$

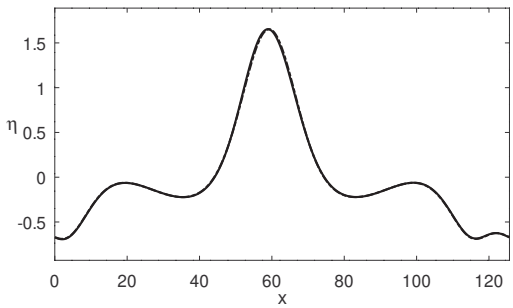

(d) $\theta = \pi/40$, $d = 0$

Figure 6.13: Graphics of $\boldsymbol{\eta}^*$ $(- \cdot -)$ and $\boldsymbol{\eta}^n$ $(—)$ for the second method and each initial guess with $l = 20\pi$, $\alpha = \beta = 0.001$, $\Delta x = 0.03068$, $\Delta t = 0.14302$ at time $t = 125.57114 = 878\Delta t$.

Profiles	e_{abs}	e_{rel}	c_n	c
$\theta = \pi/30$, $d \neq 0$	0.0113657	0.0006529	0.97291	0.97632
$\theta = \pi/40$, $d \neq 0$	0.0104325	0.0009229	0.97266	0.97618
$\theta = \pi/30$, $d = 0$	0.9085554	0.0345465	0.97080	0.97109
$\theta = \pi/40$, $d = 0$	0.6042668	0.0159830	0.97203	0.97291

Table 6.12: Errors at time $t = 125.57114 = 878\Delta t$ and wave velocities of η for the second method and each initial guess with $l = 20\pi$, $\alpha = \beta = 0.001$, $\Delta x = 0.03068$, $\Delta t = 0.14302$.

Unlike the previous methods, the third method presents better results than the initial guesses for $d \neq 0$ and the profiles did not change. Again, in the case $d = 0$, we have wave profiles with different shapes than the initial guesses, but the errors are in general smaller than the other methods. We highlight the cases in figures 6.14 ($\theta = \pi/40$), 6.16 and 6.17 in which the wave shape is quite similar to those obtained by the first method, but with different amplitudes. We also highlight the case $\alpha = 0.0001$, $l = 10\pi$ and $\theta = \pi/30$ where Newton's method did not converge and the generated wave disperses as time advances. Therefore, this is the best method to generate travelling waves among those presented here.

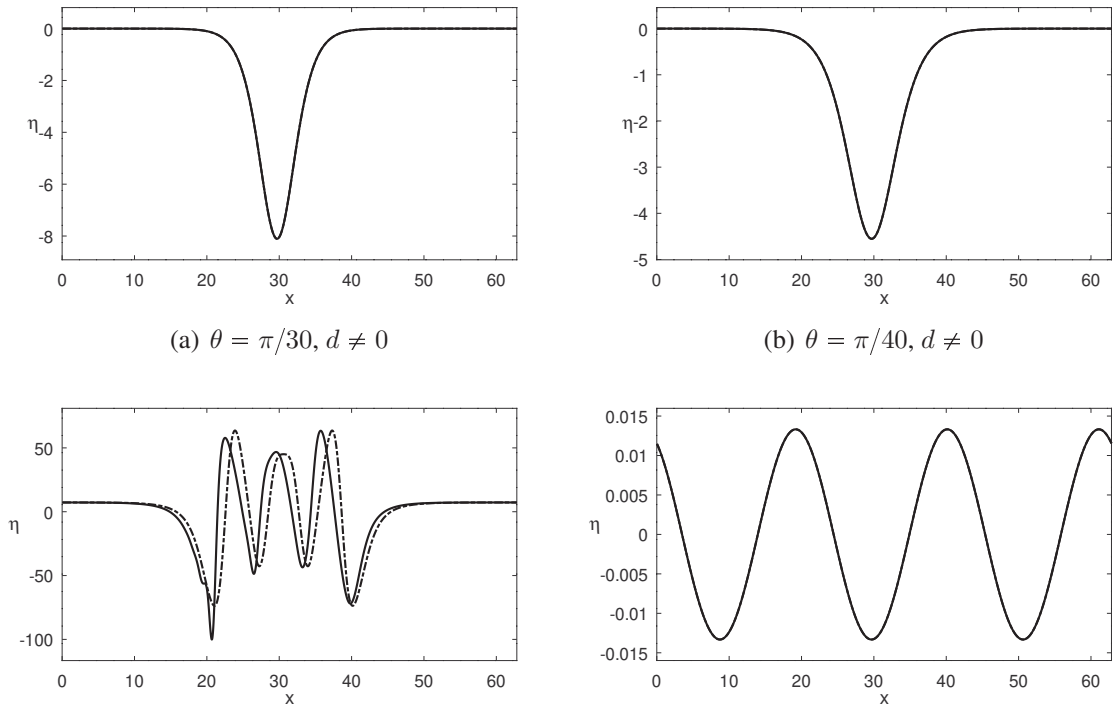

(a) $\theta = \pi/30$, $d \neq 0$

(b) $\theta = \pi/40$, $d \neq 0$

(c) $\theta = \pi/30$, $d = 0$

(d) $\theta = \pi/40$, $d = 0$

Figure 6.14: Graphics of $\boldsymbol{\eta}^*$ $(- \cdot -)$ and $\boldsymbol{\eta}^n$ $(—)$ for the third method and each initial guess with $l = 10\pi$, $\alpha = \beta = 0.0001$, $\Delta x = 0.03068$, $\Delta t = 0.08043$ at time $t = 62.81254 = 781\Delta t$.

Profiles	e_{abs}	e_{rel}	c_n	c
$\theta = \pi/30,\ d \neq 0$	0.0216556	0.0002215	0.97301	0.97302
$\theta = \pi/40,\ d \neq 0$	0.0033497	0.0000528	0.97285	0.97285
$\theta = \pi/30,\ d = 0$	1005.6112811	0.7945183	0.98733	0.97211
$\theta = \pi/40,\ d = 0$	0.0000548	0.0001285	0.97254	0.97254

Table 6.13: Errors at time $t = 62.81254 = 781\Delta t$ and wave velocities of η for the third method and each initial guess with $l = 10\pi$, $\alpha = \beta = 0.0001$, $\Delta x = 0.03068$, $\Delta t = 0.08043$.

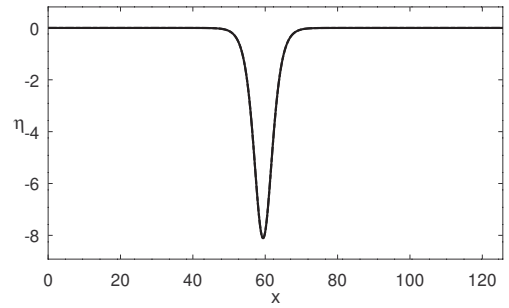

(a) $\theta = \pi/30,\ d \neq 0$

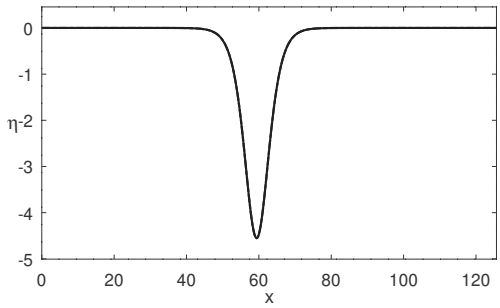

(b) $\theta = \pi/40,\ d \neq 0$

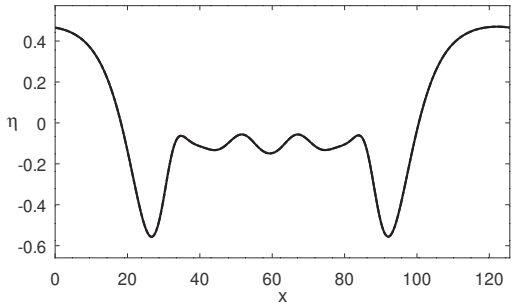

(c) $\theta = \pi/30,\ d = 0$

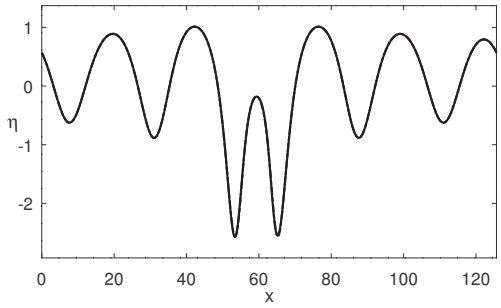

(d) $\theta = \pi/40,\ d = 0$

Figure 6.15: Graphics of $\boldsymbol{\eta}^*$ $(- \cdot -)$ and $\boldsymbol{\eta}^n$ $(—)$ for the third method and each initial guess with $l = 20\pi$, $\alpha = \beta = 0.0001$, $\Delta x = 0.03068$, $\Delta t = 0.08043$ at time $t = 125.62508 = 1562\Delta t$.

Profiles	e_{abs}	e_{rel}	c_n	c
$\theta = \pi/30,\ d \neq 0$	0.0112237	0.0001148	0.97302	0.97302
$\theta = \pi/40,\ d \neq 0$	0.0042837	0.0000675	0.97285	0.97285
$\theta = \pi/30,\ d = 0$	0.0316172	0.0016720	0.97258	0.97260
$\theta = \pi/40,\ d = 0$	0.4807426	0.0088976	0.97252	0.97253

Table 6.14: Errors at time $t = 125.62508 = 1562\Delta t$ and wave velocities of η for the third method and each initial guess with $l = 20\pi$, $\alpha = \beta = 0.0001$, $\Delta x = 0.03068$, $\Delta t = 0.08043$.

Profiles	e_{abs}	e_{rel}	c_n	c
$\theta = \pi/30,\ d \neq 0$	0.0010299	0.0000593	0.97301	0.97302
$\theta = \pi/40,\ d \neq 0$	0.0004463	0.0000398	0.97284	0.97285
$\theta = \pi/30,\ d = 0$	0.0000014	0.0000140	0.97253	0.97253
$\theta = \pi/40,\ d = 0$	0.0000019	0.0000179	0.97252	0.97252

Table 6.15: Errors at time $t = 62.78557 = 439\Delta t$ and wave velocities of η for the third method and each initial guess with $l = 10\pi$, $\alpha = \beta = 0.001$, $\Delta x = 0.03068$, $\Delta t = 0.14302$.

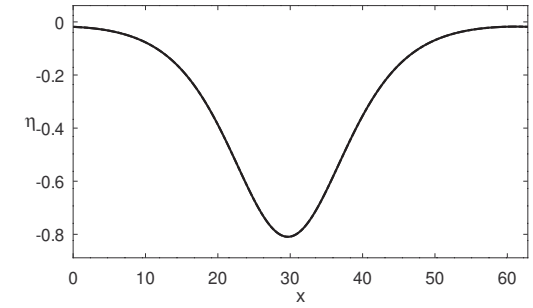

(a) $\theta = \pi/30$, $d \neq 0$

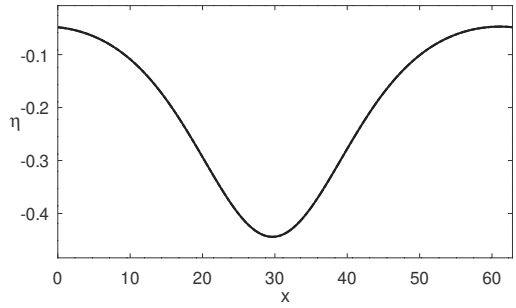

(b) $\theta = \pi/40$, $d \neq 0$

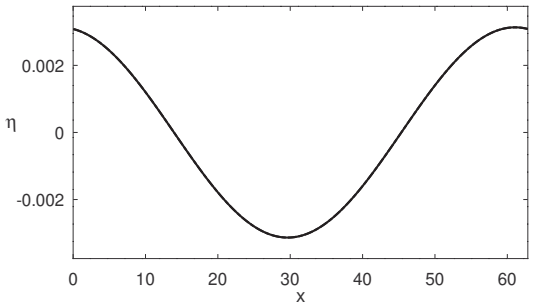

(c) $\theta = \pi/30$, $d = 0$

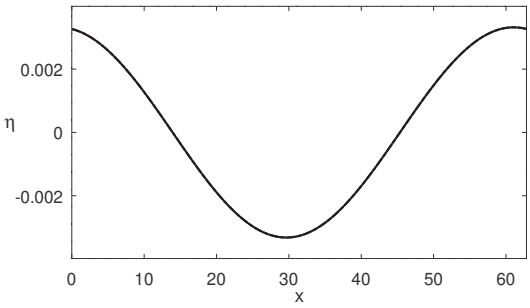

(d) $\theta = \pi/40$, $d = 0$

Figure 6.16: Graphics of $\boldsymbol{\eta}^*$ $(- \cdot -)$ and $\boldsymbol{\eta}^n$ (—) for the third method and each initial guess with $l = 10\pi$, $\alpha = \beta = 0.001$, $\Delta x = 0.03068$, $\Delta t = 0.14302$ at time $t = 62.78557 = 439\Delta t$.

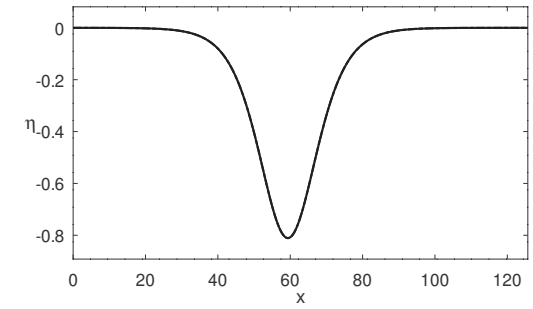

(a) $\theta = \pi/30$, $d \neq 0$

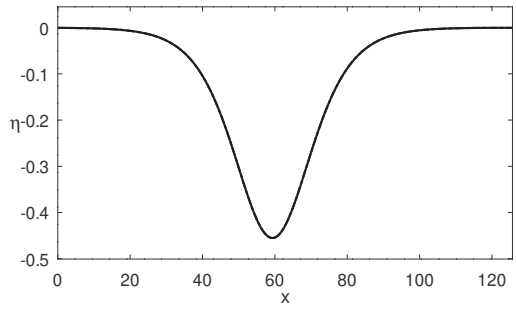

(b) $\theta = \pi/40$, $d \neq 0$

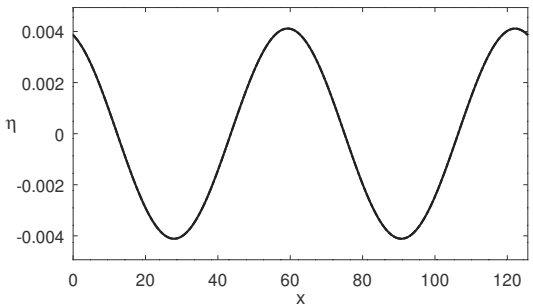

(c) $\theta = \pi/30$, $d = 0$

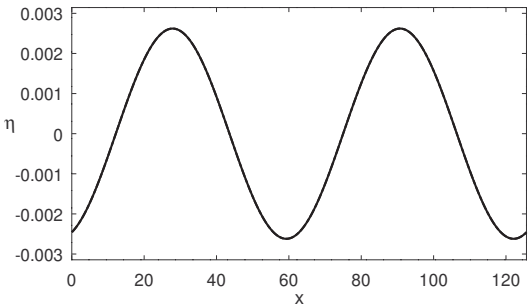

(d) $\theta = \pi/40$, $d = 0$

Figure 6.17: Graphics of $\boldsymbol{\eta}^*$ $(- \cdot -)$ and $\boldsymbol{\eta}^n$ (—) for the third method and each initial guess with $l = 20\pi$, $\alpha = \beta = 0.001$, $\Delta x = 0.03068$, $\Delta t = 0.14302$ at time $t = 125.57114 = 878\Delta t$.

The travelling wave solutions of the rILW equation perform satisfactorily as travelling waves for the nonlinear system (2.5), this can be explained by the similarity of the phase velocities

Profiles	e_{abs}	e_{rel}	c_n	c
$\theta = \pi/30$, $d \neq 0$	0.0013371	0.0000769	0.97301	0.97302
$\theta = \pi/40$, $d \neq 0$	0.0000405	0.0000036	0.97285	0.97285
$\theta = \pi/30$, $d = 0$	0.0000169	0.0000910	0.97253	0.97253
$\theta = \pi/40$, $d = 0$	0.0000035	0.0000298	0.97252	0.97253

Table 6.16: Errors at time $t = 125.57114 = 878\Delta t$ and wave velocities of η for the third method and each initial guess with $l = 20\pi$, $\alpha = \beta = 0.001$, $\Delta x = 0.03068$, $\Delta t = 0.14302$.

of both models. The third method provides the better results to obtain travelling waves for system (2.5), especially when $d \neq 0$. Therefore, the simplifications made in order to have a system with fewer equations and variables and consequently faster and easier to solve, did not prove to be advantageous, since in the first method the errors continued to be of the same order and in the second they were greater.

A result that is consistent for all methods and almost all initial guesses is the wave velocity. Except from the bad cases we always have $c_{\text{met}} \approx c_n$ and this approximation is better in the third method where we find a five-digit precision agreement is some experiments. In all cases we get $c_n \approx 0.97$ which indicates that the velocity c of the travelling wave solution for system (2.5) is smaller than 1, contrary to the initial hypothesis based on travelling wave results for other similar models. Also the velocity changes a little depending on the profile and the parameters.

In the results of the three methods we see that the parameter d is very important for the shape of the obtained waves. If for $d \neq 0$, calculated by (6.6), the initial conditions remain practically unchanged, for $d = 0$ we obtain several different shapes of travelling waves. In addition to the results presented here, extra experiments for higher α and β values can be found in Appendix B. Therefore, based on all the experiments presented in this chapter, the nonlinear system (2.5) probably admit many different forms of travelling waves solutions and the theoretical existence of this kind of solution will be studied in future works.

Chapter 7

Numerical methods for non-flat bottom models

Since the numerical results of the methods for the flat bottom models proved to be very robust we can take advantage of them and propose numerical methods for the non-flat bottom models. Let us proceed as in the flat bottom case and begin the discretization considering the linearized version of system (2.8) that is given by

$$\begin{cases} \eta_t = \dfrac{1}{M(\xi)} u_\xi, \\ \\ u_t - \dfrac{\rho_2}{\rho_1}\dfrac{\sqrt{\beta}}{M(\xi)}\mathcal{T}\big[u\big]_{\xi t} - \dfrac{\beta}{3M(\xi)}\left(\dfrac{u_{\xi t}}{M(\xi)}\right)_\xi = \dfrac{1}{M(\xi)}\eta_\xi. \end{cases} \tag{7.1}$$

Our aim is to put system (7.1) in the form

$$\begin{cases} \eta_t = \dfrac{1}{M(\xi)} u_\xi, \\ \\ \psi_t = \dfrac{1}{M(\xi)}\eta_\xi, \end{cases} \tag{7.2}$$

where ψ does not have t-derivatives of u. To do this we use the quotient rule to obtain

$$\left(\frac{u_{\xi t}}{M(\xi)}\right)_\xi = \frac{u_{\xi\xi t}}{M(\xi)} - \frac{M'(\xi)}{M^2(\xi)} u_{\xi t},$$

thus we get system (7.1) in the form of system (7.2) defining

$$\psi = u - \frac{\rho_2}{\rho_1}\frac{\sqrt{\beta}}{M(\xi)}\mathcal{T}\big[u\big]_\xi - \frac{\beta}{3M^2(\xi)} u_{\xi\xi} + \frac{\beta M'(\xi)}{3M^3(\xi)} u_\xi.$$

Since u and η are $2l$-periodic with respect to the variable ξ, we define a uniform grid on the interval $[0, 2l]$, that is, $\xi_j = j\Delta\xi,\ j = 1, \ldots, N$ where $N \in \mathbb{N}$ is even and $\Delta\xi = 2l/N$, the last element ξ_N is also identified with $\xi = 0$. We define the approximations $\boldsymbol{u}$ and $\boldsymbol{\eta}$ analogously to the flat bottom case.

Denoting $M = \operatorname{diag}(M(\xi_i)),\ i = 1, 2, \ldots, N$, we obtain easily the discretization of the right hand side terms of system (7.1) which are $M^{-1}C\boldsymbol{u}$ and $M^{-1}C\boldsymbol{\eta}$, where C is defined in Chapter 4 using the finite difference scheme since it proved to be the best option in the flat bottom case. For the left hand side of the second equation we cannot proceed directly with the spectral approach as in the flat bottom case, and we must do the discretization term by term.

For the discretization of $\mathcal{T}\big[u\big]_\xi$ and $u_{\xi\xi}$ we use matrices $T = \frac{1}{N}\overline{F}^T\hat{T}F$ and $S = \frac{1}{N}\overline{F}^T\hat{S}F$

defined in Chapter 6. The discretization of $M'(\xi)$ and u_ξ is made using matrix C but we will consider two options for it: the spectral scheme which can be more appropriate for the dispersive terms and finite difference which presents better stability conditions. Thus, denoting $Q = \mathrm{diag}(C\boldsymbol{m})$ where $\boldsymbol{m}$ is a vector whose entries are $m_i = M(\xi_i)$, $i = 1, \ldots, N$, we obtain the following discretization of ψ

$$\boldsymbol{\psi} = \left(I - \frac{\rho_2}{\rho_1}\sqrt{\beta}M^{-1}T - \frac{\beta}{3}M^{-2}S + \frac{\beta}{3}M^{-3}QC \right) \boldsymbol{u} = P\boldsymbol{u}.$$

The spatial discretization results in a system of Ordinary Differential Equations in the matrix form below and the time advancing is performed with the RK4 method.

$$\begin{cases} \boldsymbol{\eta}_t = M^{-1}C\boldsymbol{u}, \\ P\boldsymbol{u}_t = M^{-1}C\boldsymbol{\eta}. \end{cases}$$

Once the discretization of the linear system is complete, let us obtain the discretization of the nonlinear system. For that, let us rewrite system (2.8) as

$$\begin{cases} \eta_t &= E_1(\eta, u), \\ \psi_t &= E_2(\eta, u), \end{cases}$$

where

$$E_1(\eta, u) = \frac{1}{M(\xi)}(u_\xi - \alpha\eta u_\xi - \alpha u\eta_\xi),$$

$$E_2(\eta, u) = \frac{1}{M(\xi)}(\eta_\xi - \alpha u u_\xi).$$

The discretization of E_1 and E_2 is done similarly to the one done in the flat bottom case, only multiplying by matrix M^{-1}.

Now we must take care of the stability conditions. The coefficient M may affect negatively the stability conditions obtained for the flat bottom linear model making them more restrictive. Although a von Neumann analysis can be done using the method of frozen coefficients, due to the expression of Matrix P this work is considerably difficult and will not be done at this moment.

In view of this we establish a numerical procedure to obtain an appropriate Δt. Since it is not expected that the amplitude of η increases, we set a Δt^* which satisfies a stability condition in theorem 4.3 and run the method until a fixed time T or until the criteria $\|\boldsymbol{\eta}^n\|_\infty > 2\|\boldsymbol{\eta}^0\|_\infty$ is achieved. Then we set a smaller Δt and restart the method from $t = 0$. This procedure is repeated until the criteria $\|\boldsymbol{\eta}^n\|_\infty > 2\|\boldsymbol{\eta}^0\|_\infty$ is not achieved twice in a row.

For the experiments we set $l = 8\pi$, $N = 2^{10}$ $\rho_1 = 1$, $\rho_2 = 2$, $h_1 = 0.1$ and $h_2 = 3.505$. The values of β, α and the initial Δt, which is given by the condition (4.14), are defined in each test. The other values are calculated by the relations $L = h_1/\sqrt{\beta}$ and $\delta = h_2/L$. As initial condition we will use two options: the Gaussian profile $\overline{\eta}(x) = 0.1\exp(-2(x - l/2)^2)$ where u_0 is set as $\widehat{u}_0(k) = v(k\pi/l)\widehat{\eta}_0(k)$ and the travelling wave obtained in the previous chapter by the third method with $d \neq 0$. Thereby we can compare the behavior of a regular wave and a travelling wave in a non-flat bottom configuration.

For a non-flat topography, even a very simple one, the computation of the coefficient $M(\xi)$ demands a considerably high computational cost. Because of this, in the following experiments we proceed as in [25] and assume that $M(\xi) = 1 + n(\xi)$, where $n(\xi)$ describes periodic fluctuations. As we see in [17, 18, 19], this choice is not far from the real coefficient that comes from mapping a periodic piecewise linear topography.

Let us begin with the periodic slowly-varying coefficient M given by

$$M(\xi) = \begin{cases} 1 + 0.5\sin(5\xi) & \text{if } \xi \in [6\pi, 12\pi], \\ 1 & \text{otherwise.} \end{cases}$$

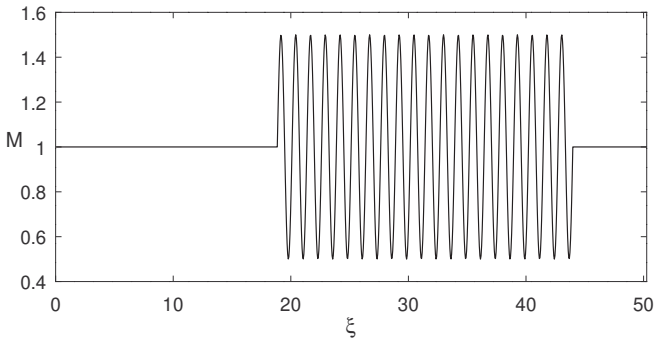

Figure 7.1: Periodic slowly-varying coefficient M.

We can see that the initial choice of $\Delta t = 0.10173$, which is stable for the flat bottom models, does not work well and provides an unstable solution as figure 7.2 illustrates. The results of the numerical procedure to obtain a stable Δt for the non-flat bottom linear model with $\beta = 0.0001$ are presented in tables 7.1 and 7.2 for spectral diferentiation and finite difference, respectively. Using $\Delta t = 0.08139$ we obtain a stable solution for both cases including the nonlinear methods as presented in figures 7.3 and 7.4.

Figure 7.5 shows the influence of the coefficient M in the model comparing the solutions of flat and non-flat nonlinear methods for the same initial condition and parameters. Besides the wave train that is characteristic of the problem, another kind of waves appear in the solution of the non-flat bottom method that are a result of the Bragg's phenomenon. The period of these waves is expected to be twice the period of the non-constant part of M that is 1.2566, [12]. Since the estimated period of the waves from Bragg's phenomenon is 2.5525 the experiments are consistent with the expected results.

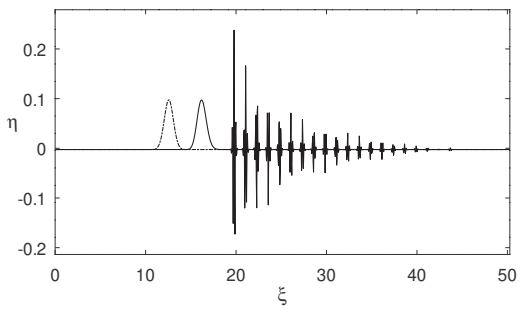

(a) $t = 0$ $(\cdots)$ and $t = 37\Delta t$ (—). SP

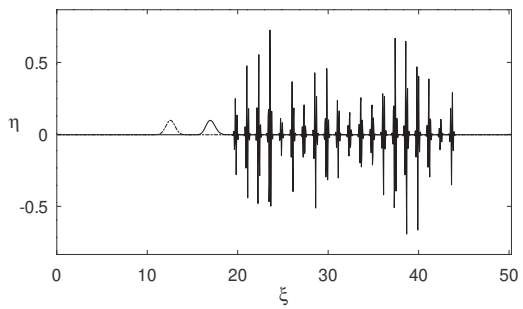

(b) $t = 0$ $(\cdots)$ and $t = 45\Delta t$ (—). FD

Figure 7.2: Solutions η for the non-flat linear method with $l = 8\pi$, $\beta = 0.0001$, $\Delta\xi = 0.04909$, $\Delta t = 0.10173$ and slowly-varying coefficient.

Δt	t	$\|\boldsymbol{\eta}^n\|_\infty$
$\Delta t = 0.10173$	$t = 37\Delta t = 3.76406$	0.23787
$0.95\Delta t = 0.09664$	$t = 60\Delta t = 5.79869$	0.51034
$0.9\Delta t = 0.09156$	$t = 171\Delta t = 15.65647$	0.27645
$0.85\Delta t = 0.08647$	$t = 1156\Delta t = 99.96134$	0.07387
$0.8\Delta t = 0.08139$	$t = 1228\Delta t = 99.94099$	0.07408

Table 7.1: Stability analysis for non-flat linear method with slowly-varying coefficient, spectral scheme, $\beta = 0.0001$ and $\|\boldsymbol{\eta}^0\|_\infty = 0.09751$.

Δt	t	$\|\boldsymbol{\eta}^n\|_\infty$
$\Delta t = 0.10173$	$t = 45\Delta t = 4.57792$	0.72449
$0.95\Delta t = 0.09664$	$t = 69\Delta t = 6.66850$	0.20363
$0.9\Delta t = 0.09156$	$t = 202\Delta t = 18.49478$	0.28927
$0.85\Delta t = 0.08647$	$t = 1156\Delta t = 99.96134$	0.07387
$0.8\Delta t = 0.08139$	$t = 1228\Delta t = 99.94099$	0.07408

Table 7.2: Stability analysis for non-flat linear method with slowly-varying coefficient, finite difference, $\beta = 0.0001$ and $\|\boldsymbol{\eta}^0\|_\infty = 0.09751$.

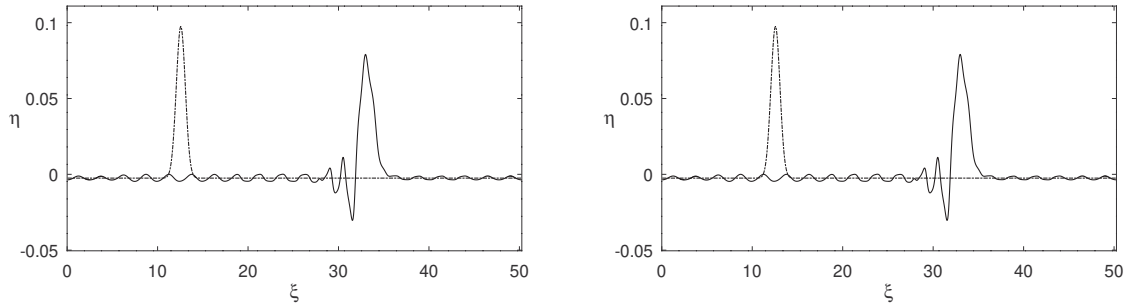

(a) Spectral scheme. (b) Finite difference.

Figure 7.3: Solutions η for the non-flat linear method at $t = 0$ $(\cdots)$ and $t = 900\Delta t$ (—) with $l = 8\pi$, $\beta = 0.0001$, $\Delta\xi = 0.04909$, $\Delta t = 0.081385$ and slowly-varying coefficient.

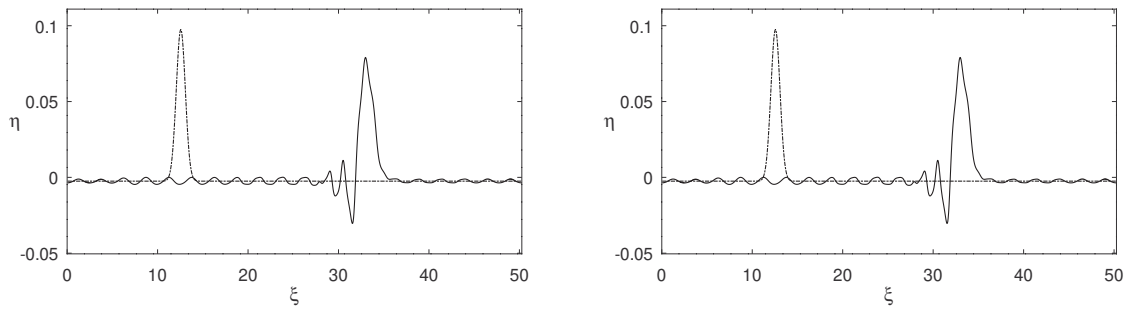

(a) Spectral scheme. (b) Finite difference.

Figure 7.4: Solutions η for the non-flat nonlinear method at $t = 0$ $(\cdots)$ and $t = 900\Delta t$ (—) with $l = 8\pi$, $\alpha = \beta = 0.0001$, $\Delta\xi = 0.04909$, $\Delta t = 0.081385$ and slowly-varying coefficient.

The solutions obtained for the non-flat nonlinear system using the travelling wave solution are illustrated in figure 7.6. We cannot see the existence of Bragg's phenomenon in this case as when we use the gaussian profile. Despite some oscillations in the wave their shape is well preserved considering the bottom. In order to understand these results let us analyze the Fourier

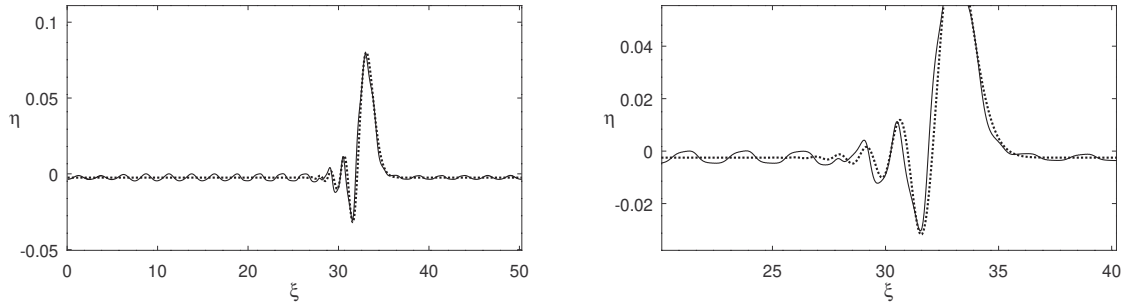

(a) Solutions with SP differentiation (b) Detail

Figure 7.5: Solutions η at $t = 900\Delta t$ for flat nonlinear method $(\cdots)$ and non-flat nonlinear method (—) with $l = 8\pi$, $\alpha = \beta = 0.0001$, $\Delta\xi = 0.04909$, $\Delta t = 0.081385$ and slowly-varying coefficient.

modes of the solutions. Starting with the gaussian profile we can see that the coefficient M affects the solutions mostly in the modes between -100 and 100 approximately (figures 7.7 and 7.8) and the nonzero Fourier modes of M are concentrated in the same region (figure 7.9). Thus the effects of M is on the same range of modes but the result is different since the Fourier modes of both solutions are considerable different.

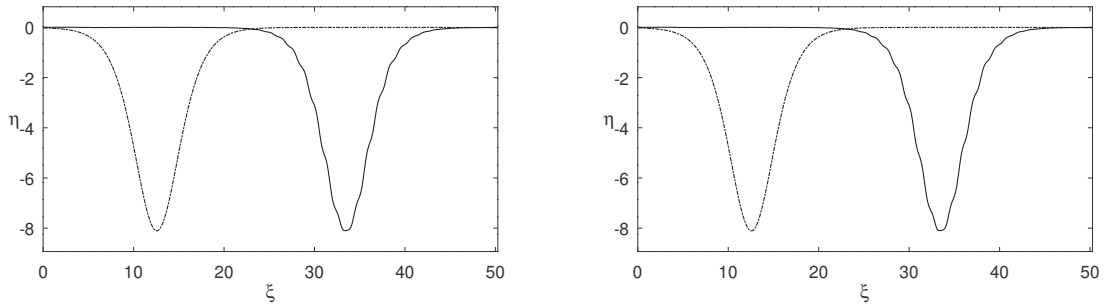

(a) Spectral scheme (b) Finite difference

Figure 7.6: Solutions η for the non-flat nonlinear method at $t = 0$ $(\cdots)$ and $t = 900\Delta t$ (—) with $l = 8\pi$, $\alpha = \beta = 0.0001$, $\Delta\xi = 0.04909$, $\Delta t = 0.08139$ and slowly-varying coefficient.

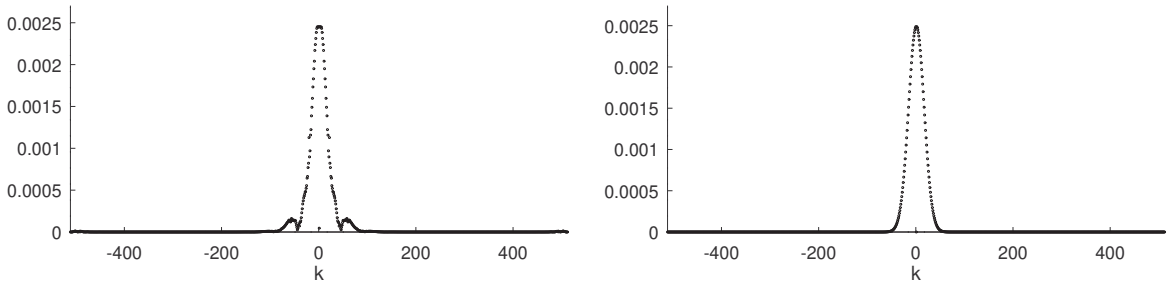

(a) Non-flat bottom

(b) Flat bottom

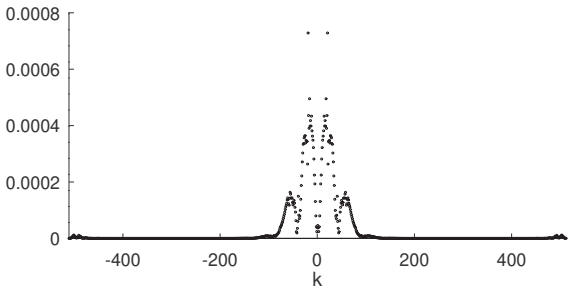

(c) Difference module

Figure 7.7: Fourier modes $|\hat{\eta}^n|$ of solutions η for the non-flat nonlinear method at $t = 900\Delta t$ with $l = 8\pi$, $\alpha = \beta = 0.0001$, $\Delta\xi = 0.04909$, $\Delta t = 0.081385$ and slowly-varying coefficient.

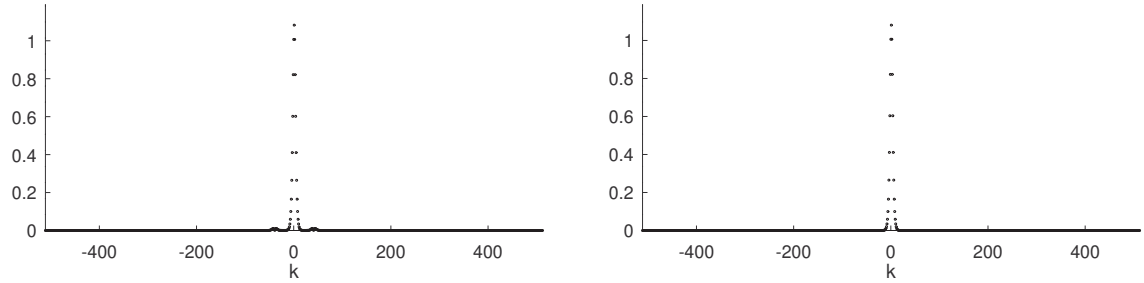

(a) Non-flat bottom

(b) Flat bottom

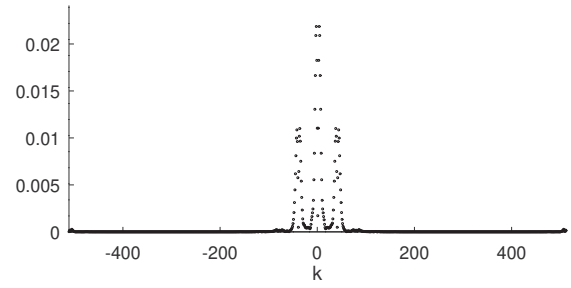

(c) Difference module

Figure 7.8: Fourier modes $|\hat{\eta}^n|$ of solutions η for the non-flat nonlinear method with $l = 8\pi$, $\alpha = \beta = 0.0001$, $\Delta\xi = 0.04909$, $\Delta t = 0.081385$ and slowly-varying coefficient.

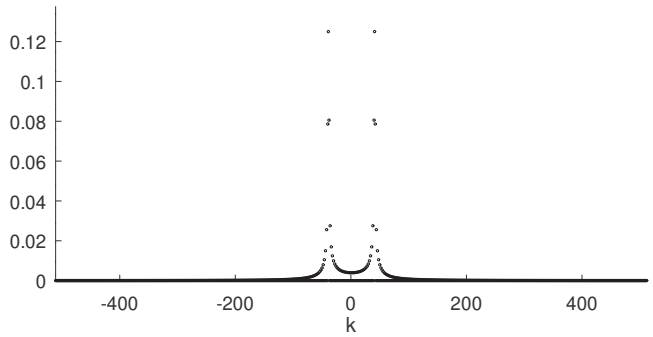

Figure 7.9: Fourier modes of periodic slowly-varying coefficient M.

Tables 7.3 and 7.4 present the numerical procedure to obtain a stable Δt for the non-flat bottom linear model for spectral diferentiation and finite difference, respectively. As in the case with $\beta = 0.0001$, the initial choice of $\Delta t = 0.18091$ which is stable for the flat bottom models provides an unstable solution. A stable solution is obtained using $\Delta t = 0.12663$ for both cases including the nonlinear methods as presented in figures 7.10 and 7.11. The Bragg's phenomenon is also present in these experiments as shown in figure 7.12 and the estimated period of the waves is 2.5525 as in the previous tests.

Δt	t	$\|\boldsymbol{\eta}^n\|_\infty$
$\Delta t = 0.18091$	$t = 19\Delta t = 3.43723$	0.87871
$0.95\Delta t = 0.17186$	$t = 23\Delta t = 3.95282$	0.41103
$0.9\Delta t = 0.16282$	$t = 31\Delta t = 5.04730$	0.58025
$0.85\Delta t = 0.15377$	$t = 49\Delta t = 7.53478$	0.23604
$0.8\Delta t = 0.14473$	$t = 188\Delta t = 27.20841$	0.19799
$0.75\Delta t = 0.13568$	$t = 737\Delta t = 99.99633$	0.04025
$0.7\Delta t = 0.12663$	$t = 789\Delta t = 99.91492$	0.04044

Table 7.3: Stability analysis for non-flat linear method with slowly-varying coefficient, spectral scheme, $\beta = 0.001$ and $\|\boldsymbol{\eta}^0\|_\infty = 0.09751$.

Δt	t	$\|\boldsymbol{\eta}^n\|_\infty$
$\Delta t = 0.18091$	$t = 19\Delta t = 3.43723$	0.80933
$0.95\Delta t = 0.17186$	$t = 23\Delta t = 3.95282$	0.40835
$0.9\Delta t = 0.16282$	$t = 31\Delta t = 5.04730$	0.47720
$0.85\Delta t = 0.15377$	$t = 49\Delta t = 7.53478$	0.22905
$0.8\Delta t = 0.14473$	$t = 196\Delta t = 28.36621$	0.22426
$0.75\Delta t = 0.13568$	$t = 737\Delta t = 99.99633$	0.04025
$0.7\Delta t = 0.12663$	$t = 789\Delta t = 99.91492$	0.04044

Table 7.4: Stability analysis for non-flat linear method with slowly-varying coefficient, finite difference $\beta = 0.001$ and $\|\boldsymbol{\eta}^0\|_\infty = 0.09751$.

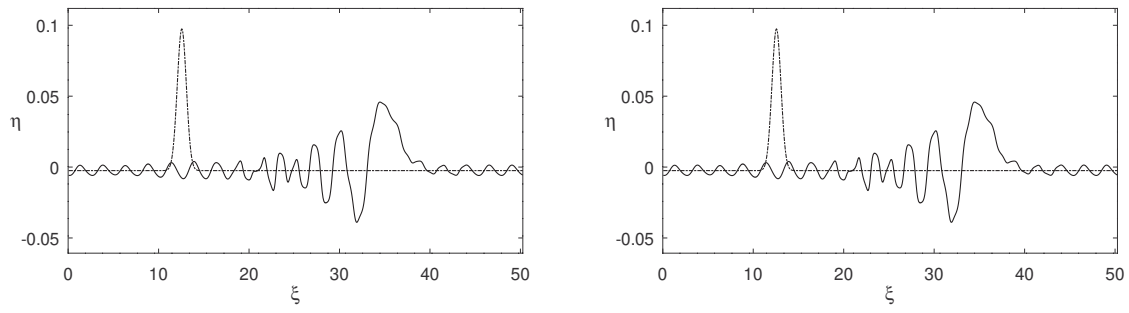

(a) Spectral scheme

(b) Finite difference

Figure 7.10: Solutions η for the non-flat linear method at $t = 0$ $(\cdots)$ and $t = 600\Delta t$ (—) with $l = 8\pi$, $\beta = 0.001$, $\Delta\xi = 0.04909$, $\Delta t = 0.12663$ and slowly-varying coefficient.

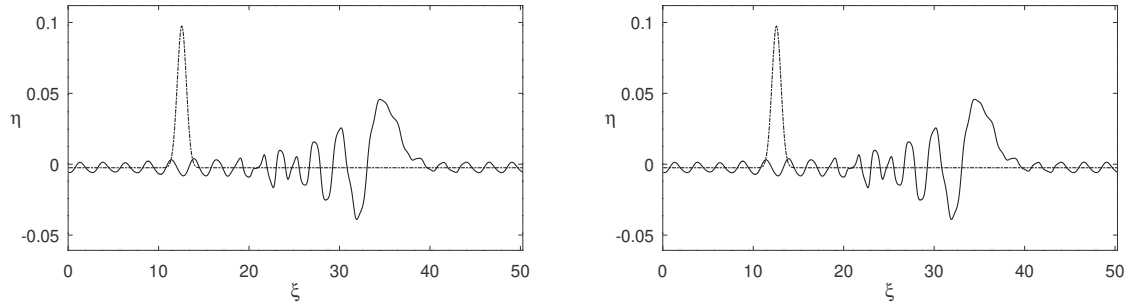

(a) Spectral scheme (b) Finite difference

Figure 7.11: Solutions η for the non-flat nonlinear method at $t = 0$ $(\cdots)$ and $t = 600\Delta t$ (—) with $l = 8\pi$, $\alpha = \beta = 0.001$, $\Delta\xi = 0.04909$, $\Delta t = 0.12663$ and slowly-varying coefficient.

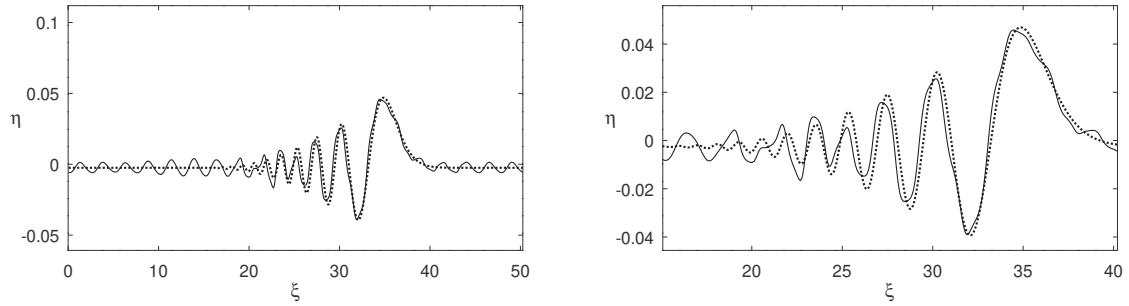

(a) Solutions with SP differentiation (b) Detail

Figure 7.12: Solutions η at $t = 600\Delta t$ for flat nonlinear method $(\cdots)$ and non-flat nonlinear method (—) with $l = 8\pi$, $\alpha = \beta = 0.001$, $\Delta\xi = 0.04909$, $\Delta t = 0.12663$ and slowly-varying coefficient.

Figure 7.13 shows that the travelling wave has a similar behavior to the case with $\alpha = \beta = 0.0001$ and we cannot see the Bragg's phenomenon. Also, when we analyze the Fourier modes of the solutions we see that the effects of the coefficient M are very similar to the previous ones.

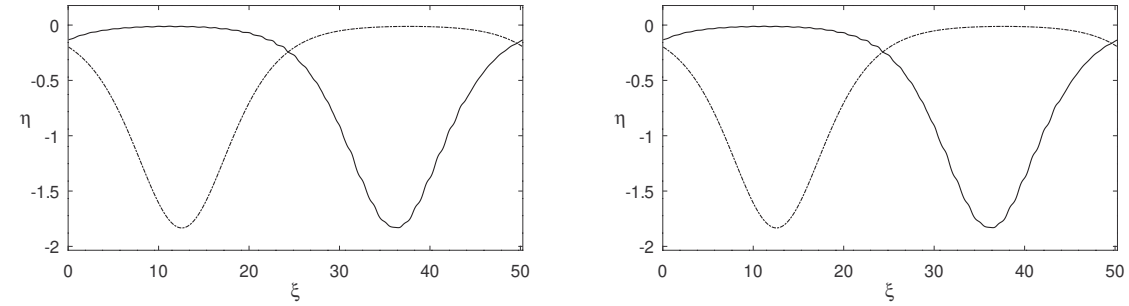

(a) Spectral scheme (b) Finite difference

Figure 7.13: Solutions η for the non-flat nonlinear method at $t = 0$ $(\cdots)$ and $t = 600\Delta t$ (—) with $l = 8\pi$, $\alpha = \beta = 0.001$, $\Delta\xi = 0.04909$, $\Delta t = 0.12663$ and slowly-varying coefficient.

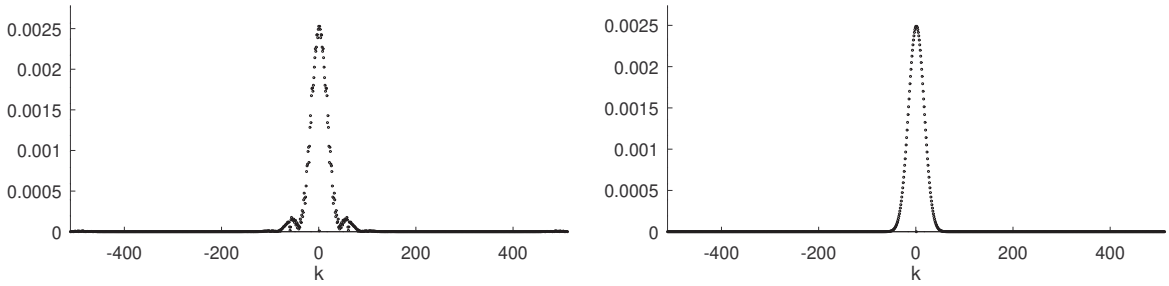

(a) Non-flat bottom

(b) Flat bottom

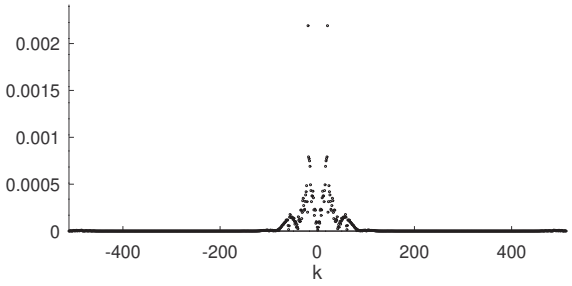

(c) Difference module

Figure 7.14: Fourier modes $|\hat{\eta}^n|$ of solutions η for the non-flat nonlinear method at $t = 600\Delta t$ with $l = 8\pi$, $\alpha = \beta = 0.001$, $\Delta\xi = 0.04909$, $\Delta t = 0.12663$ and slowly-varying coefficient.

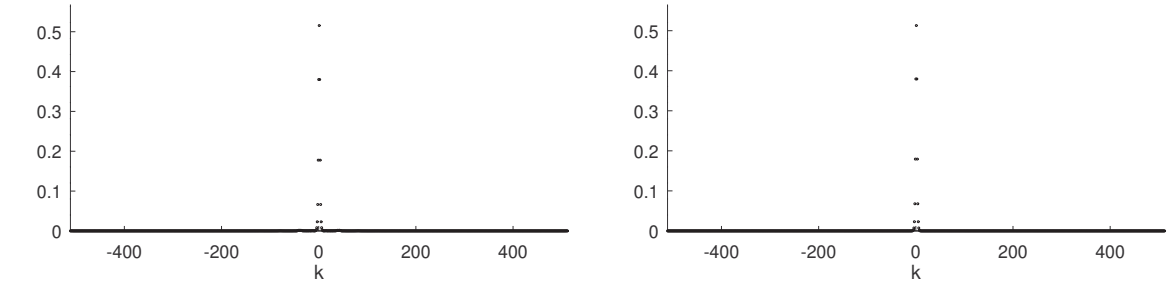

(a) Non-flat bottom

(b) Flat bottom

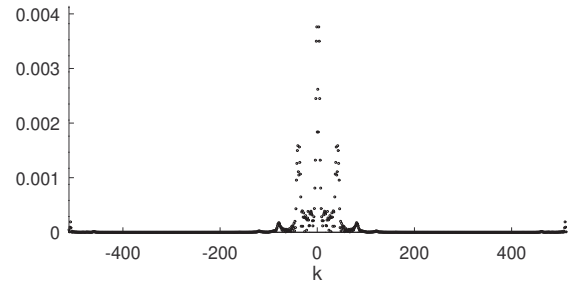

(c) Difference module

Figure 7.15: Fourier modes $|\hat{\eta}^n|$ of solutions η for the non-flat nonlinear method at $t = 600\Delta t$ with $l = 8\pi$, $\alpha = \beta = 0.001$, $\Delta\xi = 0.04909$, $\Delta t = 0.12663$ and slowly-varying coefficient.

Now we will consider the periodic rapidly-varying coefficient M given by

$$M(\xi) = \begin{cases} 1 + 0.5\sin(15\xi) & \text{if } \xi \in [6\pi, 12\pi] \\ 1 & \text{otherwise.} \end{cases}$$

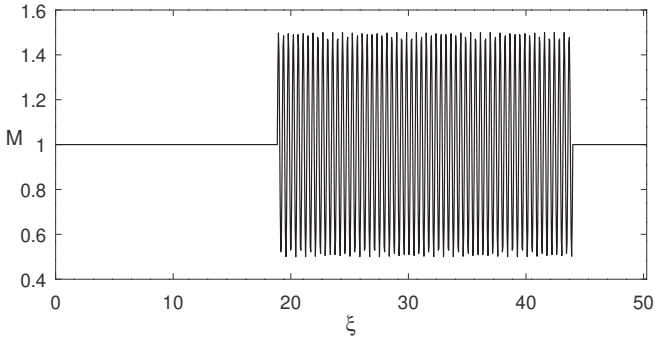

Figure 7.16: Periodic rapidly-varying coefficient M.

In this case of rapidly-varying coefficient, for $\alpha = \beta = 0.0001$ the stability condition (4.14) presents a stable Δt as tables 7.5 and 7.6 and figures 7.17 and 7.18 show. Differently from the case of slowly-varying coefficient there are no waves from the Bragg's phenomenon. In fact, the effect of the coefficient consist in a slightly lower speed propagation as illustrates figure 7.23. The travelling wave is also well preserved in this case as presented in figure 7.21.

Δt	t	$\|\boldsymbol{\eta}^n\|_\infty$
$\Delta t = 0.10173$	$t = 982\Delta t = 99.90030$	0.07482
$0.95\Delta t = 0.09664$	$t = 1034\Delta t = 99.93082$	0.07483
$0.9\Delta t = 0.09156$	$t = 1092\Delta t = 99.98169$	0.07483

Table 7.5: Stability analysis for non-flat nonlinear method with rapidly-varying coefficient, spectral scheme, $\beta = 0.0001$ and $\|\boldsymbol{\eta}^0\|_\infty = 0.09751$.

Δt	t	$\|\boldsymbol{\eta}^n\|_\infty$
$\Delta t = 0.10173$	$t = 982\Delta t = 99.90030$	0.07482
$0.95\Delta t = 0.09664$	$t = 1034\Delta t = 99.93082$	0.07483
$0.9\Delta t = 0.09156$	$t = 1092\Delta t = 99.98169$	0.07483

Table 7.6: Stability analysis for non-flat nonlinear method with rapidly-varying coefficient, finite difference scheme, $\beta = 0.0001$ and $\|\boldsymbol{\eta}^0\|_\infty = 0.09751$.

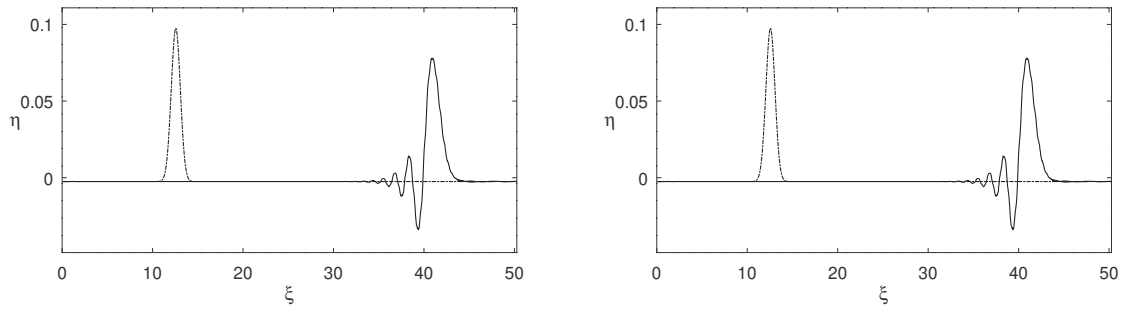

(a) Spectral scheme (b) Finite difference

Figure 7.17: Solutions η for the non-flat nonlinear method at $t = 0$ $(\cdots)$ and $t = 800\Delta t$ (—) with $l = 8\pi$, $\alpha = \beta = 0.0001$, $\Delta x = 0.04909$, $\Delta t = 0.10173$ and rapidly-varying coefficient.

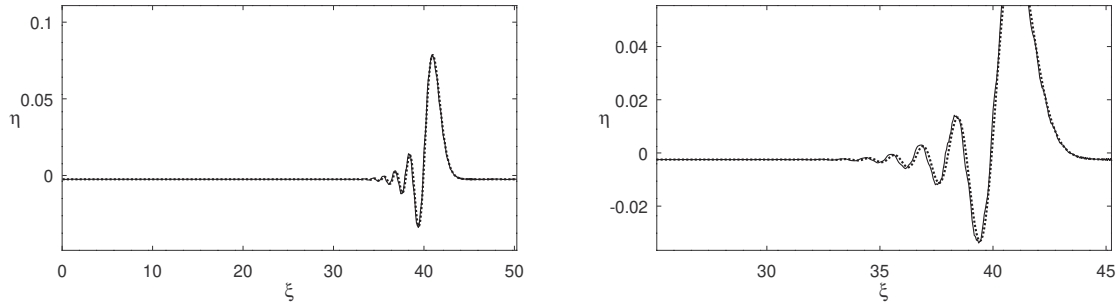

(a) Solutions with SP differentiation (b) Detail

Figure 7.18: Solutions η at $t = 800\Delta t$ for flat nonlinear method $(\cdots)$ and non-flat nonlinear method (—) with $l = 8\pi$, $\alpha = \beta = 0.0001$, $\Delta\xi = 0.04909$, $\Delta t = 0.10173$ and rapidly-varying coefficient.

Figure 7.19 shows the Fourier modes of the solutions for the gaussian profile. We can see that the effects of M are smaller and distributed in a bigger range which is comparable with the modes of the coefficient presented in figure 7.20. Although small, the effects of the coefficient M in the solution are apparent in figure 7.22. In both cases an instability appears for large values of $|k|$, but it is controlled and does not pollute the solutions obtained.

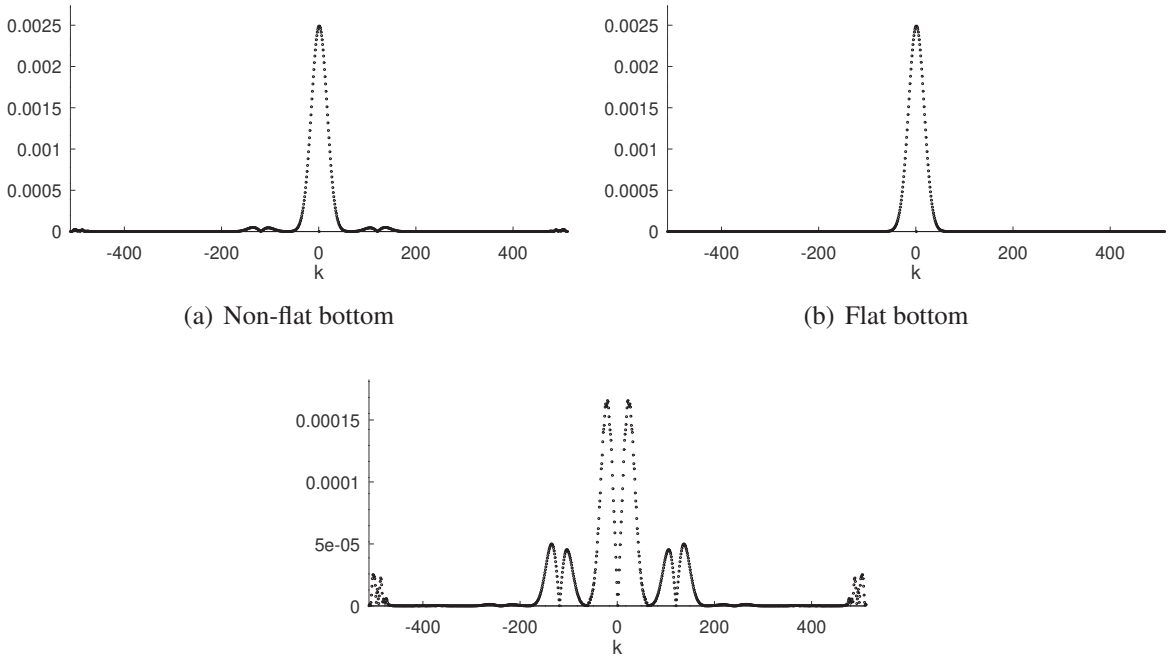

(a) Non-flat bottom (b) Flat bottom

(c) Difference module

Figure 7.19: Fourier modes $|\hat{\eta}^n|$ of solutions η for the non-flat nonlinear method at $t = 800\Delta t$ with $l = 8\pi$, $\alpha = \beta = 0.0001$, $\Delta x = 0.04909$, $\Delta t = 0.10173$ and rapidly-varying coefficient.

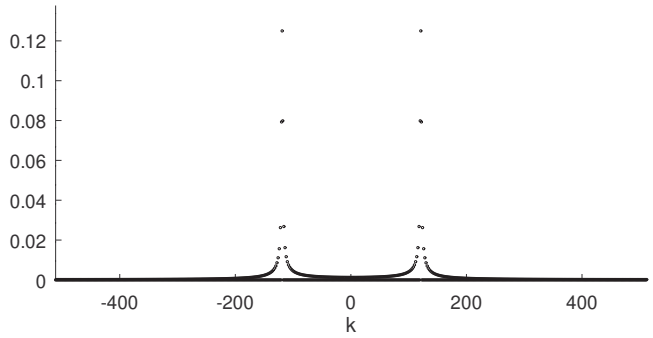

Figure 7.20: Fourier mode of periodic rapidly-varying coefficient M.

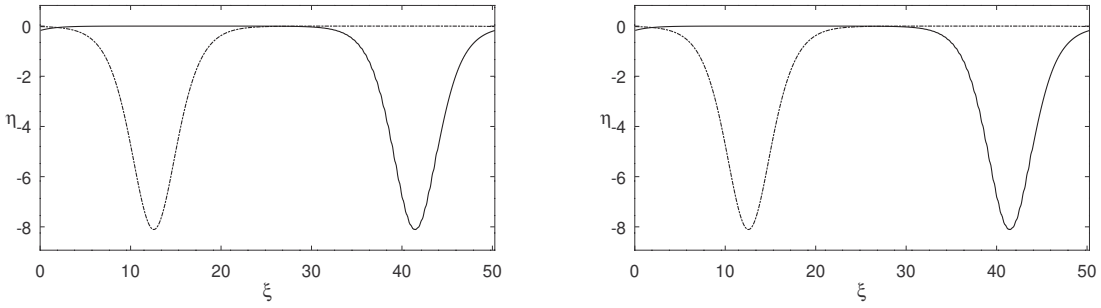

(a) Spectral scheme

(b) Finite difference

Figure 7.21: Solutions η for the non-flat nonlinear method at $t = 0$ $(\cdots)$ and $t = 800\Delta t$ (—) with $l = 8\pi$, $\alpha = \beta = 0.0001$, $\Delta\xi = 0.04909$, $\Delta t = 0.10173$ and rapidly-varying coefficient.

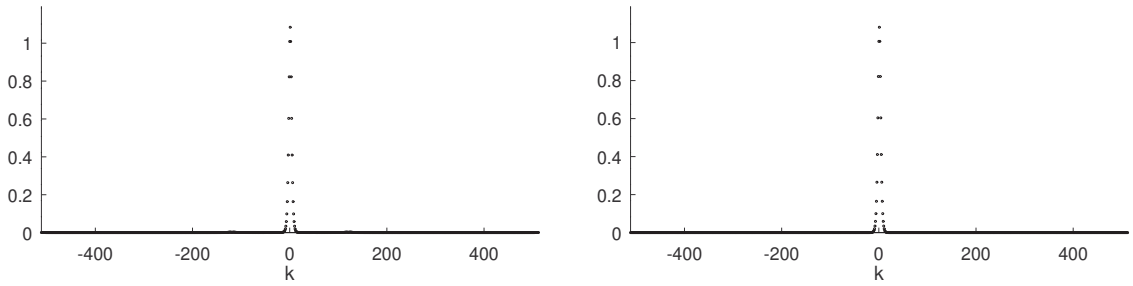

(a) Non-flat bottom

(b) Flat bottom

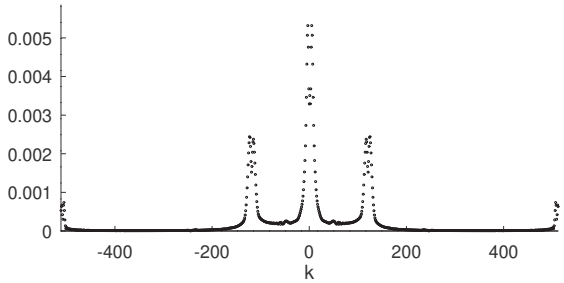

(c) Difference module

Figure 7.22: Solutions η for the non-flat nonlinear method at $t = 800\Delta t$ with $l = 8\pi$, $\alpha = \beta = 0.0001$, $\Delta x = 0.04909$, $\Delta t = 0.10173$ and rapidly-varying coefficient.

In the case of $\alpha = \beta = 0.001$ we do not have a stable Δt from the stability condition (4.14) as tables 7.5 and 7.6 present. Using $\Delta t = 0.14473$ the solutions obtained are stable

in both cases for the nonlinear methods as presented in figures 7.17 and 7.18. As in the tests with $\alpha = \beta = 0.0001$ and rapidly-varying coefficient there are no waves from the Bragg's phenomenon, just a slightly lower speed propagation as before that is shown in figure 7.23. Again, the shape of the travelling wave is well preserved as illustrated in figure 7.26.

Δt	t	$\|\boldsymbol{\eta}^n\|_\infty$
$\Delta t = 0.18091$	$t = 28\Delta t = 5.06540$	0.21780
$0.95\Delta t = 0.17186$	$t = 45\Delta t = 7.73377$	0.21425
$0.9\Delta t = 0.16282$	$t = 173\Delta t = 28.16722$	0.19672
$0.85\Delta t = 0.15377$	$t = 650\Delta t = 99.95110$	0.04277
$0.8\Delta t = 0.14473$	$t = 690\Delta t = 99.86065$	0.04283

Table 7.7: Stability analysis for non-flat nonlinear method with rapidly-varying coefficient, spectral scheme, $\beta = 0.001$ and $\|\boldsymbol{\eta}^0\|_\infty = 0.09751$.

Δt	t	$\|\boldsymbol{\eta}^n\|_\infty$
$\Delta t = 0.18091$	$t = 30\Delta t = 5.42721$	0.38065
$0.95\Delta t = 0.17186$	$t = 49\Delta t = 8.42122$	0.29919
$0.9\Delta t = 0.16282$	$t = 208\Delta t = 33.86579$	0.23822
$0.85\Delta t = 0.15377$	$t = 650\Delta t = 99.95110$	0.04275
$0.8\Delta t = 0.14473$	$t = 690\Delta t = 99.86065$	0.04282

Table 7.8: Stability analysis for non-flat nonlinear method with rapidly-varying coefficient, finite difference scheme, $\beta = 0.001$ and $\|\boldsymbol{\eta}^0\|_\infty = 0.09751$.

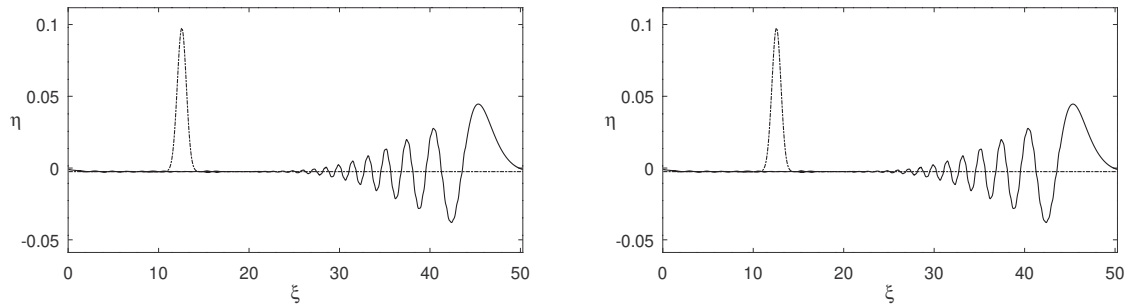

(a) Spectral scheme (b) Finite difference

Figure 7.23: Solutions η for the non-flat nonlinear method at $t = 0$ $(\cdots)$ and $t = 600\Delta t$ (—) with $l = 8\pi$, $\alpha = \beta = 0.001$, $\Delta\xi = 0.04909$, $\Delta t = 0.14473$ and rapidly-varying coefficient.

Figures 7.25 and 7.27 show the Fourier modes of the solutions with a gaussian initial profile and an approximate travelling wave from the flat case, respectively, for $\alpha = \beta = 0.001$. Again we can see that the effects of M are smaller and distributed in a bigger range as for $\alpha = \beta = 0.0001$. An analogous instability appeared for large values of $|k|$, which is controlled and does not pollute the solutions obtained.

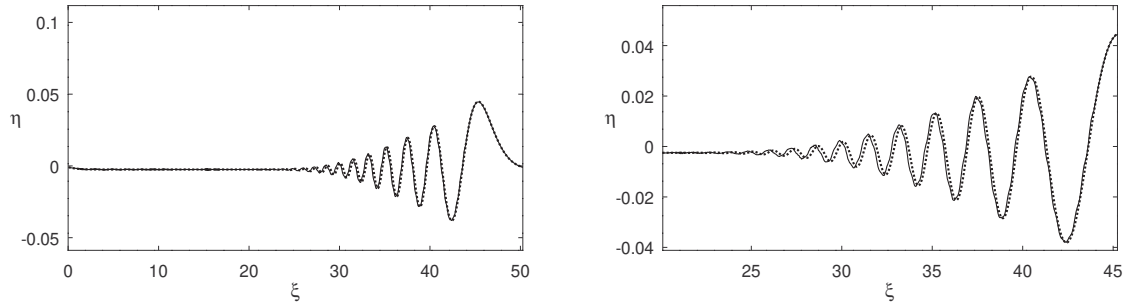

(a) Solutions with SP differentiation (b) Detail

Figure 7.24: Solutions η at $t = 600\Delta t$ for flat nonlinear method $(\cdots)$ and non-flat nonlinear method (—) with $l = 8\pi$, $\alpha = \beta = 0.001$, $\Delta\xi = 0.04909$, $\Delta t = 0.14473$ and rapidly-varying coefficient.

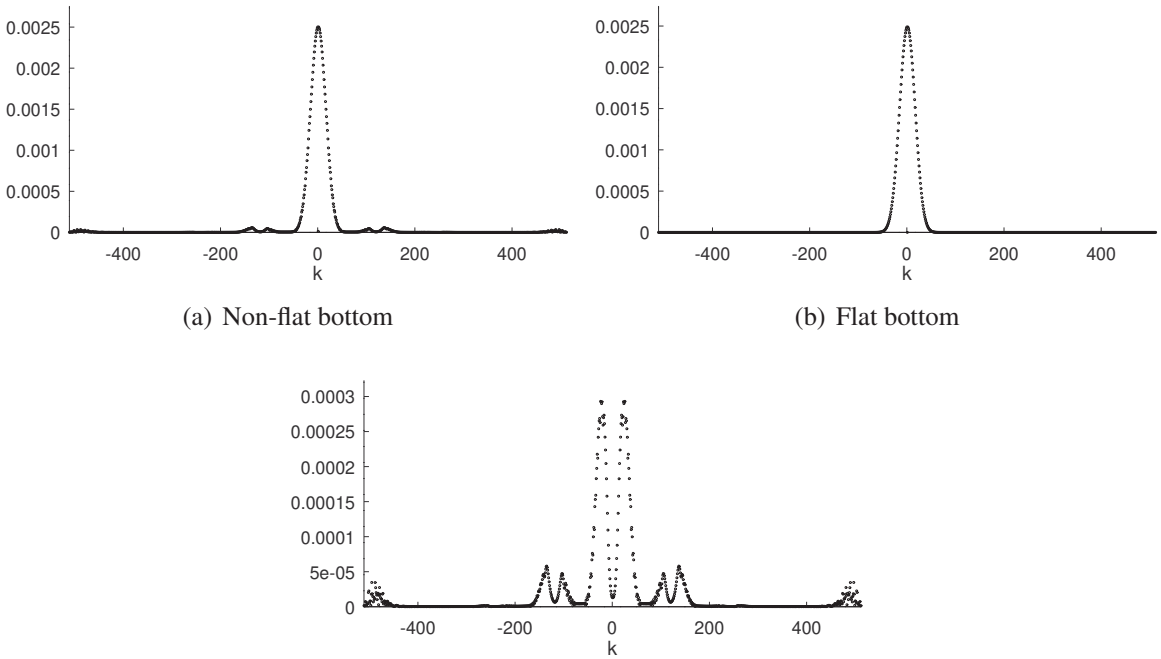

(a) Non-flat bottom (b) Flat bottom

(c) Difference module

Figure 7.25: Fourier modes $|\hat{\eta}^n|$ of solutions η for the non-flat nonlinear method at $t = 600\Delta t$ with $l = 8\pi$, $\alpha = \beta = 0.001$, $\Delta\xi = 0.04909$, $\Delta t = 0.14473$ and rapidly-varying coefficient.

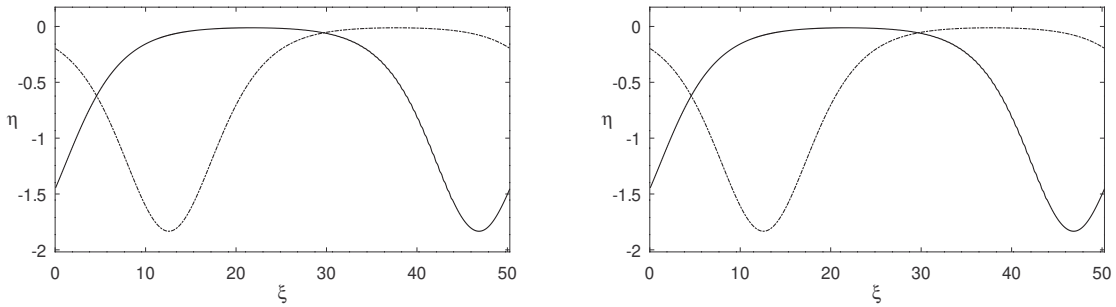

(a) Spectral scheme (b) Finite difference

Figure 7.26: Solutions η for the non-flat nonlinear method at $t = 0$ $(\cdots)$ and $t = 600\Delta t$ (—) with $l = 8\pi$, $\alpha = \beta = 0.001$, $\Delta\xi = 0.04909$, $\Delta t = 0.14473$ and rapidly-varying coefficient.

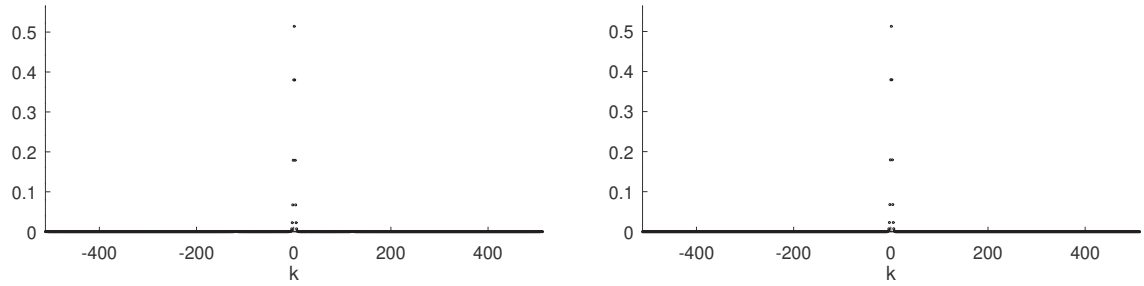

(a) Non-flat bottom

(b) Flat bottom

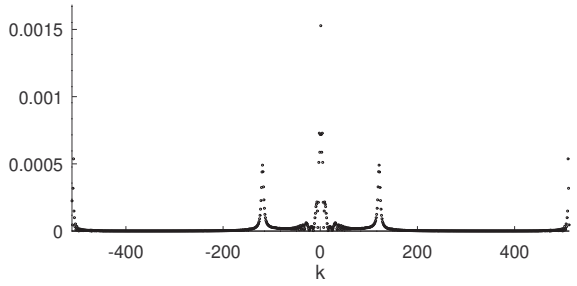

(c) Difference module

Figure 7.27: Fourier modes $|\hat{\eta}^n|$ of solutions η for the non-flat nonlinear method at $t = 600\Delta t$ with $l = 8\pi$, $\alpha = \beta = 0.001$, $\Delta\xi = 0.04909$, $\Delta t = 0.14473$ and rapidly-varying coefficient.

The numerical methods proposed for the non-flat bottom models perform well and are important to understand the effects of the coefficient M in the solutions. When the slowly-varying coefficient is used we see the effects of Bragg's phenomenon which are strong in the gaussian profile and weak in the travelling wave. On the other hand, as expected, when the rapidly-varying coefficient is used the effects are small and the shape of the solution differs little from the flat bottom case. Also, there is no significant difference in terms of stability and computational cost between the spectral scheme and the finite difference in the discretization of the first order derivatives in ψ.

Chapter 8

Conclusions

Some works about the internal wave models deduced by Ruiz de Zarate in [25] have been published recently. The existence of solutions in Sobolev spaces for flat bottom models was proved by Brodzinski in [7]. Also, a very efficient numerical scheme for these same models was presented by the author in [16]. In this work, new results for these models were presented.

The methods for the flat bottom models served as the base for the schemes for the non-flat bottom models (7.1) and (2.8). Instead of a theoretical stability analysis for the non-flat bottom the stability conditions for the flat bottom methods were used as starting points for a numerical procedure to get a good choice of Δt in terms of stability for each experiment. The effects of the coefficient M in the solutions were studied in some cases where the Bragg's phenomenon appears when considering a slowly-varying coefficient M and a small loss of velocity was noted when considering a rapidly-varying coefficient M.

Works on the fixed-point index theory were studied with the aim of proving the existence of traveling waves for the nonlinear system (2.5). Unfortunately, due to some characteristics of the system, the method cannot be successfully applied. However, it was possible to prove the existence of travelling wave solutions for the regularized finite depth Benjamin equation (2.9) obtained by asymptotic analysis from system (2.5). In future works the existence of non periodic travelling waves for this equation can be proven and also numerical methods to compute them can be proposed.

The approach proposed by the author in [16] to obtain travelling waves for the nonlinear system (2.5) was improved and now we have an efficient method to compute travelling waves. Furthermore, in the search for a good initial guess for the aforementioned method, it was found that the travelling wave solutions of the rILW equation perform satisfactorily as travelling waves for the nonlinear system (2.5). The good numerical results obtained here are a motivation to continue the study of theoretical existence of travelling waves for the nonlinear system (2.5) in future works.

References

[1] Daniel Alfaro Vigo, Saulo Oliveira, Ailín Ruiz de Zárate, and André Nachbin, *Fully discrete stability and dispersion analysis for a linear dispersive internal wave model*, Computational and Applied Mathematics **33** (2013), 203–221.

[2] J.R. Apel, L.A. Ostrovsky, Y.A. Stepanyants, and J.F. Lynch, *Internal solitons in the ocean*, Tech. report, Woods Hole Oceanographic Institution, 2006.

[3] U. M. Ascher and L. R. Petzold, *Computer methods for ordinary differential equations and differential-algebraic equations*, Society for Industrial and Applied Mathematics, 1998.

[4] T. B. Benjamin, *Internal waves of permanent form in fluids of great depth*, Journal of Fluid Mechanics **29** (1967), no. 3, 559–592.

[5] ———, *A new kind of solitary wave*, Journal of Fluid Mechanics **245** (1992), 401–411.

[6] ———, *Solitary and periodic waves of a new kind*, Philosophical Transactions of the Royal Society of London **354** (1996), 1775–1806.

[7] J. S. Brodzinski, *Estudo de um modelo dispersivo não linear para ondas internas*, Ph.D. thesis, UFPR, 2016.

[8] J. W. Brown and R. V. Churchill, *Complex variables and applications*, McGraw-Hill, 2009.

[9] Wooyoung Choi and Roberto Camassa, *Fully nonlinear internal waves in a two-fluid system*, Journal of Fluid Mechanics **396** (1999), 1–36.

[10] T. N. dos Santos, *Ondas viajantes*, Monography, UFPR, 2010.

[11] P. G. Drazin and R. S Johnson, *Solitons: An introduction*, Cambridge University Press, 1989.

[12] E. Guazzeli, V. Rey, and M. Belzons, *Higher order bragg reflection of gravity surface waves by periodic beds*, Journal of Fluid Mechanics **245** (1992), 301–317.

[13] Karl R. Helfrich and W. Kendall Melville, *Long nonlinear internal waves*, Annual Review of Fluid Mechanics **38** (2006), 395–425.

[14] R. Iorio Jr and V. Iorio, *Fourier analysis and partial differential equations*, Cambridge University Press, 2001.

[15] R. I. Joseph, *Solitary waves in a finite depth fluid*, Journal of Physics A Mathematical General **10** (1977), no. 12, L225–L227.

[16] Willian Carlos Lesinhovski, *Análise de von neumann de um modelo dispersivo de ondas internas*, Master's thesis, UFPR, 2017.

[17] J. C. Munoz and A. Nachbin, *Dispersive wave attenuation due to orographic forcing*, SIAM Journal of Applied Mathematics **64** (2004), 977–1001.

[18] J. C. Munoz and A Nachbin, *Stiff microscale forcing and solitary wave refocusing*, SIAM Multiscale Modeling and Simulation **3** (2005), 680–705.

[19] Nachbin, *A terrain-following boussinesq system*, SIAM Journal on Applied Mathematics **63** (2003), 905–922.

[20] A. Nachbin and A. Ruiz de Zarate, *Tópicos introdutórios à análise complexa aplicada*, IMPA, 2010.

[21] Fridtjof Nansen, *Farthest north: The epic adventure of a visionary explorer*, Skyhorse Publishing Inc., 2008.

[22] F. M. A. Natali, *Propriedades de positividade e estabilidade de ondas viajantes periódicas*, Ph.D. thesis, UNICAMP, 2007.

[23] F. A. Pipicano, *Ondas viajeras periódicas para un sistema benjamin-ono regularizado*, Master's thesis, Universidad Del Vale, 2016.

[24] F. A. Pipicano and J. C. M. Grajales, *Existence of periodic travelling wave solutions for a regularized benjamin-ono system*, Journal of Differential Equations **259** (2015), 7503–7528.

[25] Ailín Ruiz de Zárate, *A reduced model for internal waves interacting with submarine structures at intermediate depth*, Ph.D. thesis, IMPA, 2007.

[26] Ailín Ruiz de Zárate, Daniel Alfaro Vigo, André Nachbin, and And Choi, *A higher-order internal wave model accounting for large bathymetric variations*, Studies in Applied Mathematics **122** (2009), 275–294.

[27] G. Strang, *Introduction to applied mathematics*, Cambridge University Press, 1986.

[28] Bruce R. Sutherland, *Internal gravity waves*, Cambridge University Press, 2010.

[29] G. B. Whitham, *Linear and nonlinear waves*, Wiley, 2011.

Appendix A

Travelling wave solutions for BBM equation

Let us deduce the travelling wave solutions for the BBM equation (6.12) and the KdV equation. Defining $a_1 = 3\alpha/2$ and $a_2 = \beta/6$ and making the change of variables $\eta^* = -a_1\eta$, $x^* = \sqrt{a_2}x$ and $t^* = \sqrt{a_2}t$ we get the equations

$$\eta_t + \eta_x + \eta\eta_x - \eta_{xxt} = 0 \tag{A.1}$$

and

$$\eta_t + \eta_x + \eta\eta_x + \eta_{xxx} = 0 \tag{A.2}$$

where asterisks are ignored.

For simplicity let us begin by equation (A.2). Supposing that there exists a travelling wave solution $\eta(x,t) = f(x-ct) = f(z)$ for equation (A.2) we obtain

$$(1-c)f' + ff' + f''' = 0.$$

Defining $\tilde{c} = c - 1$ in order to simplify the computations we get

$$-\tilde{c}f' + ff' + f''' = 0.$$

Let us suppose that $f, f', f'' \to 0$ when $z \to \pm\infty$, thus, integrating we have

$$-\tilde{c}f + \frac{f^2}{2} + f'' = 0.$$

Multiplying this by f' and integrating over again we have

$$-\tilde{c}\frac{f^2}{2} + \frac{f^3}{6} + \frac{(f')^2}{2} = 0$$

that can be simplified as

$$3(f')^2 = (3\tilde{c} - f)f^2.$$

Considering $3\tilde{c} - f > 0$ we obtain

$$\sqrt{3}|f'| = \sqrt{3\tilde{c} - f}|f|.$$

Defining the auxiliary function $g = \sqrt{3\tilde{c} - f}$ we get

$$\frac{-2\sqrt{3}gg'}{g(3\tilde{c}-g^2)}=1.$$

Thus, making some algebraic calculations we have

$$\frac{-2\sqrt{3\tilde{c}}gg'}{g(3\tilde{c}-g^2)}=\frac{g'}{\sqrt{3\tilde{c}}-g}+\frac{g'}{\sqrt{3\tilde{c}}+g}=\sqrt{\tilde{c}}.$$

Integrating this expression we obtain

$$-\log(\sqrt{3\tilde{c}}-g)+\log(\sqrt{3\tilde{c}}+g)=-\sqrt{\tilde{c}}z+d,$$

and consequently

$$\log\left(\frac{\sqrt{3\tilde{c}}+g}{\sqrt{3\tilde{c}}-g}\right)=-\sqrt{\tilde{c}}z+d,$$

which lead us to conclude that

$$g=-\sqrt{3\tilde{c}}\tanh\left(\frac{\sqrt{\tilde{c}}z+d}{2}\right).$$

So, we have that

$$f=3\tilde{c}\,\mathrm{sech}^2\left(\frac{\sqrt{\tilde{c}}z+d}{2}\right).$$

That is, the travelling wave solution of equation (A.2) is

$$f(z)=3(c-1)\,\mathrm{sech}^2\left(\frac{\sqrt{c-1}}{2}z\right),$$

and therefore, the travelling wave solution of the KdV equation is

$$\eta(y)=-\frac{3(c-1)}{a_1}\,\mathrm{sech}^2\left(\frac{\sqrt{c-1}y}{2\sqrt{a_2}}\right).$$

Analogously, supposing that there exists a travelling wave solution $\eta(x,t)=f(x-ct)=f(z)$ for the equation (A.1) we have

$$-\tilde{c}f'+ff'+cf'''=0,$$

which lead us to

$$\sqrt{3c}|f'|=\sqrt{3\tilde{c}-f}|f|.$$

So, we conclude that the travelling wave solution of the equation (A.1) is

$$f(z)=3(c-1)\,\mathrm{sech}^2\left(\frac{\sqrt{c-1}}{2\sqrt{c}}z\right).$$

Therefore, the travelling wave solution of the BBM equation (6.12) is

$$\eta(y)=-\frac{3(c-1)}{a_1}\,\mathrm{sech}^2\left(\frac{\sqrt{c-1}y}{2\sqrt{ca_2}}\right).$$

Appendix B

Extra travelling wave experiments

Here we present some extra experiments for the three methods to obtain travelling waves using higher values of α and β. The results presented here are consistent with the ones in chapter 6, also, we remark that the second method did not converge for $d = 0$, $\alpha = \beta = 0.01$ and $l = 20\pi$.

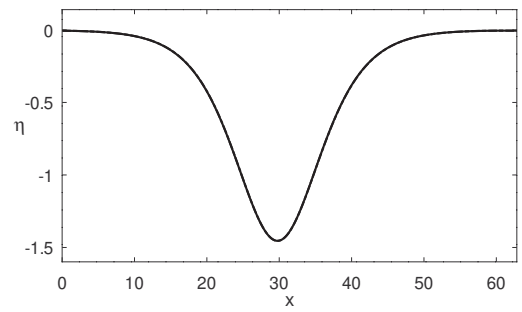

(a) $\theta = \pi/10$, $d \neq 0$

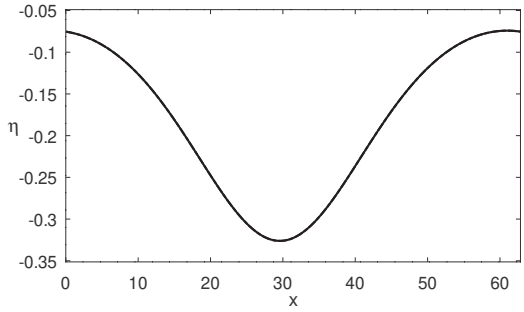

(b) $\theta = \pi/20$, $d \neq 0$

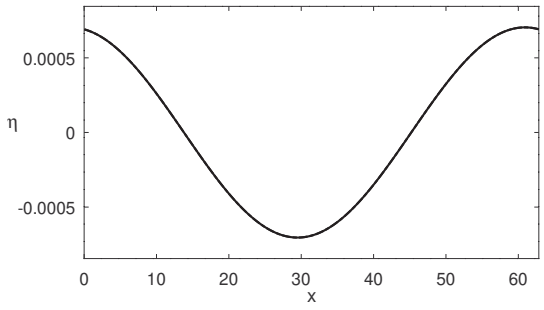

(c) $\theta = \pi/10$, $d = 0$

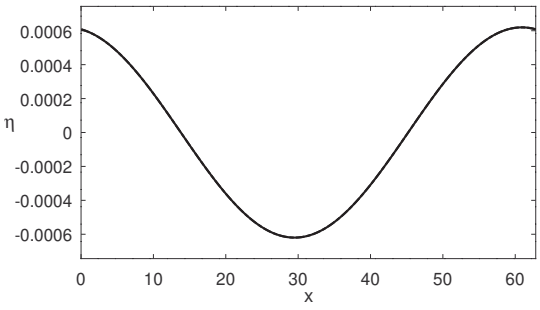

(d) $\theta = \pi/20$, $d = 0$

Figure B.1: Graphics of $\boldsymbol{\eta}^*$ $(- \cdot -)$ and $\boldsymbol{\eta}^n$ $(—)$ for the first method and each initial guess with $l = 10\pi$, $\alpha = \beta = 0.005$, $\Delta x = 0.03068$, $\Delta t = 0.21386$ at time $t = 62.66217 = 293\Delta t$.

Profiles	e_{abs}	e_{rel}	c_n	c
$\theta = \pi/10,\ d \neq 0$	0.0420997	0.0015622	0.97637	0.97598
$\theta = \pi/20,\ d \neq 0$	0.0013104	0.0001421	0.97352	0.97342
$\theta = \pi/10,\ d = 0$	0.0000037	0.0001632	0.97207	0.97209
$\theta = \pi/20,\ d = 0$	0.0000032	0.0001626	0.97207	0.97210

Table B.1: Errors at time $t = 62.66217 = 293\Delta t$ and wave velocities of η for the first method and each initial guess with $l = 10\pi$, $\alpha = \beta = 0.005$, $\Delta x = 0.03068$, $\Delta t = 0.21386$.

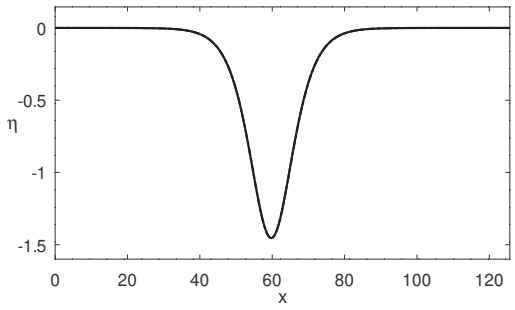

(a) $\theta = \pi/10,\ d \neq 0$

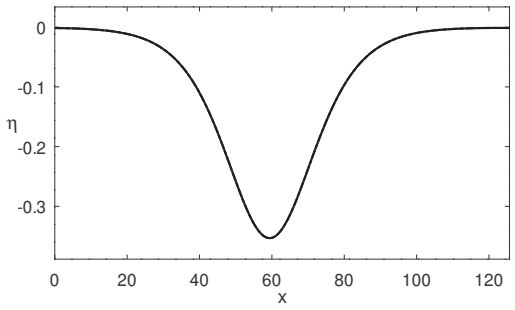

(b) $\theta = \pi/20,\ d \neq 0$

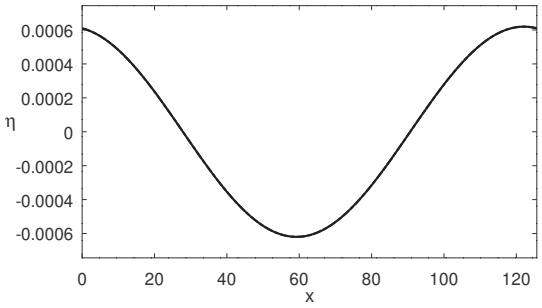

(c) $\theta = \pi/10,\ d = 0$

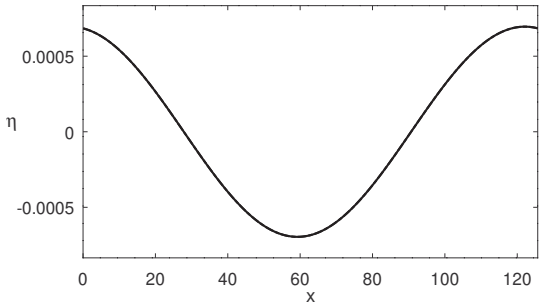

(d) $\theta = \pi/20,\ d = 0$

Figure B.2: Graphics of $\boldsymbol{\eta}^*$ $(- \cdot -)$ and $\boldsymbol{\eta}^n$ $(—)$ for the first method and each initial guess with $l = 20\pi$, $\alpha = \beta = 0.005$, $\Delta x = 0.03068$, $\Delta t = 0.21386$ at time $t = 125.53821 = 587\Delta t$.

Profiles	e_{abs}	e_{rel}	c_n	c
$\theta = \pi/10,\ d \neq 0$	0.0794506	0.0029482	0.97636	0.97598
$\theta = \pi/20,\ d \neq 0$	0.0028267	0.0003007	0.97354	0.97345
$\theta = \pi/10,\ d = 0$	0.0000017	0.0000609	0.97251	0.97250
$\theta = \pi/20,\ d = 0$	0.0000020	0.0000623	0.97251	0.97250

Table B.2: Errors at time $t = 125.53821 = 587\Delta t$ and wave velocities of η for the first method and each initial guess with $l = 20\pi$, $\alpha = \beta = 0.005$, $\Delta x = 0.03068$, $\Delta t = 0.21386$.

Profiles	e_{abs}	e_{rel}	c_n	c
$\theta = \pi/5,\ d \neq 0$	0.5650807	0.0117298	0.98917	0.98782
$\theta = \pi/10,\ d \neq 0$	0.0226095	0.0014128	0.97643	0.97597
$\theta = \pi/5,\ d = 0$	0.0000289	0.0006195	0.97165	0.97156
$\theta = \pi/10,\ d = 0$	0.0000040	0.0003549	0.97161	0.97156

Table B.3: Errors at time $t = 62.81918 = 247\Delta t$ and wave velocities of η for the first method and each initial guess with $l = 10\pi$, $\alpha = \beta = 0.01$, $\Delta x = 0.03068$, $\Delta t = 0.25433$.

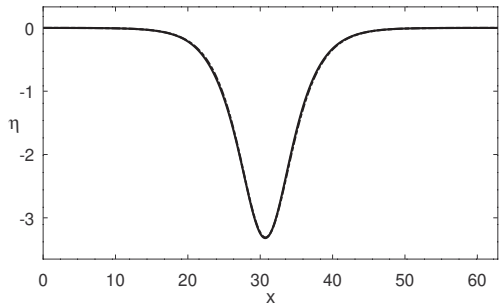

(a) $\theta = \pi/5$, $d \neq 0$

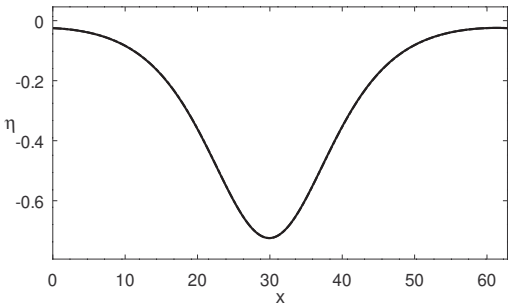

(b) $\theta = \pi/10$, $d \neq 0$

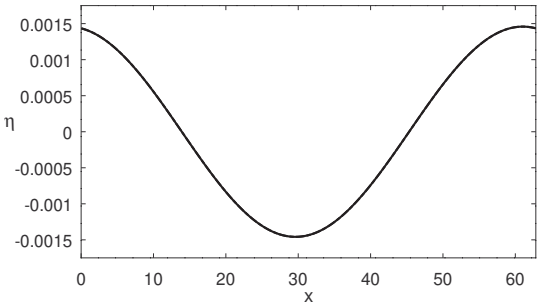

(c) $\theta = \pi/5$, $d = 0$

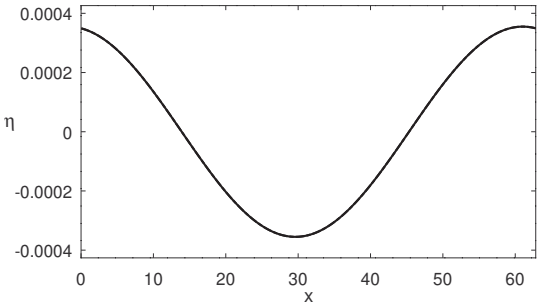

(d) $\theta = \pi/10$, $d = 0$

Figure B.3: Graphics of $\boldsymbol{\eta}^*$ $(- \cdot -)$ and $\boldsymbol{\eta}^n$ $(—)$ for the first method and each initial guess with $l = 10\pi$, $\alpha = \beta = 0.01$, $\Delta x = 0.03068$, $\Delta t = 0.25433$ at time $t = 62.81918 = 247\Delta t$.

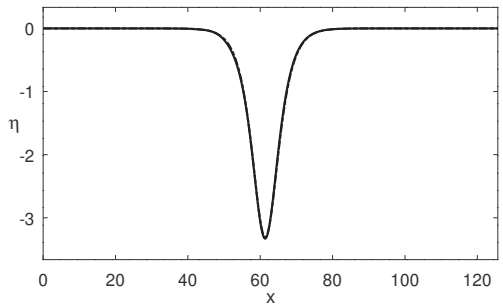

(a) $\theta = \pi/5$, $d \neq 0$

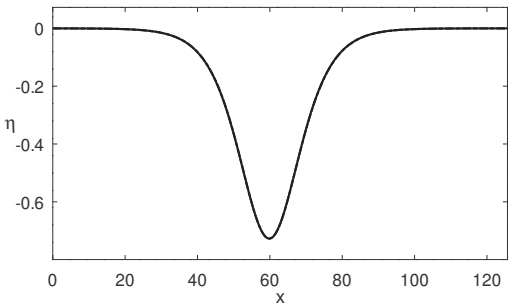

(b) $\theta = \pi/10$, $d \neq 0$

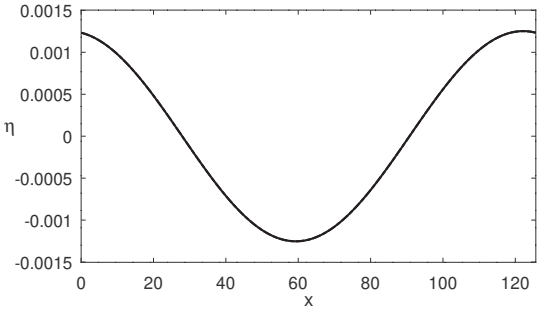

(c) $\theta = \pi/5$, $d = 0$

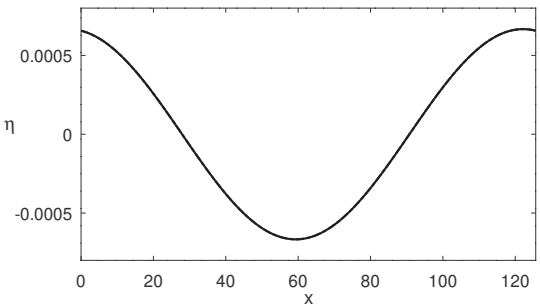

(d) $\theta = \pi/10$, $d = 0$

Figure B.4: Graphics of $\boldsymbol{\eta}^*$ $(- \cdot -)$ and $\boldsymbol{\eta}^n$ $(—)$ for the first method and each initial guess with $l = 20\pi$, $\alpha = \beta = 0.01$, $\Delta x = 0.03068$, $\Delta t = 0.25433$ at time $t = 125.63836 = 494\Delta t$.

Profiles	e_{abs}	e_{rel}	c_n	c
$\theta = \pi/5$, $d \neq 0$	0.7096486	0.0147307	0.98874	0.98782
$\theta = \pi/10$, $d \neq 0$	0.0354102	0.0022098	0.97637	0.97598
$\theta = \pi/5$, $d = 0$	0.0000091	0.0001598	0.97239	0.97236
$\theta = \pi/10$, $d = 0$	0.0000029	0.0000947	0.97238	0.97236

Table B.4: Errors at time $t = 125.63836 = 494\Delta t$ and wave velocities of η for the first method and each initial guess with $l = 20\pi$, $\alpha = \beta = 0.01$, $\Delta x = 0.03068$, $\Delta t = 0.25433$.

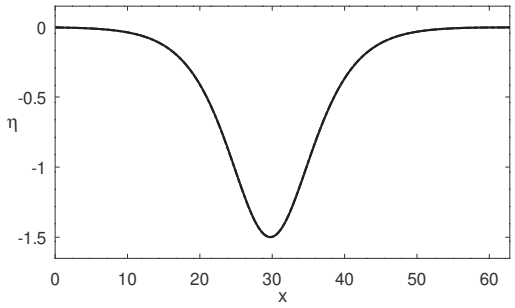

(a) $\theta = \pi/10$, $d \neq 0$

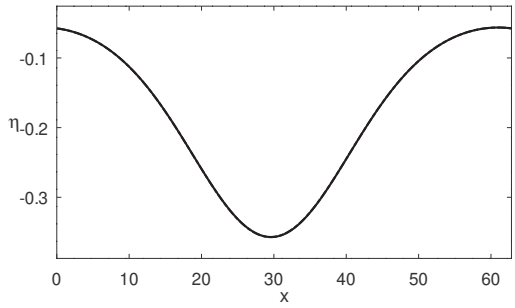

(b) $\theta = \pi/20$, $d \neq 0$

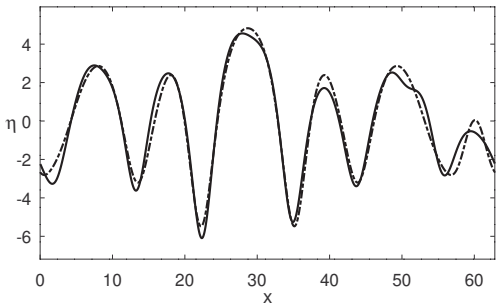

(c) $\theta = \pi/10$, $d = 0$

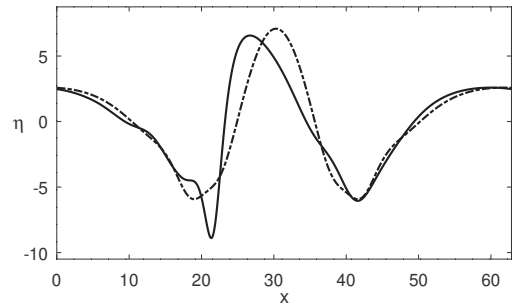

(d) $\theta = \pi/20$, $d = 0$

Figure B.5: Graphics of $\boldsymbol{\eta}^*$ $(- \cdot -)$ and $\boldsymbol{\eta}^n$ $(—)$ for the second method and each initial guess with $l = 10\pi$, $\alpha = \beta = 0.005$, $\Delta x = 0.03068$, $\Delta t = 0.21386$ at time $t = 62.66217 = 293\Delta t$.

Profiles	e_{abs}	e_{rel}	c_n	c
$\theta = \pi/10$, $d \neq 0$	0.0681512	0.0024964	0.97579	0.97887
$\theta = \pi/20$, $d \neq 0$	0.0059534	0.0006203	0.97325	0.97684
$\theta = \pi/10$, $d = 0$	20.3818830	0.1759205	0.95910	0.95864
$\theta = \pi/20$, $d = 0$	72.3643709	0.4545441	0.98475	0.95899

Table B.5: Errors at time $t = 62.66217 = 293\Delta t$ and wave velocities of η for the second method and each initial guess with $l = 10\pi$, $\alpha = \beta = 0.005$, $\Delta x = 0.03068$, $\Delta t = 0.21386$.

Profiles	e_{abs}	e_{rel}	c_n	c
$\theta = \pi/10$, $d \neq 0$	0.1012769	0.0037095	0.97590	0.97887
$\theta = \pi/20$, $d \neq 0$	0.0089135	0.0009305	0.97330	0.97672
$\theta = \pi/10$, $d = 0$	4.2724029	0.1953820	0.96770	0.98605
$\theta = \pi/20$, $d = 0$	4.4712940	0.0689461	0.96982	0.96735

Table B.6: Errors at time $t = 125.53821 = 587\Delta t$ and wave velocities of η for the second method and each initial guess with $l = 20\pi$, $\alpha = \beta = 0.005$, $\Delta x = 0.03068$, $\Delta t = 0.21386$.

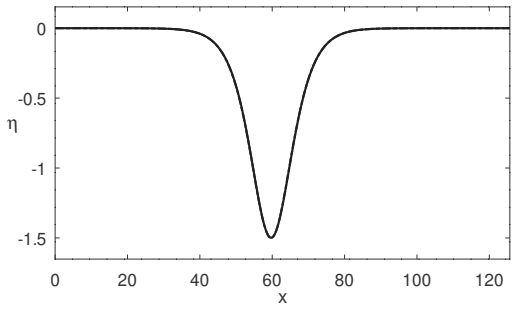

(a) $\theta = \pi/10$, $d \neq 0$

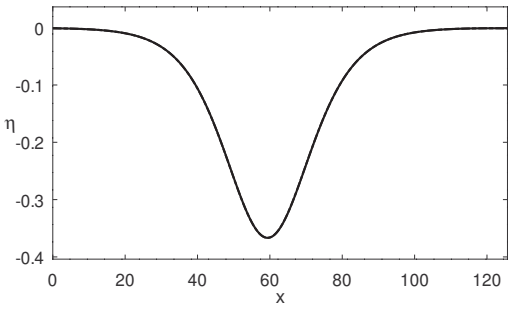

(b) $\theta = \pi/20$, $d \neq 0$

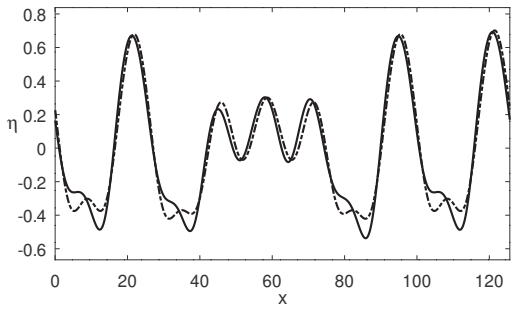

(c) $\theta = \pi/10$, $d = 0$

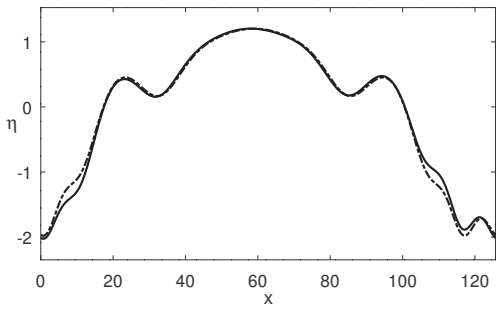

(d) $\theta = \pi/20$, $d = 0$

Figure B.6: Graphics of $\boldsymbol{\eta}^*$ $(- \cdot -)$ and $\boldsymbol{\eta}^n$ $(—)$ for the second method and each initial guess with $l = 20\pi$, $\alpha = \beta = 0.005$, $\Delta x = 0.03068$, $\Delta t = 0.21386$ at time $t = 125.53821 = 587\Delta t$.

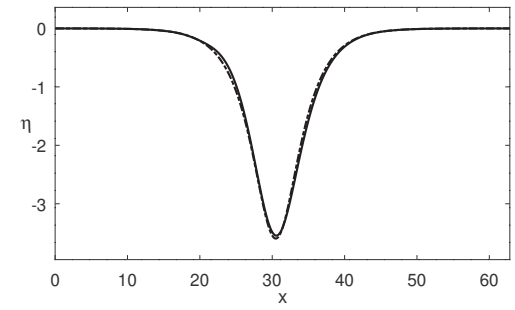

(a) $\theta = \pi/5$, $d \neq 0$

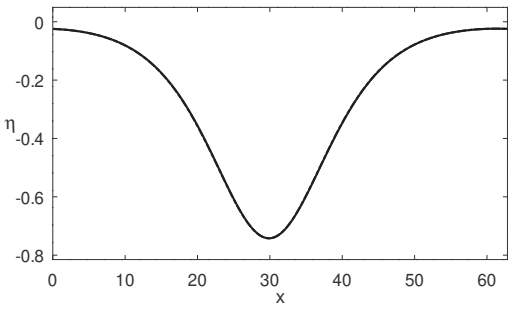

(b) $\theta = \pi/10$, $d \neq 0$

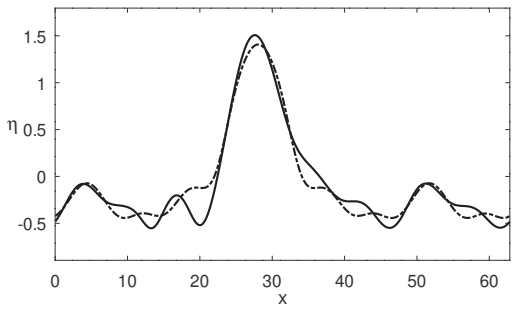

(c) $\theta = \pi/5$, $d = 0$

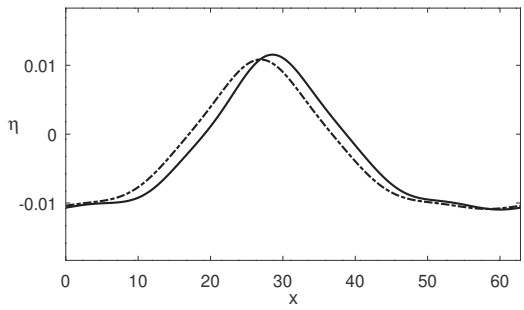

(d) $\theta = \pi/10$, $d = 0$

Figure B.7: Graphics of $\boldsymbol{\eta}^*$ $(- \cdot -)$ and $\boldsymbol{\eta}^n$ $(—)$ for the second method and each initial guess with $l = 10\pi$, $\alpha = \beta = 0.01$, $\Delta x = 0.03068$, $\Delta t = 0.25433$ at time $t = 62.81918 = 247\Delta t$.

Profiles	e_{abs}	e_{rel}	c_n	c
$\theta = \pi/5,\ d \neq 0$	1.8958617	0.0383338	0.98543	0.98788
$\theta = \pi/10,\ d \neq 0$	0.0421220	0.0026089	0.97559	0.97888
$\theta = \pi/5,\ d = 0$	5.2525438	0.2259850	0.94659	1.09918
$\theta = \pi/10,\ d = 0$	0.0769420	0.2084727	0.92843	1.36596

Table B.7: Errors at time $t = 62.81918 = 247\Delta t$ and wave velocities of η for the second method and each initial guess with $l = 10\pi$, $\alpha = \beta = 0.01$, $\Delta x = 0.03068$, $\Delta t = 0.25433$.

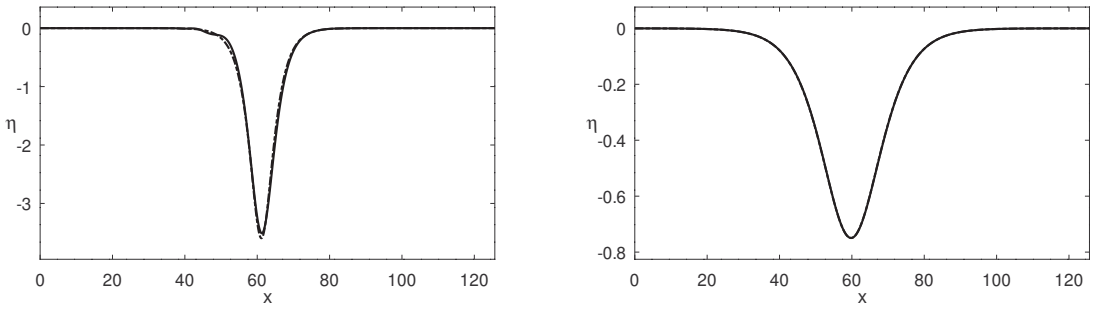

(a) $\theta = \pi/5,\ d \neq 0$ (b) $\theta = \pi/10,\ d \neq 0$

Figure B.8: Graphics of $\boldsymbol{\eta}^*$ $(- \cdot -)$ and $\boldsymbol{\eta}^n$ $(—)$ for the second method and each initial guess with $l = 20\pi$, $\alpha = \beta = 0.01$, $\Delta x = 0.03068$, $\Delta t = 0.25433$ at time $t = 125.63836 = 494\Delta t$.

Profiles	e_{abs}	e_{rel}	c_n	c
$\theta = \pi/5,\ d \neq 0$	2.2611471	0.0457198	0.98682	0.98788
$\theta = \pi/10,\ d \neq 0$	0.0455760	0.0028075	0.97587	0.97887

Table B.8: Errors at time $t = 125.63836 = 494\Delta t$ and wave velocities of η for the second method and each initial guess with $l = 20\pi$, $\alpha = \beta = 0.01$, $\Delta x = 0.03068$, $\Delta t = 0.25433$.

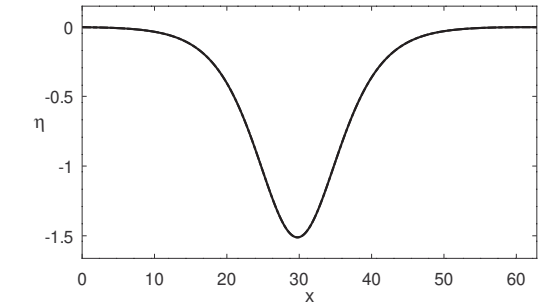

(a) $\theta = \pi/10$, $d \neq 0$

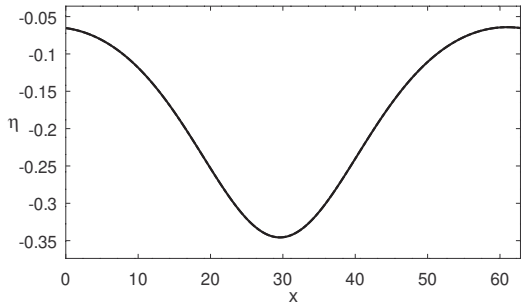

(b) $\theta = \pi/20$, $d \neq 0$

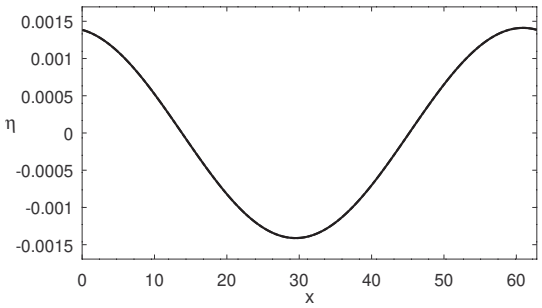

(c) $\theta = \pi/10$, $d = 0$

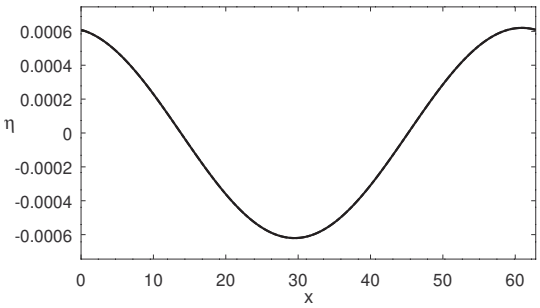

(d) $\theta = \pi/20$, $d = 0$

Figure B.9: Graphics of $\boldsymbol{\eta}^*$ $(- \cdot -)$ and $\boldsymbol{\eta}^n$ $(—)$ for the third method and each initial guess with $l = 10\pi$, $\alpha = \beta = 0.005$, $\Delta x = 0.03068$, $\Delta t = 0.21386$ at time $t = 62.66217 = 293\Delta t$.

Profiles	e_{abs}	e_{rel}	c_n	c
$\theta = \pi/10$, $d \neq 0$	0.0033280	0.0001212	0.97622	0.97621
$\theta = \pi/20$, $d \neq 0$	0.0015829	0.0001678	0.97343	0.97348
$\theta = \pi/10$, $d = 0$	0.0000075	0.0001657	0.97207	0.97210
$\theta = \pi/20$, $d = 0$	0.0000032	0.0001633	0.97207	0.97210

Table B.9: Errors at time $t = 62.66217 = 293\Delta t$ and wave velocities of η for the third method and each initial guess with $l = 10\pi$, $\alpha = \beta = 0.005$, $\Delta x = 0.03068$, $\Delta t = 0.21386$.

Profiles	e_{abs}	e_{rel}	c_n	c
$\theta = \pi/10$, $d \neq 0$	0.0001858	0.0000068	0.97621	0.97621
$\theta = \pi/20$, $d \neq 0$	0.0004649	0.0000485	0.97350	0.97351
$\theta = \pi/10$, $d = 0$	0.0000037	0.0000654	0.97251	0.97250
$\theta = \pi/20$, $d = 0$	0.0000043	0.0000675	0.97251	0.97250

Table B.10: Errors at time $t = 125.53821 = 587\Delta t$ and wave velocities of η for the third method and each initial guess with $l = 20\pi$, $\alpha = \beta = 0.005$, $\Delta x = 0.03068$, $\Delta t = 0.21386$.

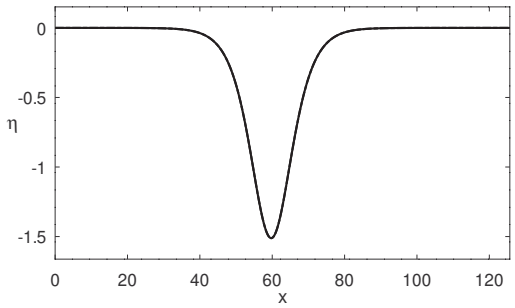

(a) $\theta = \pi/10$, $d \neq 0$

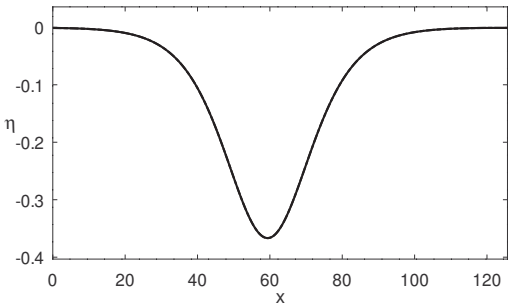

(b) $\theta = \pi/20$, $d \neq 0$

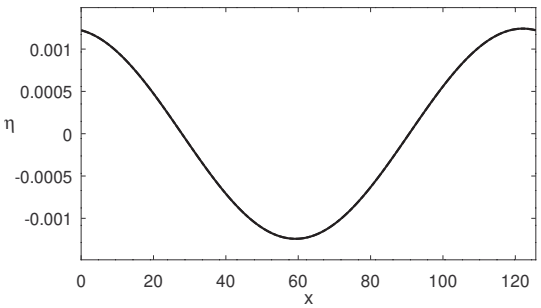

(c) $\theta = \pi/10$, $d = 0$

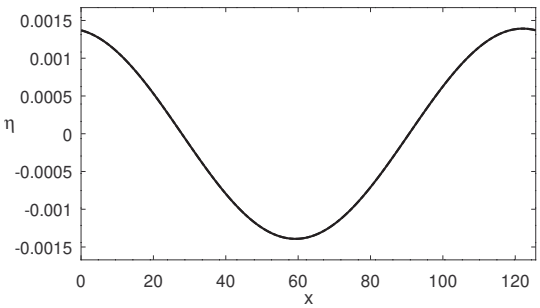

(d) $\theta = \pi/20$, $d = 0$

Figure B.10: Graphics of $\boldsymbol{\eta}^*$ $(- \cdot -)$ and $\boldsymbol{\eta}^n$ $(—)$ for the third method and each initial guess with $l = 20\pi$, $\alpha = \beta = 0.005$, $\Delta x = 0.03068$, $\Delta t = 0.21386$ at time $t = 125.53821 = 587\Delta t$.

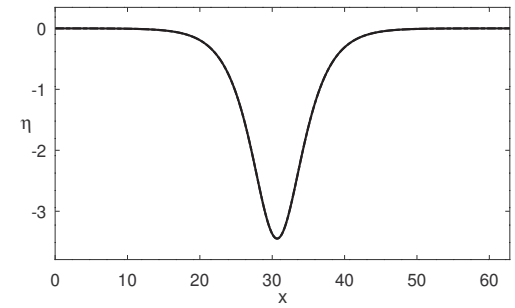

(a) $\theta = \pi/5$, $d \neq 0$

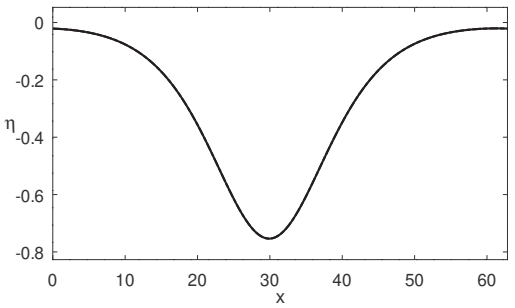

(b) $\theta = \pi/10$, $d \neq 0$

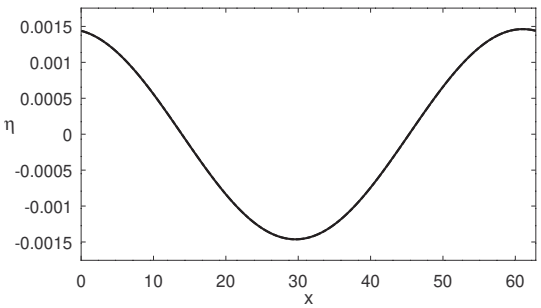

(c) $\theta = \pi/5$, $d = 0$

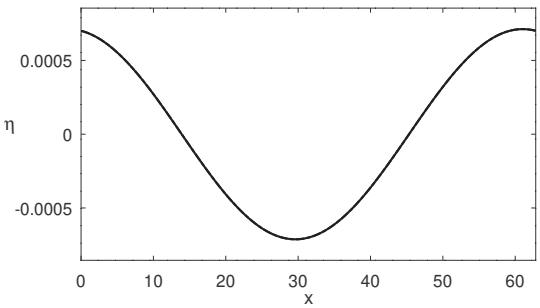

(d) $\theta = \pi/10$, $d = 0$

Figure B.11: Graphics of $\boldsymbol{\eta}^*$ $(- \cdot -)$ and $\boldsymbol{\eta}^n$ $(—)$ for the third method and each initial guess with $l = 10\pi$, $\alpha = \beta = 0.01$, $\Delta x = 0.03068$, $\Delta t = 0.25433$ at time $t = 62.81918 = 247\Delta t$.

Profiles	e_{abs}	e_{rel}	c_n	c
$\theta = \pi/5,\ d \neq 0$	0.0095141	0.0001940	0.98843	0.98842
$\theta = \pi/10,\ d \neq 0$	0.0014617	0.0000896	0.97622	0.97620
$\theta = \pi/5,\ d = 0$	0.0000290	0.0006188	0.97165	0.97156
$\theta = \pi/10,\ d = 0$	0.0000081	0.0003554	0.97161	0.97156

Table B.11: Errors at time $t = 62.81918 = 247\Delta t$ and wave velocities of η for the third method and each initial guess with $l = 10\pi$, $\alpha = \beta = 0.01$, $\Delta x = 0.03068$, $\Delta t = 0.25433$.

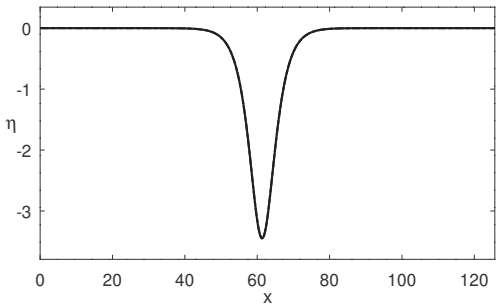

(a) $\theta = \pi/5,\ d \neq 0$

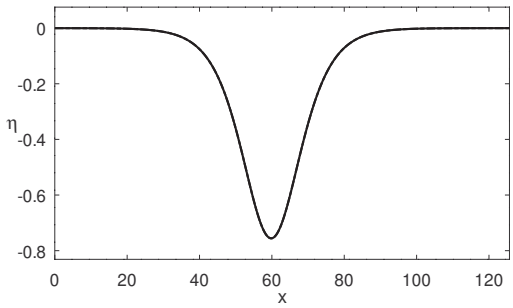

(b) $\theta = \pi/10,\ d \neq 0$

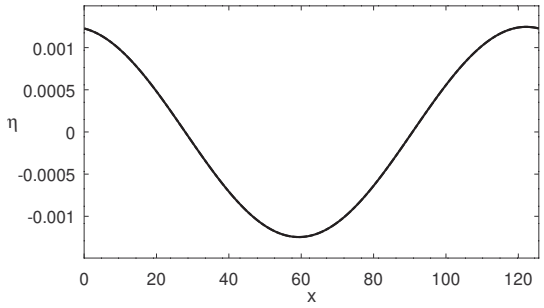

(c) $\theta = \pi/5,\ d = 0$

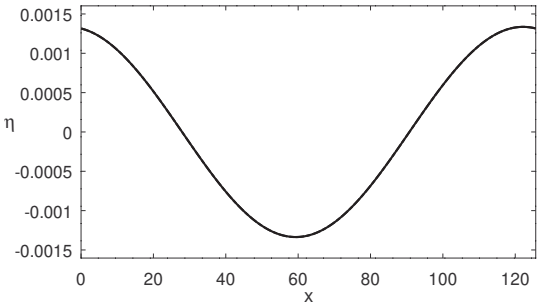

(d) $\theta = \pi/10,\ d = 0$

Figure B.12: Graphics of $\boldsymbol{\eta}^*$ $(- \cdot -)$ and $\boldsymbol{\eta}^n$ $(—)$ for the third method and each initial guess with $l = 20\pi$, $\alpha = \beta = 0.01$, $\Delta x = 0.03068$, $\Delta t = 0.25433$ at time $t = 125.63836 = 494\Delta t$.

Profiles	e_{abs}	e_{rel}	c_n	c
$\theta = \pi/5,\ d \neq 0$	0.0118725	0.0002421	0.98843	0.98842
$\theta = \pi/10,\ d \neq 0$	0.0026844	0.0001644	0.97622	0.97621
$\theta = \pi/5,\ d = 0$	0.0000090	0.0001594	0.97239	0.97236
$\theta = \pi/10,\ d = 0$	0.0000097	0.0001608	0.97239	0.97237

Table B.12: Errors at time $t = 125.63836 = 494\Delta t$ and wave velocities of η for the third method and each initial guess with $l = 20\pi$, $\alpha = \beta = 0.01$, $\Delta x = 0.03068$, $\Delta t = 0.25433$.

Appendix C

Scripts

Below we present the codes used to compute approximate solutions for the linear and nonlinear systems studied in this work, as well as the codes used to compute the travelling waves. We remark that the codes for the bidirectional models were based on those presented in [25] and the codes to compute the travelling waves were inspired in the one presented in [10]. All of them were implemented in the Octave language.

MainCode

```
%% Parameters
l = 20*pi; % period/2
N = 2^12;
%beta = 0.01;  alpha =0.01;  ab='01';
%beta = 0.005;  alpha =0.005;  ab='005';
%beta = 0.001;  alpha =0.001;  ab='001';
beta = 0.0001; alpha =0.0001; ab='0001';

deltaxi = 2 * l / N
x = (deltaxi:deltaxi:2*l);
ro1 =1; ro2 =2;
h1=0.1; h2=35.05*h1;% See Choi & Camassa, J. Fl Mech, 1999
L = h1/sqrt(beta); delta=h2/L;
parameters=[l,N,beta,alpha,ro1,ro2,h1,h2,L,delta];

%deltat = 2.061*sqrt(1+(ro2*sqrt(beta))/(ro1*delta))*deltaxi % condition 1
deltat = 2.651*sqrt(sqrt(beta)*(1+ro2/ro1)*deltaxi) % condition 2
%deltat = 2.828*sqrt(beta/3) % condition 3
Tfinal = 2*l;
Tsteps = fix(Tfinal/(deltat));

%MODEL = 'flat_linear'; md='FL';
MODEL = 'flat_weakly_nonlinear'; md='FN';
%MODEL = 'corrugated_linear'; md='CL';
%MODEL = 'corrugated_weakly_nonlinear'; md='CN';
Fund='S'; DerDisp='FD';

%WAVE='Gaus';
%WAVE='pBBM';
WAVE='prILW';
ct=pi/30;

%OPT='OP0'; %in case of one_direction
%OPT='OP1'; %first option eta
OPT='OP3'; %option u not approx
%OPT='OP5'; %complete system

%PROPAGATION = 'two_directions';
%PROPAGATION = 'one_direction';
PROPAGATION = 'traveling';

MEAN=1;

[M,matrix] = Topography(parameters,x,deltaxi,MODEL,Fund,DerDisp);
```

```
[init_eta,init_u,c] = InitialCondition(parameters,x,ct,WAVE,MEAN,PROPAGATION,OPT);
[Eta,U] = TimeAdvancing(parameters,deltaxi,deltat,Tsteps,init_eta,init_u,matrix,M,MODEL);
```

InitialData

```
function [init_eta,init_u,c] = InitialCondition(parameters,x,ct,WAVE,MEAN,PROPAGATION,OPT)
%% parameters
l=parameters(1);    N=parameters(2);
beta=parameters(3); alpha=parameters(4);
ro1=parameters(5);  ro2=parameters(6);
h1=parameters(7);   h2=parameters(8);
L=parameters(9);    delta=parameters(10);

%% initial eta guess
c=1;
switch WAVE
case {'Gaus'}
eta0 = 0.1*exp(-2*(x-l*ones(1,N)/2).^2);

case {'prILW'}
theta=ct;
lambda=delta/theta; c1=-1.5*alpha; c2=ro2*sqrt(beta)/(ro1*2);
c=1/(1+((2*c2)/delta)*theta*cot(2*theta));
aa =4*c*c2*theta*tan(theta)/(delta*c1);
eta0 = zeros(1,N);
for j=-10:1:10
eta0=eta0+aa*(cos(theta)^2)./((cos(theta)^2)*ones(1,N)+sinh((x-l+2*l*j)/lambda).^2);
end

case {'pBBM'}
c=ct;
a2= -3*alpha/2; a3=beta/6; c0=c-1; % c=sqrt(beta);
eta0=zeros(1,N);
for j=-10:1:10
eta0=eta0+(3*c0*(sech(sqrt(c0)*(x-l+2*l*j)/(2*sqrt(c)*sqrt(a3)))).^2)/a2;
end
end

%% eta mean
if MEAN==1
v=ones(1,N);
media=sum(eta0)/N;
eta0=eta0-media*v;
end

switch PROPAGATION
case 'one_direction'
init_eta=eta0;
etaeta = fft(eta0);
aux = pi*[1:N/2 -N/2 + 1:-1]/l;
omega = sqrt(1./(ones(1,N-1)+sqrt(beta)*ro2*aux.*coth(delta*aux)/ro1+beta*aux.*aux/3));
omega  = [ 1 , omega];
uu = -omega.* etaeta;
init_u = real(ifft(uu));

case 'two_directions'
init_eta=eta0;
init_u = zeros(1,N);

case 'traveling'
switch OPT
case 'OP1'
[init_eta, c]=NewtonEta1(l,N,alpha,beta,ro1,ro2,delta,eta0,c,MEAN);
init_u=-c*init_eta./(ones(1,N)-alpha*init_eta);

case 'OP3'
u0=-c*eta0./(ones(1,N)-alpha*eta0);
[init_u,c]=NewtonU2(l,N,alpha,beta,ro1,ro2,delta,u0,c,MEAN);
init_eta=init_u./(alpha*init_u -c*ones(1,N));

case 'OP5'
u0=-c*eta0./(ones(1,N)-alpha*eta0);
[init_eta,init_u,c]=NewtonS(l,N,alpha,beta,ro1,ro2,delta,eta0,u0,c,MEAN);
%init_eta=[init_eta(N/4 +1:N) init_eta(1:N/4)];
```

```
%init_u=[init_u(N/4 +1:N) init_u(1:N/4)];
end
end
end
```

defineV

```
function V = defineV(eta,u,MODEL,parameters,matrix)
%% parameters
l=parameters(1);    N=parameters(2);
beta=parameters(3); alpha=parameters(4);
ro1=parameters(5);  ro2=parameters(6);
h1=parameters(7);   h2=parameters(8);
L=parameters(9);    delta=parameters(10);

uu = fft(u);
aux = [1:N/2 -N/2 + 1:-1];
aux = pi*aux/l; % 2l period
kernel = (ones(1,N-1) + sqrt(beta)*ro2*aux.*coth(h2*aux/L)/ro1 + beta*aux.*aux/3);
kernel = [1 + sqrt(beta)*L*ro2/(ro1*h2), kernel];

switch lower(MODEL)
case 'flat_linear'
V = real(ifft(kernel.*uu));
case 'flat_weakly_nonlinear'
V = real(ifft(kernel.*uu));
case 'corrugated_linear'
V = matrix*(u');
V = V';
case 'corrugated_weakly_nonlinear'
V = matrix*(u');
V = V';
end
```

computeu

```
function u = computeu(eta,V,MODEL,parameters,matrix)
%% parameters
l=parameters(1);    N=parameters(2);
beta=parameters(3); alpha=parameters(4);
ro1=parameters(5);  ro2=parameters(6);
h1=parameters(7);   h2=parameters(8);
L=parameters(9);    delta=parameters(10);

VV = fft(V);
aux = [1:N/2 -N/2 + 1:-1];
aux = pi*aux/l;
kernel = (ones(1,N-1) + sqrt(beta)*ro2*aux.*coth(h2*aux/L)/ro1 + beta*aux.*aux/3);
kernel = [1 + sqrt(beta)*L*ro2/(ro1*h2), kernel];

switch MODEL
case 'flat_linear'
u = real(ifft(VV./kernel));
case 'flat_weakly_nonlinear'
u = real(ifft(VV./kernel));
case 'corrugated_linear'
u = matrix\(V).';
u = u.';
case 'corrugated_weakly_nonlinear'
u = matrix\(V).';
u = u.';
end
```

RK4step

```
function [eta_next,V_next] = RK4step(eta,u,V,deltaxi,deltat,MODEL,parameters,matrix,M)

switch MODEL
case 'flat_linear'
[K1,KK1] = computeE(eta,u,deltaxi,MODEL,parameters,M);

Phi_KK1 = computeu(eta,KK1,MODEL,parameters,matrix);
```

```
[K2,KK2]=computeE(eta+deltat*K1/2,u+deltat*Phi_KK1/2,deltaxi,MODEL,parameters,M);

Phi_KK2 = computeu(eta,KK2,MODEL,parameters,matrix);
[K3,KK3]=computeE(eta+deltat*K2/2,u+deltat*Phi_KK2/2,deltaxi,MODEL,parameters,M);

Phi_KK3 = computeu(eta,KK3,MODEL,parameters,matrix);
[K4,KK4]=computeE(eta+deltat*K3,u+deltat*Phi_KK3,deltaxi,MODEL,parameters,M);

case 'flat_weakly_nonlinear'
[K1,KK1] = computeE(eta,u,deltaxi,MODEL,parameters,M);

Phi_KK1 = computeu(eta,KK1,MODEL,parameters,matrix);
[K2,KK2]=computeE(eta+deltat*K1/2,u+deltat*Phi_KK1/2,deltaxi,MODEL,parameters,M);

Phi_KK2 = computeu(eta,KK2,MODEL,parameters,matrix);
[K3,KK3]=computeE(eta+deltat*K2/2,u+deltat*Phi_KK2/2,deltaxi,MODEL,parameters,M);

Phi_KK3 = computeu(eta,KK3,MODEL,parameters,matrix);
[K4,KK4]=computeE(eta+deltat*K3,u+deltat*Phi_KK3,deltaxi,MODEL,parameters,M);

case 'corrugated_linear'
[K1,KK1] = computeE(eta,u,deltaxi,MODEL,parameters,M);

u_KK1 = computeu(eta + deltat*K1/2,V + deltat*KK1/2,MODEL,parameters,matrix);
[K2,KK2]=computeE(eta+deltat*K1/2,u_KK1,deltaxi,MODEL,parameters,M);

u_KK2 = computeu(eta + deltat*K2/2,V + deltat*KK2/2,MODEL,parameters,matrix);
[K3,KK3]=computeE(eta + deltat*K2/2,u_KK2,deltaxi,MODEL,parameters,M);

u_KK3 = computeu(eta + deltat*K3,V + deltat*KK3,MODEL,parameters,matrix);
[K4,KK4] = computeE(eta + deltat*K3,u_KK3,deltaxi,MODEL,parameters,M);

case 'corrugated_weakly_nonlinear'
[K1,KK1] = computeE(eta,u,deltaxi,MODEL,parameters,M);

u_KK1 = computeu(eta + deltat*K1/2,V + deltat*KK1/2,MODEL,parameters,matrix);
[K2,KK2] = computeE(eta + deltat*K1/2,u_KK1,deltaxi,MODEL,parameters,M);

u_KK2 = computeu(eta + deltat*K2/2,V + deltat*KK2/2,MODEL,parameters,matrix);
[K3,KK3] = computeE(eta + deltat*K2/2,u_KK2,deltaxi,MODEL,parameters,M);

u_KK3 = computeu(eta + deltat*K3,V + deltat*KK3,MODEL,parameters,matrix);
[K4,KK4] = computeE(eta + deltat*K3,u_KK3,deltaxi,MODEL,parameters,M);
end

eta_next = eta + deltat*(K1+2*K2+2*K3+K4)/6;
V_next = V+ deltat*(KK1+2*KK2+2*KK3+KK4)/6;
```

computeE

```
function [E,F] = computeE(eta,u,deltaxi,MODEL,parameters,M)
%% parameters
l=parameters(1);    N=parameters(2);
beta=parameters(3); alpha=parameters(4);

%finite difference differentiation
u_xi=(8*([u(2:N) u(1)]-[u(N) u(1:N-1)])+[u(N-1:N) u(1:N-2)]-[u(3:N) u(1:2)])/(12*deltaxi);
eta_xi=(8*([eta(2:N) eta(1)]-[eta(N) eta(1:N-1)])+[eta(N-1:N) eta(1:N-2)]- ...
[eta(3:N) eta(1:2)])/(12*deltaxi);

switch MODEL

case 'flat_linear'
E =  u_xi ;
F =  eta_xi ;
case 'flat_weakly_nonlinear'
E =  (ones(1,N) - alpha*eta).*u_xi - alpha* u .* eta_xi ;
F =  eta_xi - alpha* u.*u_xi ;
case 'corrugated_linear'
E =  u_xi./M ;
F =  eta_xi./M ;  %there is another way to compute it.
case 'corrugated_weakly_nonlinear'
E = ((ones(1,N) - alpha*eta).*u_xi - alpha* u .* eta_xi)./M ;
```

```
F = (eta_xi - alpha* u.*u_xi)./M ;
end
```

Topography

```
function [M,matrix] = Topography(parameters,x,deltaxi,MODEL,Fund,DerDisp)
l=parameters(1);    N=parameters(2);
beta=parameters(3); alpha=parameters(4);
ro1=parameters(5);  ro2=parameters(6);
h1=parameters(7);   h2=parameters(8);
L=parameters(9);    delta=parameters(10);

switch MODEL
case {'corrugated_linear','corrugated_weakly_nonlinear'}
switch Fund
case 'S'
x_part = (3*l/4:deltaxi:7*l/4);
M = 1+ 0.5*sin(5*x_part);
M = [ones(1,3*N/8 - 1) M ones(1,N/8) ];
case 'R'
x_part = (3*l/4:deltaxi:7*l/4);
M = 1+ 0.5*sin(15*x_part);
M = [ones(1,3*N/8 - 1) M ones(1,N/8) ];
end

%% definition of matrices
w = exp(2*pi*i/N);
for j = 1:N
for k = 1:N
F(j,k) = w^((j-1)*(k-1));
end
end
auxp = pi*[1:N/2 -N/2 + 1:-1]/l;
td = [-1/delta -auxp.*coth(auxp.*delta)].';
diagonaltd = diag(td);
TD = real(F*diagonaltd*conj(F)/N);

d2=[0 -auxp.^2];
diagonald2=diag(d2);
D2=real(F*diagonald2*conj(F)/N);

switch DerDisp
case 'SP'
d=[0 i*auxp];
diagonald=diag(d);
C=real(F*diagonald*conj(F)/N);
case 'FD'
C=zeros(N,N);
a=zeros(1,N);
a(2)=2/(3*deltaxi); a(3)=-1/(12*deltaxi); a(N-1)=1/(12*deltaxi); a(N)=-2/(3*deltaxi);
C(1,:)=a;
for j=2:N
C(j,:)=[C(j-1,N) C(j-1,1:N-1)];
end
end

Mm = diag(1./M);
CM=diag(C*M');
matrix=(eye(N) - sqrt(beta)*ro2*Mm*TD/ro1 -beta*Mm^2*D2/3+beta*Mm^3*CM*C/3);

otherwise
M=ones(1,N);
matrix=eye(N);
end
end
```

TimeAdvancing

```
function [Eta,U]=TimeAdvancing(parameters,deltaxi,deltat,Tsteps,init_eta,init_u,matrix,M,MODEL)
l=parameters(1);    N=parameters(2);
beta=parameters(3); alpha=parameters(4);
ro1=parameters(5);  ro2=parameters(6);
h1=parameters(7);   h2=parameters(8);
L=parameters(9);    delta=parameters(10);
```

```
Eta=zeros(Tsteps+1,N);
U=zeros(Tsteps+1,N);
Eta(1,:) = init_eta;
U(1,:) = init_u;
V=defineV(init_eta,init_u,MODEL,parameters,matrix);

n2=norm(init_eta,2);
ninf=norm(init_eta,inf);
Final_step=Tsteps;
Tfinal=Tsteps*deltat;
for i=1:Tsteps
[eta_next,V_next] = RK4step(Eta(i,:),U(i,:),V,deltaxi,deltat,MODEL,parameters,matrix,M);
u_next = computeu(eta_next,V_next,MODEL,parameters,matrix);
n_2=norm(eta_next,2);
n_inf=norm(eta_next,inf);
Eta(i+1,:) = eta_next;
U(i+1,:) = u_next;
if   n_inf>2*ninf
Final_step=i;
Tfinal=deltat*Final_step;
break
end
V = V_next;
end

if Final_step<Tsteps
Eta([Final_step+2:Tsteps+1],:)=[];
U([Final_step+2:Tsteps+1],:)=[];
end
end
```

NewtonEta

```
function [Eta,c] = NewtonEta(l,N,alpha,beta,rho1,rho2,delta,Eta,c,MEAN)

w = exp(2*pi*i/N);
F=zeros(N,N);
for j = 1:N
for k = 1:N
F(j,k) = w^((j-1)*(k-1));
end
end
auxp = pi*[1:N/2 -N/2 + 1:-1]/l;
td = [-1/delta -auxp.*coth(auxp.*delta)]';
diagonaltd = diag(td);
ThD = real(F*diagonaltd*conj(F)/N);

diagDD=[0 -auxp.^2]';
diagonalDD=diag(diagDD);
DD=real(F*diagonalDD*conj(F)/N);

J=zeros(N+1);
v=ones(1,N);
Eta=Eta';
var=[Eta;c];
int=0;
if MEAN==0
int=v*Eta/N;
end
fun(1:N,1)=1.5*alpha*Eta.*Eta+(1-(1/c^2))*Eta-sqrt(beta)*rho2/rho1*ThD*Eta-(beta/3)*DD*Eta;
fun(N+1,1)=v*Eta/N-int;
contador = 0;
norma = 10;
while norma > 10^(-10) && contador < 10
J(1:N,1:N)=diag(3*alpha.*Eta)+(1-(1/c^2))*eye(N)-sqrt(beta)*rho2/rho1*ThD-(beta/3)*DD;
J(N+1,1:N)=v/N;
J(1:N,N+1)=(2/c^3)*Eta;

y=linsolve(J,fun);
var=var-y;
Eta=var(1:N);
c=var(N+1);
fun(1:N,1)=1.5*alpha*Eta.*Eta+(1-(1/c^2))*Eta-sqrt(beta)*rho2/rho1*ThD*Eta-(beta/3)*DD*Eta;
```

```
fun(N+1,1)=v*Eta/N-int;
norma=norm(fun,2)/(N+1);

contador = contador + 1;
end
if contador==10
fprintf('maximum number of iterations reached. Error = %.10f \n',norma)
end

Eta=Eta';
end
```

NewtonU

```
function [U,c] = NewtonU(l,N,alpha,beta,rho1,rho2,delta,U,c,MEAN)

w = exp(2*pi*i/N);
F=zeros(N,N);
for j = 1:N
for k = 1:N
F(j,k) = w^((j-1)*(k-1));
end
end
auxp = pi*[1:N/2 -N/2 + 1:-1]/l;
td = [-1/delta -auxp.*coth(auxp.*delta)]';
diagonaltd = diag(td);
ThD = real(F*diagonaltd*conj(F)/N);

diagDD=[0 -auxp.^2]';
diagonalDD=diag(diagDD);
DD=real(F*diagonalDD*conj(F)/N);

J=zeros(N+1);
v=ones(1,N);
U=U';
var=[U;c];
int=0;
if MEAN==0
int=v*(U./(alpha*U -c*v'))/N;
end

fun(1:N,1) = -c*U +0.5*alpha*U.*U -U./(alpha*U -c*v') + ...
(c*sqrt(beta))*(rho2/rho1)*ThD*U+(c*beta/3)*DD*U;
fun(N+1,1)=v*(U./(alpha*U -c*v'))/N-int;
contador = 0;
norma = 10;
while norma > 10^(-10) && contador < 10

J(1:N,1:N) = diag(alpha*U) +c*diag(1./((alpha*U -c*v').^2)) -c*eye(N) + ...
 (c*sqrt(beta))*(rho2/rho1)*ThD+(c*beta/3)*DD;
J(N+1,1:N)=-c./((alpha*U -c*v').^2)/N;
J(1:N,N+1)=(-U./((alpha*U -c*v').^2) -U + (sqrt(beta))*(rho2/rho1)*ThD*U+(beta/3)*DD*U)';
J(N+1,N+1)=v*(U./((alpha*U -c*v').^2))/N;

y=linsolve(J,fun);
var=var-y;

U=var(1:N);
c=var(N+1);

fun_F(1:N,1) = -c*U +0.5*alpha*U.*U -U./(alpha*U -c*v') +...
 (c*sqrt(beta))*(rho2/rho1)*ThD*U+(c*beta/3)*DD*U;
fun_F(N+1,1)=v*(U./(alpha*U -c*v'))/N-int;
norma=norm(fun,2)/(N+1);

contador = contador + 1;
end
if contador==10
fprintf('maximum number of iterations reached. Error = %.10f \n',norma)
end
U=U';
end
```

NewtonS

```
function [Eta,U,c] = NewtonS (l,N,alpha,beta,rho1,rho2,delta,Eta,U,c,MEAN)

w = exp(2*pi*i/N);
F=zeros(N,N);
for j = 1:N
for k = 1:N
F(j,k) = w^((j-1)*(k-1));
end
end
auxp = pi*[1:N/2 -N/2 + 1:-1]/l;
td = [-1/delta -auxp.*coth(auxp.*delta)]';
diagonaltd = diag(td);
ThD = real(F*diagonaltd*conj(F)/N);

diagDD=[0 -auxp.^2]';
diagonalDD=diag(diagDD);
DD=real(F*diagonalDD*conj(F)/N);

J=zeros(2*N+1);
fun=zeros(2*N+1,1);
v=ones(1,N);
Eta=Eta';
U=U';
var=[Eta;U;c];
int=0;
if MEAN==0
int=v*Eta/N;
end

a=sqrt(beta)*rho2/rho1;
b=(beta/3);
fun(1:N,1)=c*Eta+(v'-alpha*Eta).*U;
fun(N+1:2*N,1)=c*U-alpha*(U.^2)/2 +Eta -c*a*ThD*U-c*b*DD*U;
fun(2*N+1,1)=v*Eta/N-int;
contador = 0;
norma = 10;

while norma > 10^(-10) && contador < 10
J(1:N,1:N)=c*eye(N)-alpha*diag(U);
J(1:N,N+1:2*N)=diag(v'-alpha*Eta);
J(1:N,2*N+1)=Eta;

J(N+1:2*N,1:N)=eye(N);
J(N+1:2*N,N+1:2*N)=c*eye(N)-alpha*diag(U) -c*a*ThD-c*b*DD;
J(N+1:2*N,2*N+1)=U-a*ThD*U -b*DD*U;

J(2*N+1,1:N)=v/N;

y=linsolve(J,fun);
var=var-y;
Eta=var(1:N);
U=var(N+1:2*N);
c=var(2*N+1);
fun(1:N,1)=c*Eta+(v'-alpha*Eta).*U;
fun(N+1:2*N,1)=c*U-alpha*(U.^2)/2 +Eta -c*a*ThD*U-c*b*DD*U;
fun(2*N+1,1)=v*Eta/N-int;
norma=norm(fun,2)/(2*N+1);

contador = contador + 1;
end
if contador==10
fprintf('maximum number of iterations reached. Error = %.10f \n',norma)
end
Eta=Eta';
U=U';
end
```